Dynamic Patterning of Maternal mRNAs in the Early *C. elegans* Embryo

by

Jialing Li

B.A. University of California - Berkeley (2002)

Submitted to the Department of Physics
in partial fulfillment of the requirements for the degree of

Doctor of Philosophy

at the

MASSACHUSETTS INSTITUTE OF TECHNOLOGY

June 2012

Author .....
Department of Physics
April 6, 2012

Certified by .....
Alexander van Oudenaarden
Professor of Physics, Professor of Biology
Thesis Supervisor

Accepted by .....
Krishna Rajagopal
Professor of Physics
Chairman, Associate Department Head for Education

Dynamic Patterning of Maternal mRNAs in the Early *C. elegans* Embryo

by

Jialing Li

Submitted to the Department of Physics
on April 6, 2012, in partial fulfillment of the
requirements for the degree of
Doctor of Philosophy

Abstract

Asymmetric segregation of maternally-encoded proteins is essential to cell fate determination during early cell divisions of the *Caenorhabditis elegans* (*C. elegans*) embryo, but little is known about the patterning of maternal transcripts inside somatic lineages. In the first Chapter of this thesis, by detecting individual mRNA molecules *in situ*, we measured the densities of the two maternal mRNAs *pie-1* and *nos-2* in non-germline cells. We find that *nos-2* mRNA degrades at a constant rate in all somatic lineages, starting approximately 1 cell-cycle after each lineage separated from the germline, consistent with a model in which the germline protects maternal mRNAs from degradation. In contrast, the degradation of *pie-1* mRNAs in one somatic lineage, AB, takes place at a rate slower than that of the other lineages, leading to an accumulation of that transcript. We further show that the 3′ untranslated (UTR) region of the *pie-1* transcript at least partly encodes the AB-specific degradation delay. Our results indicate that embryos actively control maternal mRNA distributions in somatic lineages via regulated degradation, providing another potential mechanism for lineage specification.

The evolutionary fate of an allele ordinarily depends on its contribution to host fitness. Occasionally, however, genetic elements arise that are able to gain a transmission advantage while simultaneously imposing a fitness cost on their hosts. Seidel *et al.* previously discovered one such element in *C. elegans* that gains a transmission advantage through a combination of paternal-effect killing and zygotic self-rescue. In the second Chapter of this thesis we demonstrate that this element is composed of a sperm-delivered toxin, *peel-1*, and an embryo-expressed antidote, *zeel-1*. *peel-1* and *zeel-1* are located adjacent to one another in the genome and co-occur in an insertion/deletion polymorphism. *peel-1* encodes a novel four-pass transmembrane protein that is expressed in sperm and delivered to the embryo via specialized, sperm-specific vesicles. In the absence of *zeel-1*, sperm-delivered PEEL-1 causes lethal defects in muscle and epidermal tissue at the two-fold stage of embryogenesis. *zeel-1* is expressed transiently in the embryo and encodes a novel six-pass transmembrane domain fused to a domain with sequence similarity to *zyg-11*, a substrate-recognition subunit of an

E3 ubiquitin ligase. *zeel-1* appears to have arisen recently, during an expansion of the *zyg-11* family, and the transmembrane domain of *zeel-1* is required and partially sufficient for antidote activity. Although PEEL-1 and ZEEL-1 normally function in embryos, these proteins can act at other stages as well. When expressed ectopically in adults, PEEL-1 kills a variety of cell types, and ectopic expression of ZEEL-1 rescues these effects. Our results demonstrate that the tight physical linkage between two novel transmembrane proteins has facilitated their co-evolution into an element capable of promoting its own transmission to the detriment of the rest of the genome.

The Apical Epidermal Ridge (AER) in vertebrates is essential to the outgrowth of a growing limb bud. Induction and maintenance of the AER reply heavily on the coordination and signaling between two surrounding cell types: ectodermal and mesenchymal cells. In morphogenesis during embryonic development, a process called the epithelial-mesenchymal transition (EMT) occurs to transform epithelial cells into mesenchymal cells for increased cell mobility and decreased cell adhesion. To check whether the AER, which originated from the ectodermal layer, undergoes EMT for enhanced cell motility and invasiveness at an early stage of the limb outgrowth, we examined expression of biomarkers of the epithelial and mesenchymal cell types in the AER of a mouse forelimb at embryonic day 10.5 in Chapter three of this thesis. We also customized correlation-based image registration algorithm to perform image stitching for more direct visualization of a big field of tissue sample. We found that the AER surprisingly expresses both the epithelial marker and the mesenchymal marker, unlike a normal non-transitioning epithelial cell or a cell undergoing EMT. Our finding serves as a basis for potential future cell isolation experiments to further look into cell type switching of the AER and its interaction with the surrounding ectodermal and mesenchymal cells.

Thesis Supervisor: Alexander van Oudenaarden
Title: Professor of Physics, Professor of Biology

Acknowledgments

It is a pleasure to thank those who made this thesis possible. First and foremost, I am grateful to my thesis adviser, Alexander van Oudenaarden, whose support, guidance, patience, encouragement and funding are indispensable for me to develop and finish the thesis project. I am also indebted to many of my colleagues, Arjun Raj, Bernardo Pando, John Tsang, Qiong Yang and Dale Muzzey, to introduce me to experimental biology and image processing, and Rui Zhen Tan, Mei Lyn Ong, Annalisa M Pawlosky and Jan Phlipp Junker, to keep my PhD experience fun and stimulating. I also want to thank the Physics Department at MIT and all the female members of the van Oudenaarden lab, especially Anna Lyubimova, and the Administrative Assistant, Monica Wolf, for being extra supportive in my decision of balancing career and family. Last but not the least, I owe my deepest gratitude to my family. Thanks to my parents for raising me with a love of maths, science and problem-solving, and supporting me in all my pursuits. Thanks to my husband, a fellow PhD student in theoretical Physics, for staying motivational and accompanying me hurdling through grad school.

Contents

Chapter 1

Dynamic Patterning of Maternal mRNAs in the Early *C. elegans* Embryo

1.1 Introduction

C.elegans was first introduced as a model organism primarily for developmental biology and neurology researches by Sydney Brenner in 1965 [148]. It is a small, free-living, non-parasitic, soil roundworm that is easy to grow and to maintain in a laboratory environment. Mutant strains can be easily frozen down and thawed up, and it only takes a handful of animals to re-spawn a new colony. The major advantages of using *C.elegans* for biology experiments are its short life-cycle and large progeny size, which allow fast experimental turnaround and speed up the process of data collection. Admittedly, *C.elegans* is less closely-related to humans compared to higher model organisms such as mice. And yet, its anatomical and developmental simplicity allows us to *begin* to untangle the mysteries in the organization of multicellular organisms [19].

To a physicist, biological processes such as embryogenesis and regeneration are puzzling. These processes are great examples of self-organizing systems in which

ordered patterns and structures arise from a seemingly uniform field of ancestor cells, often in response to some external cue and may involve feedbacks to amplify an initial bias. Incidentally, the ideas of self-organization, patterning, and clustering have become an almost ubiquitous theme in recent years, extending from the study of protein interactions to the analysis of flocking behavior and social networks [48, 92, 97].

1.1.1 The source of patterning in development

The Turing pattern was proposed by the great mathematician Alan Turing in 1952 [135]. Turing wanted to show that combinations of known physical interactions are sufficient to explain pattern formation in biological systems. In his reaction-diffusion model, Turing demonstrated robust spatial patterns can develop autonomously in a simple system composed of a short-range activator and a long-range inhibitor. A key feature of Turing's model is that it does not require a pre-existing asymmetry and therefore is truly a self-organizing system.

The periodicity and autonomous nature of the Turing pattern might sound promising for modeling biological systems where repetitive structures form with little periodic pre-patterning (for review, see [68]). For example, a Turing-related model has been suggested to be applicable for digit formation during vertebrate limb development [94]. Miura et al. recapitulated the appearance of extra digits in a polydactylous mouse mutant with numerical simulations based on the Turing reaction-diffusion system [89].

The reaction-diffusion model is quite powerful. However, in most cases of development a cell relies on the positional information in decision makings such as which fate to adopt, whether to undergo programmed cell-death, etc. The question is where this information comes from and how the cell processes that information.

In our current understanding, a cell could gather its positional information from two potential sources. The obvious one is through morphogen diffusion and cell-cell interactions, which enable a cell to physically sense its environment and act accordingly. Alternatively, a cell is capable of knowing innately where it is in terms of lin-

eage ancestry and developmental stage. It does so by maintaining certain genetic and epigenetic markers, namely, cell fate determinants. Most cell ablation experiments performed in *C.elegans* in the 1980's failed to perturb identities of the remaining cells, suggesting cell fates might be largely intrinsically determined [128]. In the late 1980's and the 1990's, blastomere isolation experiments together with genetic screens have demonstrated cell-cell interactions also play a major role in cell-fate determination in *C.elegans* embryogenesis [47, 60, 103, 108, 134]. In conclusion, the specification of blastomere identity could depend on both intrinsic signals and external cues.

1.1.2 Founder cells and asymmetric divisions

Like most other multicellular organisms (not including the ones with the power of asexual reproduction through regeneration), *C.elegans* begin its journey of development from one single cell. From fertilization to gastrulation, five somatic founder cells are generated, through rounds of asymmetric cell divisions. These founder cells are well-characterized in terms of which germ layer their progeny contribute to [127, 126]. At 2-cell stage, the first founder cell AB is born, and its descendants are mostly ectodermal. The EMS cell is born at 4-cell stage, and further divides into two founder cells E and MS one cell-cycle later. The progeny of E cell makes up the endoderm exclusively, while MS descendants belong primarily to the mesoderm layer.

Conceivably, asymmetric cell divisions serve as an ideal strategy for self-renewal and differentiation of stem cells. Genetic screens in *C.elegans* have uncovered a family of regulator proteins called Par proteins responsible for the initial polarity establishment (following an external cue, namely, the sperm entry site) and the asymmetric partitioning of cell fate determinants during the first cell cycle [17, 36, 50, 56, 76, 91, 143]. Homologues of all-but-one Par proteins are found to exist and to be functionally conserved in higher organisms [4, 27, 78].

1.1.3 The maternal-zygotic transition

In many animals, the mother expresses and deposits a significant fraction of mRNAs into the oocyte before fertilization ([10], reviewed by [40]). The presence of these maternal transcripts allows the first few hours of embryogenesis to proceed without transcription of the embryonic genome ([33, 34], reviewed by [130]) because maternally supplied mRNAs encode proteins sufficient for establishing embryonic polarity and initializing lineage specification [15, 50, 61, 110]. During the subsequent transition from maternal to zygotic gene expression, the levels of many maternal mRNAs drop significantly, allowing zygotic transcription to assume control of the developmental program ([10], reviewed by [114]).

Because embryos lack control of maternal mRNA transcription, post-transcriptional control of maternal mRNAs is crucial for normal developmental progression. In *Drosophila melanogaster* (*D. melanogaster*), for instance, maternal mRNAs display marked spatiotemporal patterns. Examples include the localization of *nanos* and *bicoid* mRNAs to the anterior and posterior of the embryo, respectively, thus forming the protein gradients that establish the anterior-posterior axis [124]. The dominant mechanism for the localization of these mRNAs is the transport of the mRNAs, either active or passive, to its final destination ([25], reviewed by [98]). Such transportation-based mechanisms are useful in the syncytial cytoplasm of the Drosophila embryo; however, they would not be effective in the cellularized embryos in which the cellular membranes would block mRNA transport.

In a cellularized context, the remaining option for spatiotemporal patterning of maternal mRNAs is the regulation of degradation. Thus far, the evidence for this mechanism arises from the observation of the protection of maternal mRNAs in the germline of the developing organism [7, 32, 116, 147]. In *C.elegans*, *in situ* hybridization revealed that *C.elegans* maternal mRNAs fall into two primary classes based on their germline-versus-soma distributions: Class I defines transcripts with uniform densities throughout the embryo and relatively constant whole-embryo levels from fertilization through gastrulation and beyond (mostly housekeeping genes), while Class

II maternal mRNAs showed strong enrichment in the germline compared to the soma, with overall levels in the soma dropping significantly by gastrulation [10, 118]. The lack of evidence for cell-specific patterning of maternal mRNA levels in the soma, however, has led to the belief that, unlike the syncytial fly embryo, much of the early patterning of the somatic worm embryo relies largely on translational control and protein localization (reviewed by [38, 111]). Indeed, there is substantial evidence for this view; for instance, the 3' UTR regulates the translation of several maternal genes important for the patterning of the early embryo, such as *pal-1*, *glp-1* and *nos-2* [29, 37, 57, 87]. The possibility that maternal mRNA levels in the soma could be subject to lineage-specific regulation, however, remains unexplored, largely due to the inability to systematically measure the low levels of the mRNAs involved.

1.2 Experiments

In this thesis, we chose to survey the distributions of two maternally deposited mRNAs in different somatic lineages of the early *C. elegans* embryo. *C. elegans* is a powerful tool for studying processes related to embryogenesis thanks to its invariance in cell identities and positioning, which greatly facilitates experimental reproducibility. In addition, the complete lineage tree and timing of cell divisions have been previously recorded, which makes staging the embryos a simple task [5, 126].

We have studied the regulation of the stability of two maternal RNAs using a single-molecule mRNA counting method based on fluorescence *in situ* hybridization. Our data shows that in each of the somatic lineages the degradation of *nos-2* mRNA begins one cell-cycle after their separation from the germline, with rates being constant in time and very similar among the AB, EMS and C lineages. The extent of depletion of *nos-2* mRNA is always higher in AB than in EMS, due to the earlier onset of degradation in AB, an effect we have called the germline protection model. We also examined the degradation of *pie-1* mRNA, revealing somatic preservation of it in the AB lineage until the 15-cell stage, strong enough to cause a faster depletion of it in EMS than in AB. This differential regulation of *pie-1* and *nos-2* degradation

results in starkly different enrichment patterns for those two maternal mRNAs in the AB versus EMS lineages. Subsequent experiments demonstrated that the 3' UTRs contain important regulatory elements responsible for generating the different spatiotemporal patterns of *pie-1* and *nos-2* mRNA levels in the soma.

1.2.1 Results

We measured RNA abundance by computing combined RNA densities of AB descendants or EMS descendants over time. We observed that both *pie-1* and *nos-2* transcripts degraded much more quickly in somatic lineages than in the germline throughout the cell stages examined (from 1 cell to 28 cells; examples of an early and a late stage embryo shown in Fig. 1-1 A and B), consistent with previous studies of Class II maternal mRNAs [29, 118, 131]. In contrast with previous studies, however, we found that between the 1 and 4 cell stages, the combined number of mRNAs in the P_2 (P_1) and EMS (AB) cells was similar to those in their immediate ancestor, the P_1 (P_0) cell, whereas the total number of mRNAs in the ABa and ABp were lower than their immediate ancestor (AB) (Fig. 1-1 C). In other words, the percent decrease in maternal mRNA counts was significantly lower in the germ cells immediate daughters than in other somatic cells. This suggests that the onset of degradation in the somatic cells begins one cell cycle after the somatic cell divides away from the germline P cell. This could be due to the presence of mRNA protection machinery (such as P granules) inherited from the mother P cell or slow maturation of degradation machinery in the newly born somatic cell [12, 44]. Based on our data, we propose a germline protection model for somatically degraded maternal mRNA in which mRNA degradation is stalled until one cell cycle after each somatic lineage separates from the P-cell and proceeds at a constant rate thereafter (Fig. 1-2 A and B); in other words, maternal mRNAs in the direct descendants of P cells are temporarily protected. This model serves as a null-model of what one might expect to see in the absence of any lineage specific regulation of maternal transcripts.

The germline protection model further predicts the differences in mRNA density should persist at later stages of embryogenesis; in particular, the mRNA density in

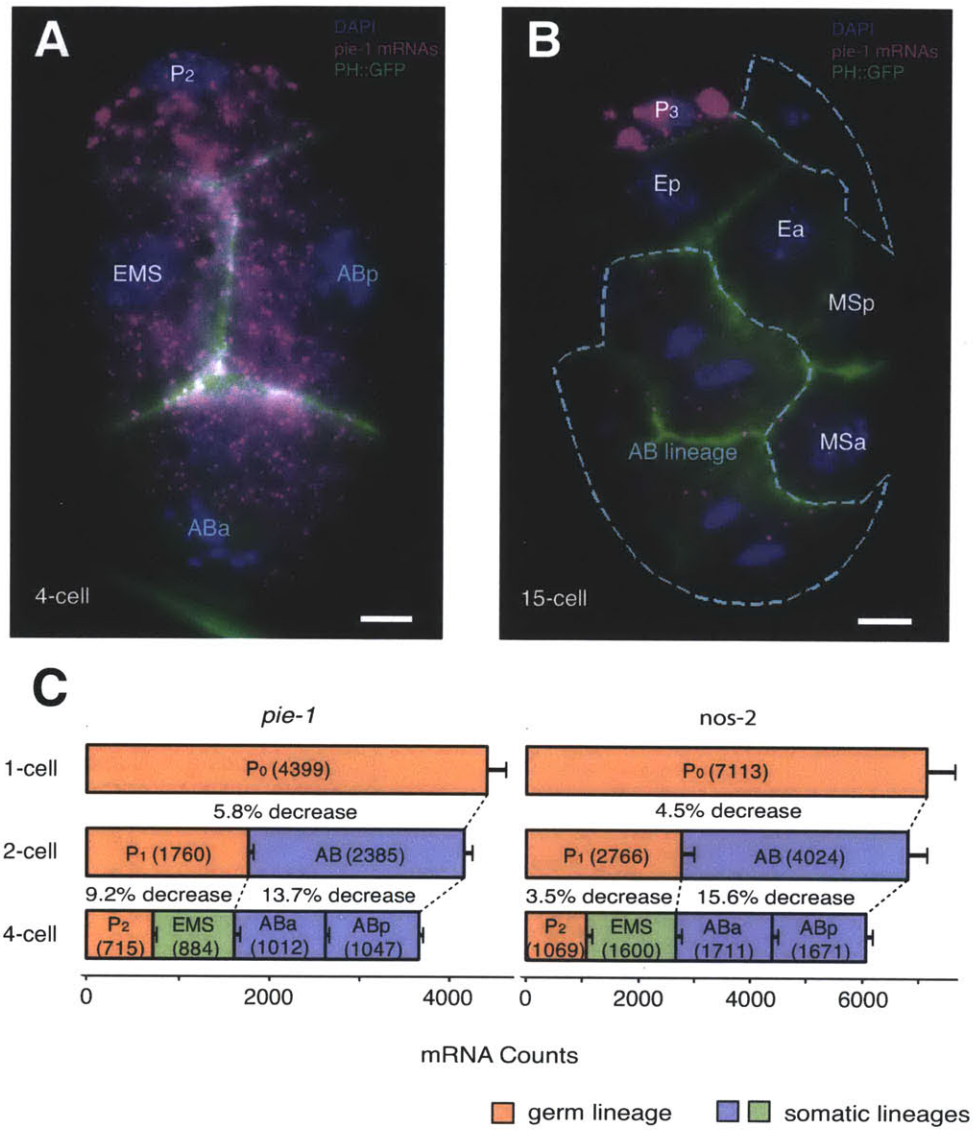

Figure 1-1: **Class II maternal mRNAs degrade faster in the soma than in germline.** (A and B) Visualization of *pie-1* transcript levels in a 4-cell embryo (A) and in a 15-cell embryo undergoing a new round of cell divisions (B) with DAPI counterstaining for the nuclei (blue) in a transgenic line with GFP cell boundary label (green). Shown in magenta are diffraction-limited spots representing individual transcripts. The dashed blue curve outlines the AB lineage in (B). Shown here are maximum projections of three planes (with a 0.3 μm interplanar space) out of thirty planes total per embryo. Scale bars are 5 μm long. (C) Counts of *pie-1* and *nos-2* mRNAs at 1 (n=13), 2 (n=8), and 4 (n=12) cell stages in GFP:PH embryos. Orange bars represent the germline P cells, and the blue and green bars indicate the somatic, AB, and EMS lineages respectively. Error bars indicate 95% confidence intervals for the sample means. Both *pie-1* and *nos-2* transcripts were degraded more rapidly in the somatic lineage (from AB to ABa plus ABp) than in the germ lineage (from P1 to P2 plus EMS); two-sample t-test: p = 0.0096 for *pie-1*, p = 0.00032 for *nos-2*.

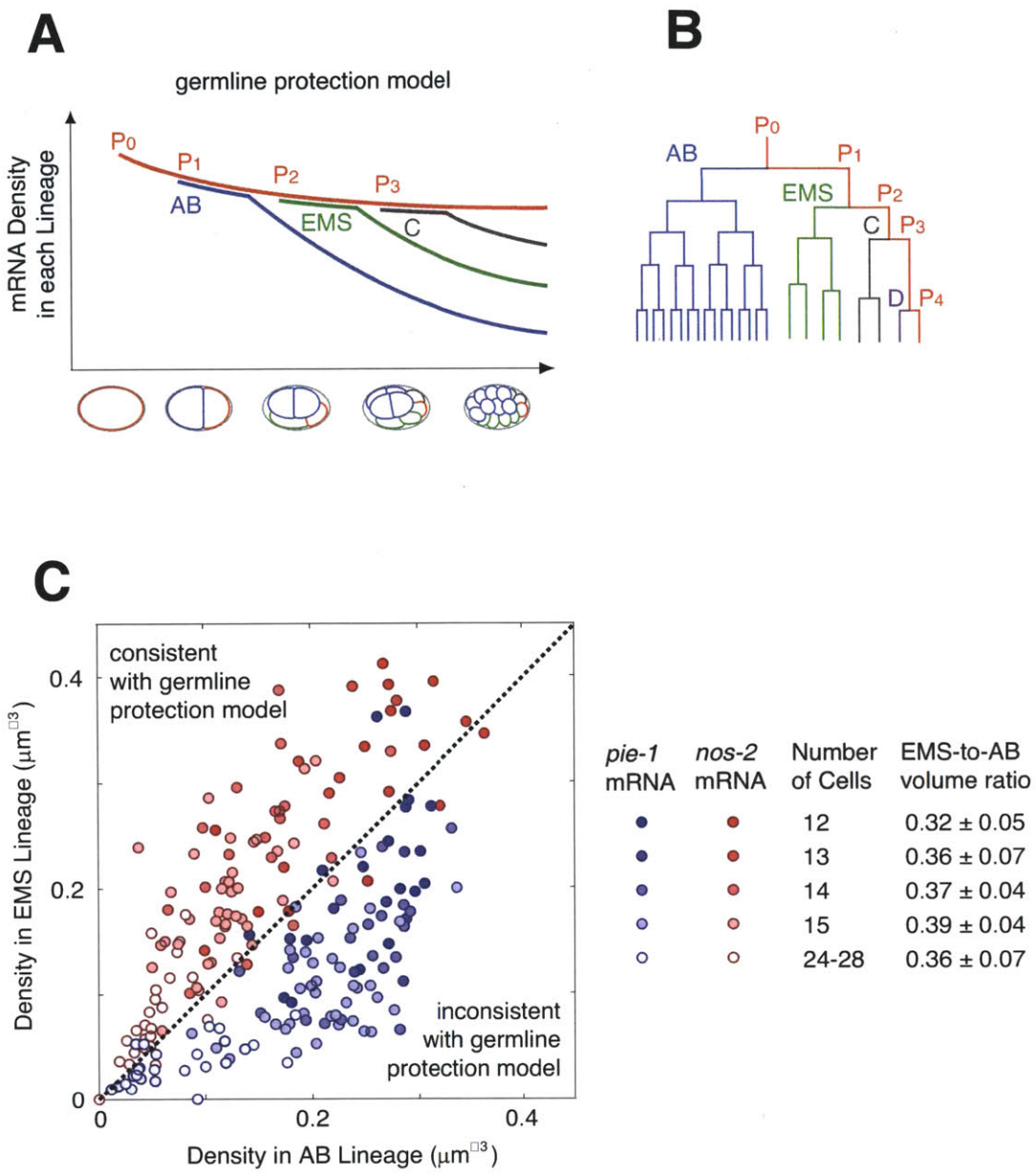

Figure 1-2: **Concentration of *pie-1* mRNA violates the germline protection model with a less-than-1 EMS-to-AB ratio.** (A) Theoretical degradation curves of maternal mRNAs in the somatic lineages based on germline protection model, predicting that the later onset of degradation would lead to a higher concentration of maternal mRNAs in EMS than in AB. (B) Lineage tree from 1 to 24 cell stages with colors corresponding to the lines in (A). (C) Densities of *pie-1* (blue) and *nos-2* (red) mRNAs in EMS versus in AB of wildtype (N2) embryos over a developmental window from 12 to 28 cell stages. Lighter spots correspond to later stages as indicated in the chart on the right. Listed on the right are the mean volume ratios between the EMS cells and the AB cells, ± errors in the volume ratio representing 95% confidence intervals for the sample means.

the EMS lineage should always be higher than in the AB lineage because EMS divides away from the P-cell one cell cycle later. To test this prediction, we measured the abundance of both *nos-2* and *pie-1* in the different lineages in embryos containing between 12 and 28 cells. We measured this abundance by computing the mRNA density rather than the total mRNA count in a lineage because the total count is rather sensitive to minor fluctuations in cell boundary identification during manual segmentation. Given that the volume ratio of EMS descendants to AB descendants is relatively constant during this developmental window (Fig. 1-2 C), the use of density rather than total count does not lead to systematic errors in our analysis. We found that *nos-2* mRNA levels were consistent with the germline protection model, with a substantially higher density of mRNAs present in the EMS lineage than in the AB lineage at virtually all cell stages (Fig. 1-2 C). Surprisingly, though, *pie-1* mRNA levels exhibited exactly the opposite behavior, with the mRNA density in the AB lineage being consistently higher than in the EMS lineage, showing that the degradation of *pie-1* is subject to lineage specific regulation.

The high density of *pie-1* in the AB lineage as compared to the EMS lineage could be due to either (or both) of two factors: a mRNA specific degradation of *pie-1* in the EMS lineage, or a mRNA specific block of degradation of *pie-1* in the AB lineage. To distinguish between these two possibilities, we quantified the degradation dynamics of both mRNAs in the AB, EMS and C lineages. In order to measure the age of our embryos, we used high resolution temporal lineage information [5] to convert number of cells into time elapsed since the first cell division. As previously mentioned, *nos-2* exhibits a degradation pattern consistent with the germline protection model. Notably, the density of *nos-2* mRNA follows an exponential curve a short time after the lineages separate from the P cell (Fig. 1-3 A), with the degradation rate computed from that curve being similar among the different lineages (Fig. 1-3 B). *pie-1* mRNA densities likewise follow a simple exponential in the EMS and C lineages, but the density curve in the AB lineage shows a biphasic behavior, in which degradation before the 15 cell stage ($\sim$74 min after first cell division) is almost three-fold slower than in the EMS and C lineages, although degradation in the AB lineage after that

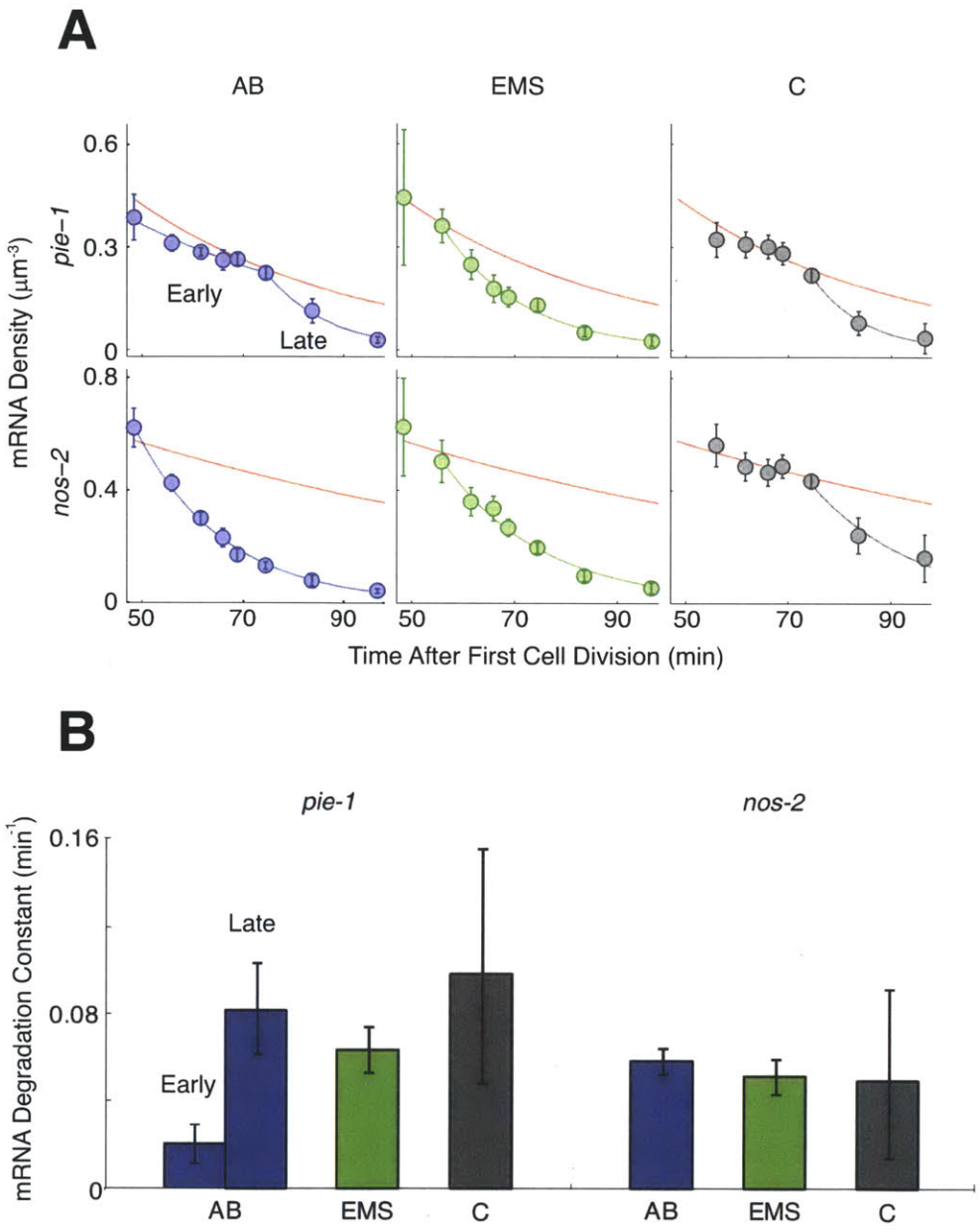

Figure 1-3: **Degradation of *pie-1* transcripts in the AB lineage proceeds at a slower rate prior to 15 cell stage (~74 min after first cell division) than thereafter.** (A) Experimentally measured degradation curves of *pie-1* and *nos-2* mRNAs in the various somatic lineages, with the estimated germline degradation curves in orange in the background. The time points used in the plots correspond to the following cell stages: 6, 8, 12, 13, 14, 15, 24 and 28. Error bars indicate 95% confidence intervals for the sample means. (B) Exponentially fitted rates of *pie-1* and *nos-2* degradation among different lineages found by the curve fitting in (A). Error bars indicate 95% confidence intervals obtained by bootstrapping (see Statistical Methods).

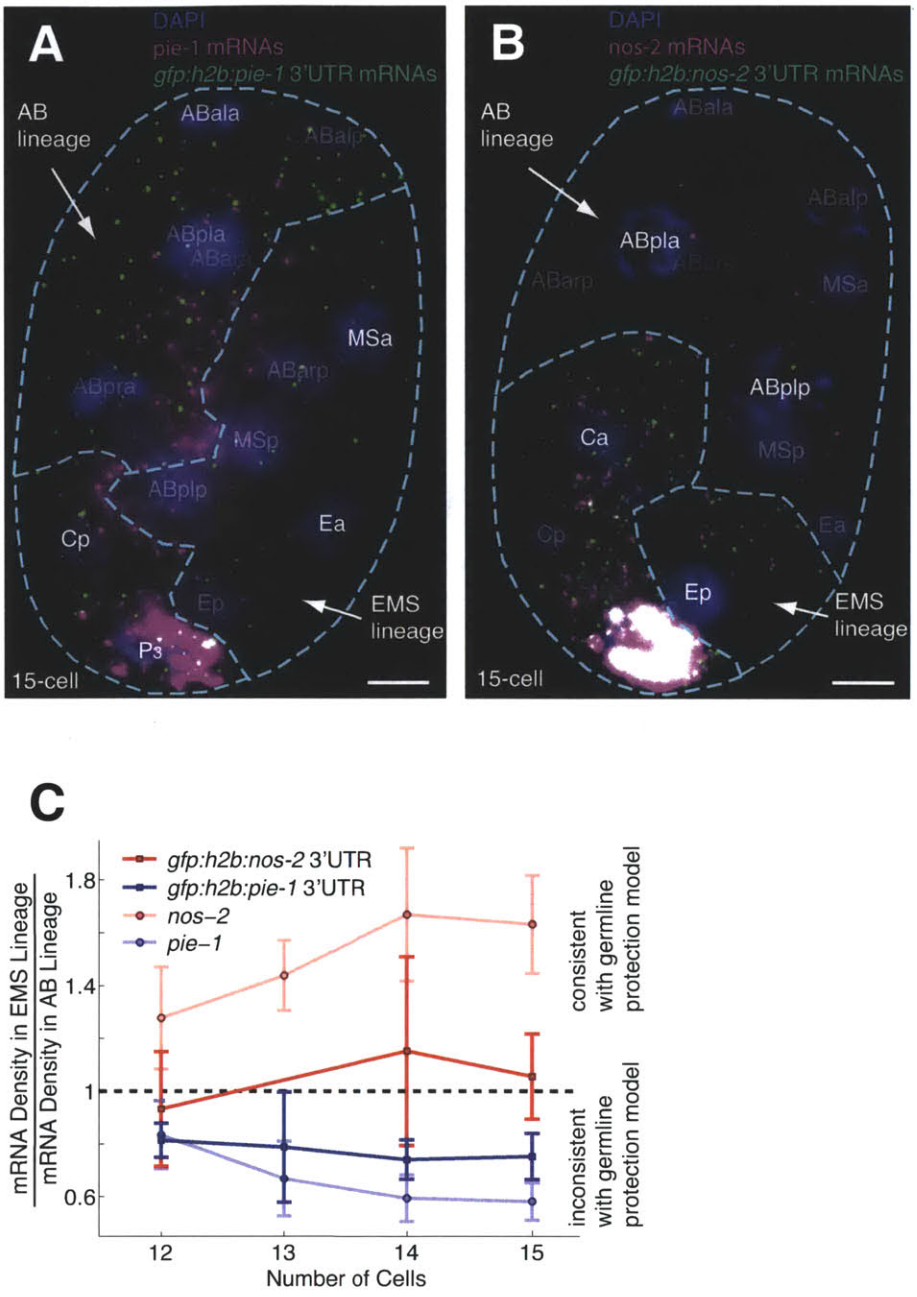

Figure 1-4: **Both *pie-1* and *nos-2* 3′ UTR can direct the mRNA degradation pattern of exogenous *gfp:h2b* transcripts.** (A and B) Simultaneous visualization of *gfp:h2b* transcripts with either *pie-1* or *nos-2* 3′ UTR and the corresponding endogenous mRNA with DAPI counter staining for the nuclei, in 15 cell stage transgenic embryos of N2 background. Shown here are maximum projections of three planes (with a 0.3 μm interplanar space) out of thirty planes total per embryo. Scale bars are 5 μm long. (C) EMS-versus-AB density ratios of the following transcripts in embryos staged from 12 to 15 cells: *gfp:h2b:pie-1* 3′ UTR, *gfp:h2b:nos-2* 3′ UTR, endogenous *pie-1* and *nos-2*. Error bars indicate 95% confidence intervals for the sample means.

time is again similar to that observed in the other lineages. These data point to a specific regulation of *pie-1* mRNA degradation in which degradation is selectively blocked in the AB lineage during a specific phase of development.

Regulation of maternal mRNAs is often encoded in the 3' UTR of the transcript [1, 8, 33]. With this in mind, we set out to test whether the 3' UTR plays a role in encoding the regulation of *pie-1* mRNA stability. To this end, we measured mRNA distributions in two strains, each containing a GFP-fused histone protein gene (*gfp:h2b*) driven by the *pie-1* promoter with either the *pie-1* or the *nos-2* 3' UTR (Fig. 1-4 A and B). We found that the *gfp:h2b* transcripts with the *nos-2* 3' UTR follow the germline protection model, while those with *pie-1* 3' UTR are more abundant in the AB lineage than in the EMS lineage in embryos containing between 12 and 15 cells (Fig. 1-4 C), qualitatively mimicking the behavior of the endogenous transcripts. The observed differential degradation in the *gfp:h2b* transcripts is not as strong as in the endogenous transcripts, suggesting the existence of additional regulatory elements in the coding portions of the transcripts. Nevertheless, our results show that the dynamics of *pie-1* and *nos-2* mRNA degradation is specific to those transcripts and is regulated via the 3' UTR.

In Zebrafish the clearance of maternal transcripts is accelerated by the MiR-430 microRNA [45]. In *C. elegans*, the loss of mir-35 or mir-51 microRNA family leads to embryonic lethality. We have examined the *pie-1* and *nos-2* transcript levels in mutant strains lacking microRNAs from either the mir-35 or the mir-51 families and failed to observe any significant changes from the wildtype distributions.

1.2.2 Materials and Methods

C. elegans strains and culture methods

We cultured *C. elegans* at 20C by following standard procedures and used the Bristol N2 as the wildtype strain [20]. We obtained the GFP cell-membrane labeling strain (OD58(P*pie-1 gfp:ph*(PLC1δ1))) from the Oegema lab [3]. The mutant strains lacking mir-35-41(*nDF50*) and mir-51(*n4473*) were gifts from the Horvitz lab [2].

Other transgenic strains used in this study were gifts from the Seydoux lab [29, 87]: JH2379(P*pie-1 gfp:h2b:pie-1* 3' UTR), JH2000(P*pie-1 gfp:h2b:nos-2* 3' UTR).

Single Molecule Fluorescence *in situ* Hybridization (FISH)

We carried out three-color single-molecule FISH procedures on *C. elegans* embryos as previously described [105], for simultaneous visualization of the two out of the three RNA species of interest (*pie-1*, *nos-2* and *gfp:h2b*) together with EMS lineage-specific transcripts (*end-3* and *med-1,2* combined). We conjugated each set of oligonucleotides targeting a unique transcript species including *pie-1*, *nos-2* and *gfp:h2b* to either tetramethylrhodamine (TMR), Cy5 or Alexa594. *end-3* and *med-1,2* probes were generated previously [104]. Signals from GFP declined but still stayed well above detection level after performing FISH. We gently squashed the embryos to ~9 micron thick before imaging. The oligonucleotide sequences of all the probes used in this study are listed in the supplementary material.

Counting mRNAs in individual cells and lineages

We identified and localized diffraction-limited spots representing single mRNA molecules using MATLAB software developed by Raj et al. [105] with slight modifications. The original software package utilizes a Mexican hat (Laplacian of Gaussian) filter for signal enhancement, in addition to manual thresholding for eliminating background noise and for positive identification of mRNA spots. A Gaussian filter smoothes out background noise and a Laplacian filter takes the spatial derivative of an image and detects rapid intensity changes between signal and background. Because an input image is composed of discrete pixels, we can apply both the Gaussian and the Laplacian filters using standard convolution methods. To speed up the image processing time, one can convolve the Gaussian filter with the Laplacian filter beforehand and apply the resulting hybrid filter to the input image altogether, given that the convolution operation is associative. The original package developed by Raj et al. [105] works nicely for resolving adjacent mRNA spots with not too small spatial separations; however, resolving diffraction-limited spots that overlap depends critically on the threshold

level and thus becomes a source of couting error. A single diffraction-limited spot has a Gaussian spread under widefield fluorescent microscope. When two diffraction-limited spots are within close proximity, their Gaussian spreads start to overlap. In the case where intensities of two overlapping Gaussian tails adds to be well above the threshold level, two spots will be mistakenly counted as one. To circumvent this issue, we identified regional maxima of the Laplacian filtered images which indicate the center locations of individual spots. Isolation of these maxima allowed us to reset the intensity in overlapping region between spots down to background level and to resolve overlapping mRNA spots regardless of the threshold chosen.

We manually segmented individual cells in embryos up to 4 cell stage based on the GFP:PH cell membrane signal. For stages beyond 4 cell and until 28 cell, we sequentially identified the different lineages (P, D, C, EMS and AB, if present) based on cell division time, sizes and locations of the nuclei with 4′,6-diamidino-2-phenylindole (DAPI) staining, together with mRNA density information. The germline (P) lineage was easily recognizable by its posterior end location and the hallmark highest concentration of maternal RNAs, *nos-2* and *pie-1*. The C cell and its descendents sit adjacently to P and their cytoplasm contain the highest density of *nos-2* mRNAs among all the somatic lineages until the birth of D at 24 cell stage. In addition, we labeled *end-3/med-1,2 mRNA* using FISH for marking the cytoplasm of EMS descendent cells. At last, after marking all the other lineages in an embryo, we tagged what remained unmarked to be the AB lineage automatically using MATLAB. We then measured the volumes of all lineages, with their shapes changing continuously throughout the 30 planes of images taken for each embryo, an 0.3 micron interplanar distance and a conversion factor of 8 camera pixels per micron. We then counted the mRNA spots inside each lineage to get the density.

Statistical methods

We assumed the mRNA degradation rates are normally distributed among the population and performed a two-sample t-test for the null hypothesis of 2-to-4 cell stage embryos having equal degradation rates of *pie-1* and *nos-2* in soma and germline (ver-

sus the alternative hypothesis of the rates being higher in soma than in germline). With one exception, we fitted each of the experimentally measured degradation curves of *pie-1* and *nos-2* mRNAs in the various somatic lineages to a single exponential decay curve with a fixed onset time consistent with the germline protection model using nonlinear least-squares. The exception is the degradation curve of *pie-1* mRNA in the AB lineage, to which we fitted two consecutive exponentially decaying curves, by allowing the onset time of the second exponential to be an additional free parameter. To obtain error estimates on degradation rates obtained from the exponential fits, we performed the same least square fitting on 5000 bootstrapped data sets (simulated data sets randomly resampled from the original data).

1.3 Discussion

We observed interesting dynamics reflecting lineage ancestry in both maternal RNA species. For *nos-2*, its densities within the somatic lineages follow essentially the same dynamics after each asymmetric cell division. After the birth of each somatic lineage, the *nos-2* density within that lineage starts out high and rapidly decreases after one cell-cycle. Therefore, the rank of *nos-2* densities from the lowest to the highest, at stages prior to gastrulation, faithfully represents the birth order of the somatic lineages. The density curves of *pie-1*, on the other hand, show two distinct behaviors. In the AB lineage, the dynamic of *pie-1* is bi-phasic, with a slower initial decay and a more rapid subsequent drop. In the EMS and C lineages, *pie-1* behaves pretty much the same as *nos-2* does. Unlike *nos-2*, however, the density of *pie-1* stayed higher in the earlier born AB lineage than in the later born EMS lineage from 8-cell to 24-cell-stage. Our result has suggested that the developing embryo intricately regulates the degradation of maternal mRNAs, so as to generate differential patterning of different mRNA species.

1.3.1 RNA-specific modulation of degradation

We can approximate the degradation of mRNAs as a simple process in which the degradation machinery (DM) binds and removes the target mRNA. (In the case of the germline lineage,the P-granules protect maternal RNAs from degradation.) The resulting mRNA density is an exponential function with a negative decay rate proportional to both the concentration of DM and the RNA-DM binding rate constant. The non-linearity in this transformation requires a fine tuning of DM concentrations and the binding constant. In other words, a small alternation in the binding efficiency between the mRNA species and its degradation machinery could cause a huge disparity in the mRNA distribution over time.

We have shown *pie-1* and *nos-2* mRNAs decay with very different kinetics through direct comparison. Moreover, we measured a rapid shift in the decay rate of *pie-1* transcripts at a specific developmental stage. Our findings, together with suggestions from previous in situ studies of other maternal transcripts such as *pos-1*, *pal-1* and *glp-1* [37, 57, 118, 119, 129], imply the existence of mRNA-specific controls of degradation. Whether these controls are direct modulations or merely secondary consequences of regulated translation is an interesting topic for future research. We cannot rule out the latter as a possibility.

If indeed our findings reflect a direct modulation in the decay process of *pie-1* mRNA, what could have caused the initial slowdown of *pie-1* mRNA degradation in AB? Perhaps the degradation of *pie-1* transcripts is actively blocked in early developmental stages. Alternatively, *pie-1* mRNA decay might require a special zygotic element. Bashirullah et al. and others previously reported the existence of distinct maternal and zygotic decay machineries in *Drosophila* and that distinct zygotic decay activities can target different maternal transcripts [8, 31]. Given our result, we speculate that *pie-1* transcripts might be targeted by a zygotic decay activity which switches on late. During the maternal-to-zygotic transition, differential timing of activation of different zygotically controlled decay machineries could be a driving force of differential patterning of distinct maternal transcripts.

One fundamental question about *C. elegans* development is how the various somatic lineages are derived from the same (germline) lineage through sequential asymmetric cell divisions and yet segregate into distinct fates. The early *C. elegans* embryo contains many strictly maternal (maternal but not embryonic) transcripts, including those of *pie-1* and *nos-2*, which can only be degraded but not newly synthesized [10]. The lack of cell specific expression presents a potential problem for using maternal mRNA to specify cell fates because in the absence of active intercellular transport of maternal transcripts (a strategy employed in the *Drosophila* syncytium, [52]), regulation of degradation is the only remaining option. Our results show that intricate regulation of degradation encoded in the 3' UTR can provide exactly such a mechanism for generating cell-specific maternal mRNA abundances, in this case, resulting in unique spatiotemporal patterns of *pie-1* and *nos-2* transcripts. By programming degradation rates in a transcript-specific manner, several maternal factors can act coordinately in generating stage- and lineage-specific expression patterns during early embryogenesis.

1.3.2 Biological significance

We were surprised to find preservation of *pie-1* maternal RNA in the AB lineage, because previous studies primarily demonstrated that the PIE-1 protein, a key regulator for germline differentiation, segregates preferentially to the P lineage and is actively degraded in the soma throughout early development [86, 132]. No patterning of PIE-1 protein has been observed in the soma to this date, likely because of the lower sensitivity of GFP tagged proteins and immunostaining methods. The single molecule FISH method we employed here detects changes in the absolute mRNA counts [105], providing us with the sensitivity to quantitatively measure differences in mRNA densities.

What possible functions might the regulated stability of *pie-1* mRNA serve? Researchers have shown that the post-translational control of the *pie-1* gene mainly serves to concentrate PIE-1 protein in the germline, so as to prevent the germline from adopting somatic fate [119]. In particular, PIE-1 represses SKN-1 in the germ

lineage and release of this repression will cause the germline to take on the EMS identity [15, 16, 84, 86]. We speculate that the spatiotemporal regulation of maternal *pie-1* transcripts, i.e. to retain higher level of *pie-1* mRNA in AB than EMS, helps reinforce the differences between AB and EMS by acting together with other somatic skn-1 repressor genes to maintain a low level of SKN-1 protein in AB. Further work is required to show the generality of such mechanisms for regulation of cell fate via regulated degradation of maternal transcripts.

Chapter 2

A novel sperm-delivered toxin causes late-stage embryo lethality and transmission ratio distortion in *C. elegans*

2.1 Introduction

The evolutionary fate of an allele ordinarily depends on the reproductive fitness of the organisms carrying it. In some cases, however, alleles are able to increase their representation in future generations while being neutral or detrimental to the fitness of their bearers. These elements, sometimes termed selfish or parasitic genes, influence transmission probabilities in a variety of ways. Some self-replicate and insert themselves into new genomic locations (*e.g.* transposons) [59]. Others act during meiosis to preferentially segregate into the oocyte [30, 41, 99] or to reduce the viability of sperm or spores inheriting alternate alleles [63, 70, 9, 136]. Still others act at the level of the zygote to destroy progeny not inheriting them. *Medea*-factors in *Tribolium* destroy non-carrier animals through a combination of maternal-effect killing and zygotic self-rescue [79]. An analogous phenomenon occurs in organisms infected by the ma-

ternally transmitted bacteria, *Wolbachia* or *Cardinium* [117, 144, 58], which modify the sperm of infected males to cause lethal defects when paired with the oocytes of uninfected females.

Previously, Seidel *et al.* discovered a nuclear-encoded element in *C. elegans* that kills non-carrier animals in a novel way [115]. This element, referred to as the *peel-1/zeel-1* element, is polymorphic within the species, and when animals carrying the *peel-1/zeel-1* element are crossed to animals lacking it, the *peel-1/zeel-1* element acts in the F1 heterozygote via paternal effect to kill F2 or backcross embryos not inheriting it. This lethality acts independently of maternal genotype and causes the *peel-1/zeel-1* element to become over-represented among the viable progeny of heterozygous sires, even while incurring a substantial fitness cost to these animals.

Paternal-effect loci are extremely rare in all of biology [21, 42], and the observed combination of nuclear-encoded, paternal-effect killing and zygotic self-rescue is unprecedented. In *C. elegans*, moreover, a paternal-effect locus whose effects can be rescued zygotically is mechanistically surprising because in this species, sperm-supplied factors are thought to act only during fertilization and first cleavage [77], whereas zygotic transcription does not begin until the four-cell stage [118].

Although the *peel-1/zeel-1* element is capable of promoting its own transmission, it rarely has the opportunity to do so in natural populations. *C. elegans* is an androdioecious species that reproduces primarily through self-fertilizing hermaphrodites. Because inbreeding is high [6], the *peel-1/zeel-1* element normally exists in the homozygous state, where no opportunity for self-promotion exists.

High inbreeding notwithstanding, out-crossing events in *C. elegans* between hermaphrodites and males do occur, albeit rarely [6, 28, 109]. And because the *peel-1/zeel-1* element is globally distributed and confers no apparent fitness disadvantage in the homozygous state [115], this element is expected to drive itself to fixation faster than a neutrally evolving locus. Consistent with this prediction, in laboratory populations where out-crossing is forced, the *peel-1/zeel-1* element fixes rapidly [115]. In natural populations, however, the *peel-1/zeel-1* element has remained polymorphic for an estimated 8 million generations [115], much longer than expected under neutrality.

One likely explanation for this paradox is that the *peel-1/zeel-1* element is tightly linked to a polymorphism maintained by balancing selection, and the tightness of this linkage maintains the *peel-1/zeel-1* element in the polymorphic state [115].

Given the unusual genetics of the *peel-1/zeel-1* element, we sought to understand its mechanism of action. Seidel *et al.* previously identified one component of the *peel-1/zeel-1* element as the gene *zeel-1* (*Y39G10AR.5*), which acts zygotically to rescue the paternal-effect killing [115]. Here we demonstrate that *zeel-1* is fully separable from the paternal-effect killing, and that this killing activity is encoded by a second gene, *peel-1* (*Y39G10AR.25*). We show that PEEL-1 acts as a sperm-supplied toxin, and ZEEL-1 an embryo-expressed antidote. We characterize the developmental defects caused by sperm-supplied PEEL-1, and we report a dose-dependent relationship between the severity of these defects and the quantity of PEEL-1 delivered to the embryo. We analyze the phylogenetic origins and functionality of each domain of *zeel-1*, and we test the tissue-autonomy of *zeel-1* rescue. Finally, in order to determine whether *peel-1* and *zeel-1* can function outside of embryogenesis, we express both genes ectopically in adults.

2.2 Experiments

2.2.1 Results

peel-1 and *zeel-1* are genetically distinct

The genetics of the *peel-1/zeel-1* element are consistent with it being composed of two interacting loci: a dominant-lethal, paternal-effect toxin, *peel-1*, and a zygotically acting antidote, *zeel-1* [115]. The activities of *peel-1* and *zeel-1* are present in the reference strain, Bristol (N2), and in approximately two-thirds of wild isolates [115]. These strains are said to carry the *peel-1/zeel-1* element. The commonly used wild strain, collected from Hawaii (CB4856), and all but two of the additional wild strains lack the activities of both *peel-1* and *zeel-1* [115]. The two remaining strains, one collected from Germany (MY19) and one collected from Utah (EG4348), exhibit the

activity of *zeel-1* but are unable to induce the paternal-effect killing [115], (Figure 2-1).

Seidel *et al.* previously mapped the *peel-1/zeel-1* element in the Bristol strain to a 62 kb interval on the left arm of chromosome I [115]. Within this interval, we identified a single gene capable of providing antidote activity. This gene, which we named *zeel-1*, encodes a 917-amino acid protein whose N-terminus is predicted to form a six-pass transmembrane domain and whose C-terminus exhibits sequence similarity to ZYG-11, a substrate-recognition subunit of an E3 ubiquitin ligase [65]. The Hawaii strain carries a 19 kb deficiency (*niDf9*) spanning *zeel-1*, and this deficiency is shared by all other wild isolates lacking the activities of both *peel-1* and *zeel-1* [115]. This deficiency is not shared by wild strains carrying the *peel-1/zeel-1* element, nor by MY19 or EG4348 [115].

The phenotype of MY19 and EG4348 demonstrates that the *zeel-1* gene is not sufficient for *peel-1* activity. Conversely, a deletion allele of *zeel-1* in the Bristol background demonstrates that *zeel-1* is also not required for it. This deletion, *tm3419*, removes 221 base pairs spanning the start codon of *zeel-1* (Figure 2-2 A). As expected, this deletion abolishes antidote activity (Figure 2-1 B); however, it does not abolish the paternal-effect killing (Figure 2-1 B). *zeel-1* is therefore genetically separable from a second, paternal-effect locus, *peel-1*. We note that as a consequence of this separability, *zeel-1* deletions in the Bristol and Hawaii backgrounds have opposite phenotypic effects: the *niDf9* deficiency is perfectly viable, whereas the *tm3419* deletion behaves as a conventional recessive-lethal mutation.

peel-1 encodes a novel, four-pass transmembrane protein of unknown function

In MY19 and EG4348, absence of *peel-1* activity is tightly linked to the 62 kb *peel-1* interval [115], (Figure 2-1 C), suggesting that these strains carry loss-of-function alleles of *peel-1*, rather than extra-genic suppressors. In addition, sequence analysis of the *peel-1* interval in MY19 [115] and EG4348 (see Materials and Methods) indicates that absence of *peel-1* activity in these strains is not caused by recombination

A

Cross	% Embryo lethality (total)
EG4348/Bristol selfing ♀	0% (275)
EG4348/Bristol ♂ x Hawaii ♀	0.7% (280)
EG4348/Hawaii selfing ♀	0.7% (285)
EG4348/Hawaii ♂ x Hawaii ♀	0.3% (372)
Bristol/Hawaii selfing ♀	23% (209)
Bristol/Hawaii ♂ x Hawaii ♀	51.2% (242)

B

Cross	% Embryo lethality (total) Expected	Observed
$\frac{zeel\text{-}1(tm3419)}{zeel\text{-}1(+)\ peel\text{-}1(+)}$ selfing ♀	~25%	24.2% (1009)
$\frac{zeel\text{-}1(tm3419)}{zeel\text{-}1(\Delta)\ peel\text{-}1(\Delta)}$ selfing ♀	~100%	99.4% (994)
$\frac{zeel\text{-}1(tm3419)}{zeel\text{-}1(\Delta)\ peel\text{-}1(\Delta)}$ ♂ x $\frac{zeel\text{-}1(\Delta)\ peel\text{-}1(\Delta)}{zeel\text{-}1(\Delta)\ peel\text{-}1(\Delta)}$ ♀	100%	100% (881)

C

peel-1 activity	*bli-3* genotype *bli-3(e767)*	+
Present	44	2
Absent	12	41

Figure 2-1: ***peel-1* and *zeel-1* are genetically separable.** (A) Wild isolate EG4348 was crossed to Bristol and Hawaii, and lethality was scored among embryos collected from self-fertilizing F1 hermaphrodites and F1 males backcrossed to Hawaii hermaphrodites. A control cross, using F1 individuals derived from a cross between Bristol and Hawaii, was performed in parallel. (B) Embryo lethality was scored among embryos collected from three crosses: (i) self-fertilizing *zeel-1(tm3419)/zeel-1(+)peel-1(+)* hermaphrodites, (ii) self-fertilizing *zeel-1(tm3419)/zeel-1(Δ)peel-1(Δ)* hermaphrodites, and (iii) *zeel-1(tm3419)/zeel-1(Δ)peel-1(Δ)* males mated to *zeel-1(Δ)peel-1(Δ)/zeel-1(Δ)peel-1(Δ)* hermaphrodites. The allelic nature of peel-1 on the haplotype carrying *zeel-1(tm3419)* is purposefully omitted because the goal of this experiment was to determine whether the deletion *tm3419* disrupts *peel-1* activity. Expected values were calculated under the hypothesis that *tm3419* creates a null allele of *zeel-1* but does not affect *peel-1*. Among embryos sired by hermaphrodites, slight decreases from 25% and 100% are expected because the paternal-effect killing is not fully penetrant when sperm derive from hermaphrodites [115]. (C) Absence of *peel-1* activity in EG4348 is genetically linked to *bli-3*, which is located on the left-hand tip of chromosome I, 10 cM from the *peel-1* interval. EG4348 was crossed to a strain of the Bristol background carrying *bli-3(e767)*, and F2 chromosomes were scored for *peel-1* activity and presence of the *bli-3(e767)* allele.

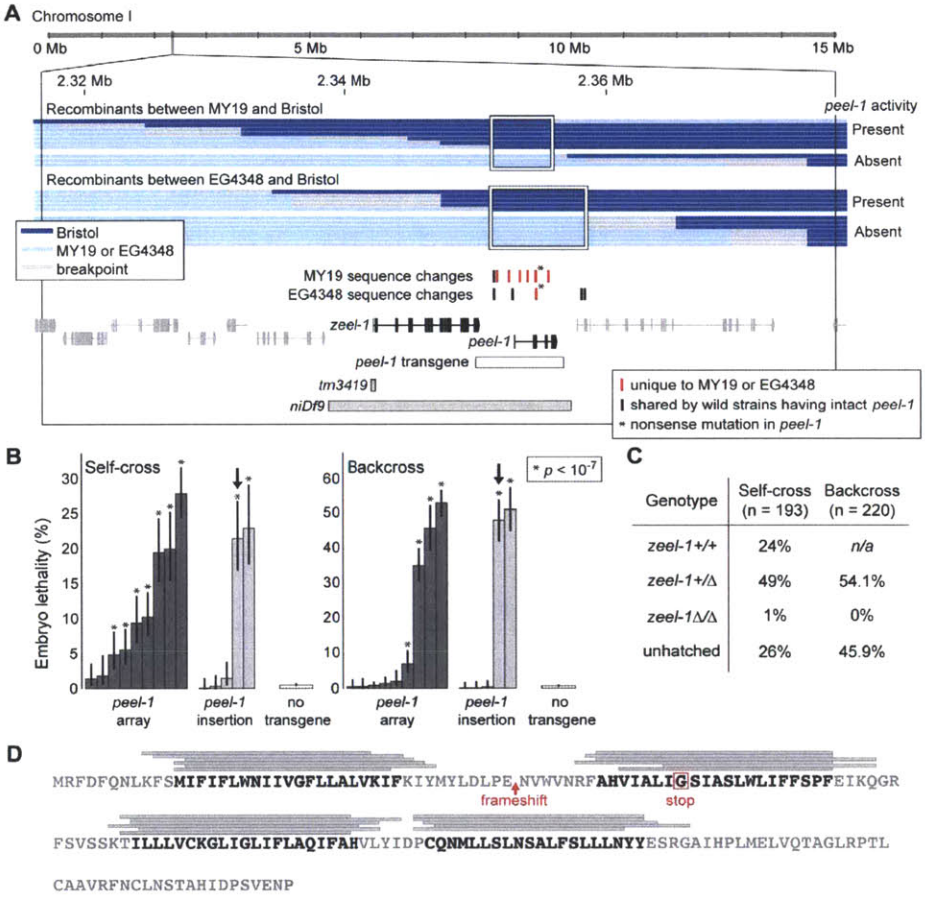

Figure 2-2: ***peel-1* is located adjacent to *zeel-1* and encodes a four-pass transmembrane protein.**

(A) The large black box outlines the genomic region to which *peel-1* was mapped previously [115]. Horizontal bars represent the recombinants used to map the *peel-1* mutations in strains MY19 and EG4348. The maximum intervals defined by these mapping experiments are outlined by white boxes. Adjoining breakpoints are excluded because they contain no sequence changes relative to Bristol. Below the recombinants, tick marks indicate all sequence changes in MY19 or EG4348 located within the boxed intervals. Horizontal bars represent the *peel-1* transgene, the *zeel-1*(*tm3419*) deletion allele, and the deficiency, *niDf9*. *niDf9* is carried by the Hawaii strain and by all other wild isolates lacking the activities of both *peel-1* and *zeel-1* [115].

(B) The Bristol allele of the *peel-1* transgene shown in (A) was tested for its ability to restore *peel-1* activity to animals carrying the *peel-1* nonsense mutation found in EG4348. To test for *peel-1* activity, transgenic animals were crossed to the Hawaii

Figure 2-2:
strain, and embryo lethality was scored from self-fertilizing F1 hermaphrodites (self-cross) and F1 males backcrossed to Hawaii hermaphrodites (backcross). Nine independent extra-chromosomal arrays and five independent single-copy genomic insertions were tested. For each array or insertion, 200 to 650 embryos were scored per self-cross or backcross. Ten control replicates were performed in parallel, each including 200 to 400 embryos. The global mean of these replicates is shown by the no transgene bars, and lethality for each individual replicate was less than 1.5%. Error bars indicate 95% binomial confidence intervals, calculated using the Agresti-Coull method [139]. *, $p < 10^{-7}$E, one-tailed binomial test relative to the mean of the control replicates. The observed variability among extra-chromosomal arrays was expected because of germline silencing [66]. The three single-copy insertions showing no *peel-1* activity probably represent incomplete insertion events, which are a common outcome of the MosSCI method [43]. Arrows indicate the insertion used for further analysis in (C).
(C) To confirm that the lethality observed in (B) was limited to *zeel-1*(Δ) embryos, an additional self-cross and backcross were performed using the insertion marked in (B). All hatched progeny were genotyped at *zeel-1*. In both crosses, the genotype frequencies among surviving progeny differed significantly from their Mendelian expectations (χ^2 tests, $p < 10^{-9}$). *n/a*, not applicable.
(D) The amino acid sequence of PEEL-1. Grey bars indicate predicted transmembrane helices, as predicted by (from top to bottom): TopPred [54], Tmpred [123], TMHMM [53], SOSUI [112], PHDhtm [137], and HMMTOP [13]. Regions predicted by at least four algorithms are highlighted in black. The frameshift in MY19 and the stop codon in EG4348 are indicated in red.

breaking apart the *peel-1/zeel-1* element. We hypothesized, therefore, that MY19 and EG4348 carry secondary, loss-of-function mutations in *peel-1*, and we reasoned that by identifying these mutations, we would be able to identify *peel-1* itself.

To accomplish this goal, we crossed MY19 and EG4348 to a strain of the Bristol background and generated recombinant chromosomes across the *peel-1* interval. Using these recombinants, we mapped the causative mutations in MY19 and EG4348 to regions of less then 10 kb (Figure 2-2 A). We then sequenced these regions to identify all sequence changes relative to Bristol. After excluding those sequence changes shared by one or more wild strains having intact *peel-1* activity (Figure 2-2 A, Figure 2-3), we defined six candidate mutations in MY19 and a single candidate mutation in EG4348.

The candidate mutations in MY19 and EG4348 reside in the intergenic interval immediately downstream of *zeel-1* (Figure 2-2 A). We searched for genes in this interval using targeted RT-PCR on Bristol animals, and we discovered a previously unannotated transcript. This transcript encodes a 174-amino acid protein (Figure 2-2 A,D), and three observations confirm this gene to be *peel-1*. First, the single candidate mutation in EG4348 and one of the candidate mutations in MY19 produce nonsense mutations in this transcript, consistent with the phenotype of these strains (frameshift in MY19; glycine to stop codon in EG4348) (Figure 2-2 A,D; Figure 2-3). Second, this gene is absent in the Hawaii strain and in all other wild isolates lacking the activities of both *peel-1* and *zeel-1* (Figure 2-2 A). Third, when we expressed the Bristol allele of this gene transgenically in a strain carrying the nonsense mutation found in EG4348, *peel-1* activity was restored (Figure 2-2 B-C).

PEEL-1 is a hydrophobic protein containing four predicted transmembrane helices (Figure 2-2 D). Neither the peptide nor the nucleotide sequence of *peel-1* has any detectable sequence similarity to any other gene in C. elegans or in the GenBank sequence database. Although *peel-1* and *zeel-1* are located adjacent to one another in the genome and oriented in the same direction, we were unable to recover transcripts carrying both genes (data not shown), demonstrating that *peel-1* and *zeel-1* are not isoforms of a single transcript or cistrons in an operon. We conclude that the *peel-1/zeel-1* element is composed of a 19 kb insertion carrying two distinct genes: *peel-1*,

which kills embryos via paternal-effect; and *zeel-1*, which acts zygotically to rescue this lethality.

Henceforth we refer to the Bristol alleles of *peel-1* and *zeel-1* as *peel-1(+)* and *zeel-1(+)* and the Hawaii alleles as *peel-1(Δ)* and *zeel-1(Δ)*. We use the term *peel-1*-affected embryos to refer to *zeel-1(Δ)* embryos fathered by a *peel-1(+)* animal.

peel-1 mRNA is expressed in spermatocytes, and the protein localizes to fibrous body-membranous organelles

As expected for a paternal-effect gene, *peel-1* is expressed exclusively in sperm. In both males and hermaphrodites, a GFP reporter driven by the *peel-1* promoter was expressed strongly in spermatocytes but not in any other tissue (Figure 2-5 A). In *fem-1(ts)* mutants, which lack sperm [22], *peel-1* expression via quantitative RT-PCR was undetectable in hermaphrodites and over 100-fold reduced in males (Figure 2-5 C). Residual expression in males probably reflects incomplete penetrance of the *fem-1(ts)* allele, because *fem-1(ts)* males occasionally produce a small number of sperm [22], and another sperm-specific gene, *spe-9* [122], also showed residual expression in males (Figure 2-5 C).

The sperm-specific expression of *peel-1* suggested that the paternal-effect killing occurs through delivery to the embryo of either sperm-supplied *peel-1* transcripts or sperm-supplied PEEL-1 protein. To distinguish between the two, we searched for *peel-1* transcripts in mature sperm via single-molecule fluorescence *in situ* hybridization (FISH). *peel-1* transcripts were observed in spermatocytes but not in mature sperm (Figure 2-4), thus excluding such transcripts as the likely mediators of *peel-1* toxicity.

Next, we searched for PEEL-1 protein both by tagging PEEL-1 with GFP and by staining sperm with an antibody raised against the C-terminal 15 amino acids of PEEL-1. Both experiments demonstrate that PEEL-1 protein is packaged into sperm, and this packaging is mediated by localization of PEEL-1 to sperm-specific vesicles called fibrous body-membranous organelles (FB-MOs) (Figure 2-6 A). PEEL-1::GFP was visible in mature sperm (Figure 2-6 E-F), and at each stage of spermatogenesis, its localization matched the pattern expected for a protein located in the membranes

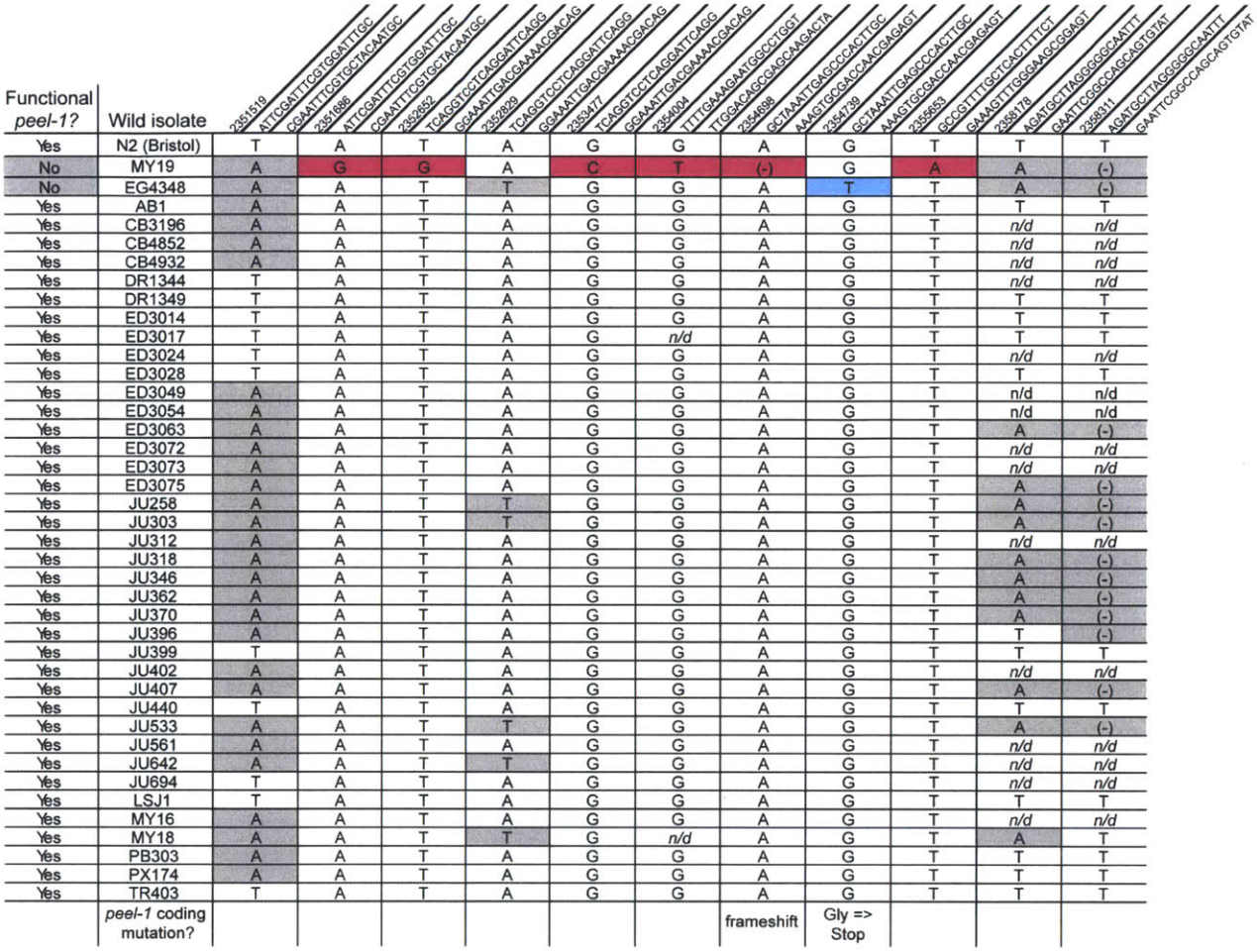

Functional *peel-1*?	Wild isolate	2351519 ATTCGATTTCGTGGATTTGC	2351686 CGAATTTCGTGCTACAATGC	2352652 ATTCGATTTCGTGGATTTGC	2352829 CGAATTTCGTGCTACAATGC	2353477 TCAGGTCCTCAGGATTCAGG	2354004 GGAAATTGACGAAAACGACAG	2354698 TCAGGTCCTCAGGATTCAGG	2354739 GGAAATTGACGAAAACGACAG	2355653 TTTTGAAAGATGGCCTGGT	2356178 TTCGACAGCGAGCAAGACTA	2356311 GCTAAATTGAGCCCACTTGC	2356693 AAGTGCGACCAACGAGAGT	2356778 GCTAAATTGAGCCCACTTGC	2356811 AAAGTGCGACCAACGAGAGT	2358178 GCCGTTTTGCTCACTTTTCT	2358311 GAAAGTTTGGGAAGCGGAGT	2358778 AGATGCTTAGGGGGCAATTT	2358811 GAATTCGGCCAGCAGTGTAT	2359278 AGATGCTTAGGGGGCAATTT	2359311 GAATTCGGCCAGCAGTGTAT
Yes	N2 (Bristol)	T	A	T	A	G	G	A	G	T	T	T									
No	MY19	A	G	G	A	C	T	(-)	G	A	A	(-)									
No	EG4348	A	A	T	T	G	G	A	T	T	A	(-)									
Yes	AB1	A	A	T	A	G	G	A	G	T	T	T									
Yes	CB3196	A	A	T	A	G	G	A	G	T	*n/d*	*n/d*									
Yes	CB4852	A	A	T	A	G	G	A	G	T	*n/d*	*n/d*									
Yes	CB4932	A	A	T	A	G	G	A	G	T	*n/d*	*n/d*									
Yes	DR1344	T	A	T	A	G	G	A	G	T	*n/d*	*n/d*									
Yes	DR1349	T	A	T	A	G	G	A	G	T	T	T									
Yes	ED3014	T	A	T	A	G	G	A	G	T	T	T									
Yes	ED3017	T	A	T	A	G	*n/d*	A	G	T	T	T									
Yes	ED3024	T	A	T	A	G	G	A	G	T	*n/d*	*n/d*									
Yes	ED3028	T	A	T	A	G	G	A	G	T	T	T									
Yes	ED3049	A	A	T	A	G	G	A	G	T	n/d	n/d									
Yes	ED3054	A	A	T	A	G	G	A	G	T	n/d	n/d									
Yes	ED3063	A	A	T	A	G	G	A	G	T	A	(-)									
Yes	ED3072	A	A	T	A	G	G	A	G	T	*n/d*	*n/d*									
Yes	ED3073	A	A	T	A	G	G	A	G	T	*n/d*	*n/d*									
Yes	ED3075	A	A	T	A	G	G	A	G	T	A	(-)									
Yes	JU258	A	A	T	T	G	G	A	G	T	A	(-)									
Yes	JU303	A	A	T	T	G	G	A	G	T	A	(-)									
Yes	JU312	A	A	T	A	G	G	A	G	T	*n/d*	*n/d*									
Yes	JU318	A	A	T	A	G	G	A	G	T	A	(-)									
Yes	JU346	A	A	T	A	G	G	A	G	T	A	(-)									
Yes	JU362	A	A	T	A	G	G	A	G	T	A	(-)									
Yes	JU370	A	A	T	A	G	G	A	G	T	A	(-)									
Yes	JU396	A	A	T	A	G	G	A	G	T	T	(-)									
Yes	JU399	T	A	T	A	G	G	A	G	T	T	T									
Yes	JU402	A	A	T	A	G	G	A	G	T	*n/d*	*n/d*									
Yes	JU407	A	A	T	A	G	G	A	G	T	A	(-)									
Yes	JU440	T	A	T	A	G	G	A	G	T	T	T									
Yes	JU533	A	A	T	T	G	G	A	G	T	A	(-)									
Yes	JU561	A	A	T	A	G	G	A	G	T	*n/d*	*n/d*									
Yes	JU642	A	A	T	T	G	G	A	G	T	*n/d*	*n/d*									
Yes	JU694	T	A	T	A	G	G	A	G	T	*n/d*	*n/d*									
Yes	LSJ1	T	A	T	A	G	G	A	G	T	T	T									
Yes	MY16	A	A	T	A	G	G	A	G	T	*n/d*	*n/d*									
Yes	MY18	A	A	T	T	G	*n/d*	A	G	T	A	T									
Yes	PB303	A	A	T	A	G	G	A	G	T	T	T									
Yes	PX174	A	A	T	A	G	G	A	G	T	T	T									
Yes	TR403	T	A	T	A	G	G	A	G	T	T	T									
	peel-1 coding mutation?							frameshift	Gly => Stop												

Figure 2-3: **Some MY19 and EG4348 sequence changes are shared with wild isolates having intact *peel-1*.** All of the sequence changes in MY19 and EG4348 located within the boxed intervals shown in Figure 2-2 A were genotyped in a panel of 38 wild strains shown previously to have intact *peel-1* activity [115]. The position of each polymorphism (WormBase release May 2008 WS190/ce6) and the primers used to amplify and sequence it are listed diagonally above each column. Alleles unique to MY19 are shown in pink, alleles unique to EG4348 are shown in cyan, and alleles shared by at least one additional wild strain are shown in grey. Polymorphisms affecting the amino acid sequence of *peel-1* are indicated in the bottom row. *n/d*, not determined; (-), single base-pair deletion.

of FB-MOs: in early spermatocytes, PEEL-1::GFP localized to cytoplasmic puncta (Figure 2-6 B), but after the pachytene stage, these puncta dissociated into a mesh-like web (Figure 2-6 B-D); after the completion of spermatogenesis, PEEL-1::GFP re-condensed into puncta located at the spermatid cortex (Figure 2-6 E); and after sperm activation, these puncta localized opposite the newly formed pseudopod (Figure 2-6 F). This localization pattern was replicated by the anti-PEEL-1 antibody (Figure 2-6 G), and staining with this antibody overlapped perfectly with a marker of FB-MOs (Figure 2-6 H-I).

We also discovered that the leader peptide of PEEL-1 can act as a sperm-localization signal. Our P*peel-1::GFP* reporter, which expressed untagged GFP, showed diffuse localization in spermatocytes and was excluded from sperm (Figure 2-5 B). This exclusion was not surprising because GFP is a heterologous protein, and trafficking of cellular components into sperm is tightly regulated [16]. Nevertheless, when we tagged GFP with the *N*-terminal 12 amino acids of PEEL-1 (MRFDFQNLKFSM), its localization changed dramatically. The tagged version of GFP localized to a reticulated structure within spermatocytes, and this structure was trafficked into sperm (Figure 2-5 B). To our knowledge, this result represents the first identification of a sperm localization signal in *C. elegans*.

peel-1-affected embryos show late-stage defects in muscle and epidermal tissue

Unlike other known paternal-effect genes [21, 42], sperm-supplied PEEL-1 does not cause defects until late in development. In *peel-1*-affected embryos, early embryogenesis, gastrulation, epidermal enclosure, and early elongation occur normally (Figure 2-7 C). Then, at the two-fold stage of elongation, when all major tissues have begun differentiating and nearly all embryonic cell divisions have already occurred, the majority of *peel-1*-affected embryos arrest elongation and fail to begin rolling within their eggshells. Shortly thereafter, the bulk of the embryo compresses inward, towards the mid-embryo bend, and the head and tail become flaccid and thin (Figure 2-7 D). Approximately two hours later, cytoplasm begins leaking from the external

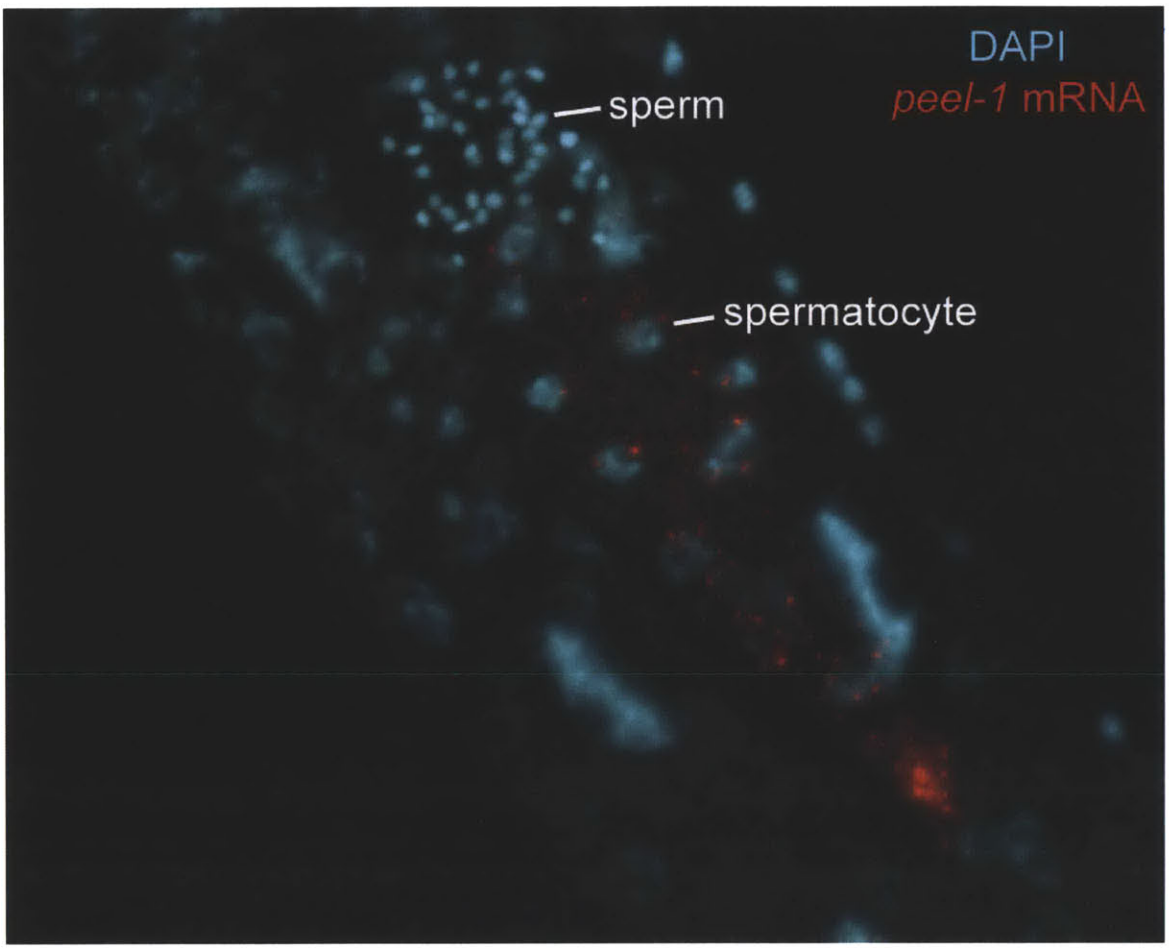

Figure 2-4: ***peel-1* mRNA is not present in sperm.** *peel-1* mRNAs were visualized in a wild-type, L4 hermaphrodite using single-molecule fluorescence *in situ* hybridization. *peel-1* mRNAs are shown in red, and nuclei are stained with DAPI (cyan). Sperm and spermatocyte nuclei are labeled.

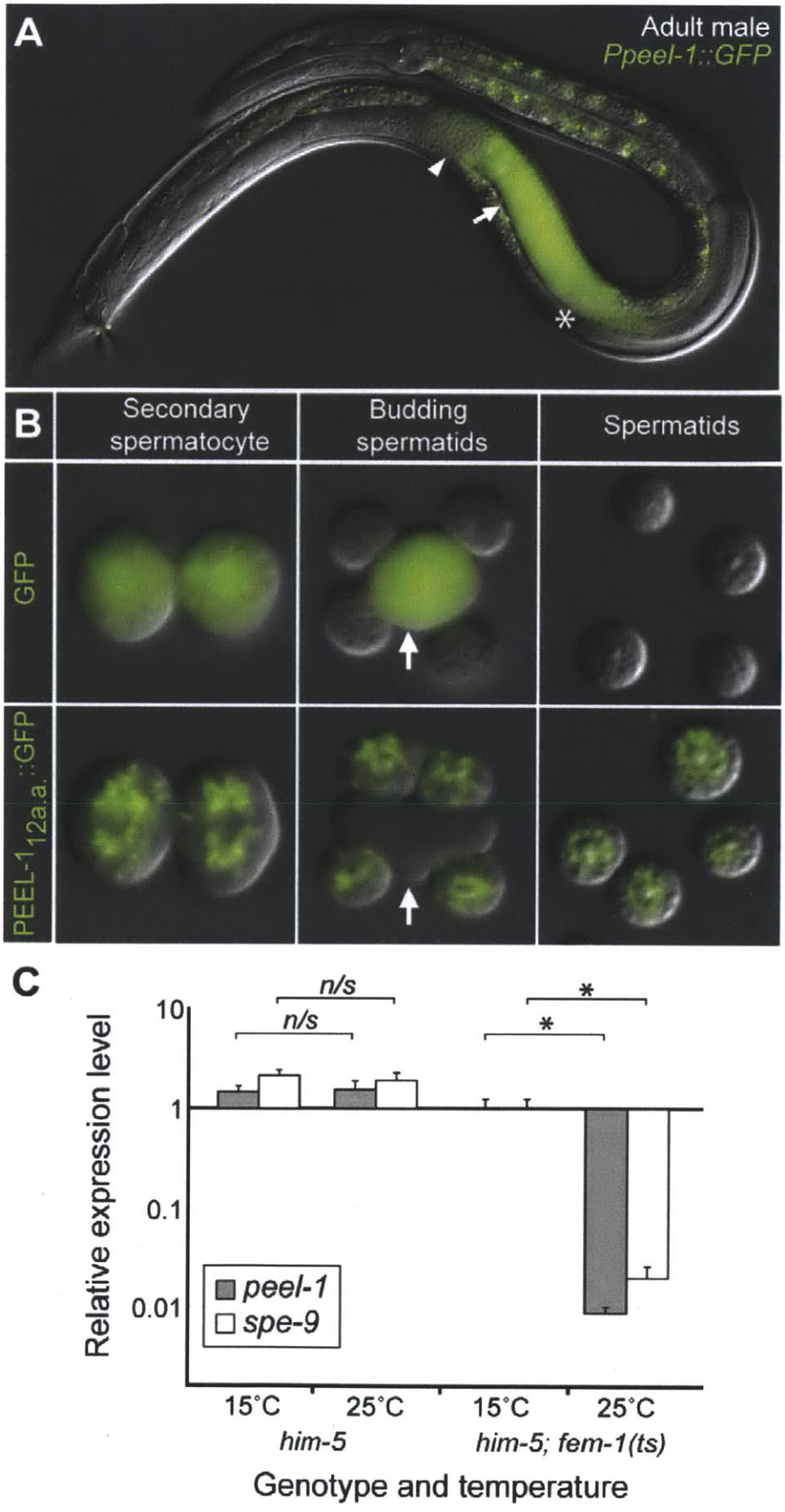

Figure 2-5: ***peel-1*** **is expressed exclusively in sperm and carries an *N*-terminal sperm localization signal.**

Figure 2-5:
(A) Adult male expressing *Ppeel-1::GFP*. The tube-like gonad begins at the asterisk, extends toward the head, folds over on itself, and then extends toward the tail. The arrow and arrowhead indicate spermatocytes and sperm, respectively. Fluorescence outside the gonad is auto-fluorescence. Nomarski and fluorescence channels are overlaid.
(B) Secondary spermatocytes, budding spermatids, and mature spermatids expressing either untagged GFP or GFP tagged with the N-terminal 12 amino acids of PEEL-1 ($PEEL-1_{12a.a.}::GFP$). Arrows indicate residual bodies. Nomarski and fluorescence channels are overlaid.
(C) Relative expression levels of *peel-1* and *spe-9* in *him-5(e1490)* and *him-5(e1490) fem-1(hc17ts)* adult males at the permissive (15C) and restrictive (25C) temperatures. *him-5(e1490)* was included to aid in collection of males. Expression levels were calculated relative to the *him-5(e1490) fem-1(hc17ts)* 15C sample. Runs were performed in triplicate and standard deviations are shown. *, $p < 10^{-5}$, one-tailed Students t-test on the normalized expression levels. *n/s*, $p > 0.05$.

epidermis, and the lumen of the excretory cell distends to form large vacuoles (Figure 2-7 D).

The defects observed in *peel-1*-affected embryos indicate severe malfunction of muscle and epidermal tissue. The phenotype of paralysis and two-fold arrest is characteristic of a complete absence of the function of body-wall muscle [90, 145]. The shape changes observed after the two-fold arrest indicate detachment of body-wall muscle fibers from the overlying epidermis [14]. Epidermal leakage and distention of the excretory cell, the only epidermal cell located in the interior of the animal, indicate further deterioration of both external and internal epidermis. These four defects paralysis and two-fold arrest, muscle-epidermal detachment, epidermal leakage, and excretory cell distention are not known to occur as side-effects of one another [145, 71], suggesting that sperm-supplied PEEL-1 may affect each tissue independently.

Paralysis and two-fold arrest have only two known causes: defective sarcomere assembly and lack of muscle contraction [90, 145]. To distinguish between the two, we examined (i) the localization of perlecan, a basement membrane protein required for sarcomere recruitment [145]; and (ii) the structure of actin and myosin myofilaments, which assemble downstream of all other sarcomere proteins [90]. In *peel-1*-affected embryos, perlecan localized normally (Figure 2-7 I-J). Likewise, actin and myosin

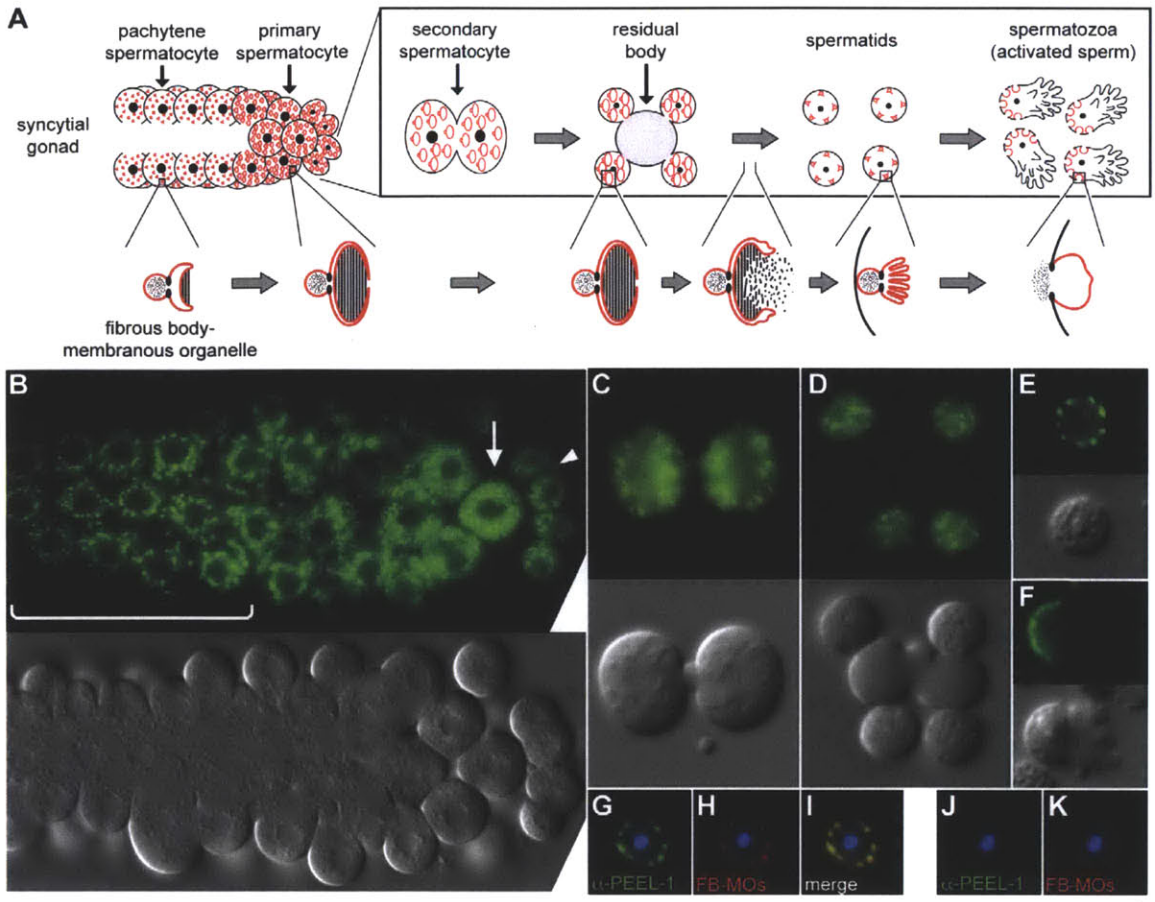

Figure 2-6: **PEEL-1 localizes to fibrous body-membranous organelles.** (A) Diagram of spermatogenesis and fibrous body-membranous organelle (FB-MO) development, adapted with permission from [77]. FB-MOs develop in pachytene spermatocytes as membrane-bound organelles having a head region separated by a collar-like constriction from a set of membrane folds (lower panel; red). As spermatogenesis proceeds, the membrane folds grow and extend into arm-like protrusions, enveloping bundles of polymerized Major Sperm Protein, referred to as fibrous bodies (hatched region). Coincident with budding of spermatids from the residual body, the membrane folds of FB-MOs retract, and the fibrous bodies depolymerize into the cytoplasm. The FB-free MOs then move to a position just inside the plasma membrane, and upon sperm activation, they fuse with the plasma membrane opposite the pseudopod.
(B-F) Nomarski and fluorescence images of spermatocytes and sperm expressing *PEEL-1::GFP*. Panels in (B) show the proximal arm of a male gonad, oriented with pachytene spermatocytes towards the left (bracketed region). Arrow and arrowhead indicate primary and secondary spermatocytes, respectively. Panels in (C-F) show higher resolution images of the following stages: secondary spermatocyte (C); budding spermatids (D); unactivated spermatid (E); and activated spermatozoan (F).
(G-K) Spermatids were dissected from *peel-1(+)* (G-I) or *peel-1(Δ)* (J-K) males and stained with anti-PEEL-1 (green) and the FB-MO marker, 1CB4 (red) [96]. Nuclei are stained with DAPI (blue).

filaments assembled correctly, except for slight abnormalities in regions of muscle detachment (Figure 2-7 K-N). We conclude that in *peel-1*-affected embryos, the phenotype of paralysis and two-fold arrest results from a defect in muscle contraction, not sarcomere assembly.

Next, to determine the cause of muscle-epidermal detachment, we examined trans-epidermal attachments, the specialized structures that span the epidermal syncytium and anchor it to underlying muscle [71]. A weakening of these structures is known to cause muscle-epidermal detachment [26], and consistent with this causality, in *peel-1*-affected embryos these structures were highly disorganized. As visualized by VAB-10A and intermediate filaments, trans-epidermal attachments did not organize into evenly spaced, circumferentially oriented bands. Instead, these bands were clumpy, disordered, and non-uniform in width (Figure 2-7 O-R). This disorganization occurred even in areas where muscles remained attached, suggesting it to be the cause of muscle detachment, rather than an effect of it. In addition, in areas highest stress, such as the mid-embryo bend, staining in post-arrest embryos (but not pre-arrest embryos) was often absent altogether (Figure 2-7 P). This absence implies that trans-epidermal attachments in *peel-1*-affected embryos are so weak that in areas of highest stress, they rupture entirely.

peel-1 toxicity is dose-dependent

Although the majority of *peel-1*-affected embryos display the aforementioned defects in muscle and epidermal tissue, the severity of these defects is variable and depends on the sex [115] and age of the sperm parent. Male-sired embryos always arrest paralyzed at the two-fold stage, always exhibit epidermal leakage, and never hatch ($n > 2{,}000$). Some hermaphrodite-sired embryos, on the other hand, elongate past the two-fold stage (Figure 2-7 E) or do not exhibit epidermal leakage. Occasionally, hermaphrodite-sired embryos even hatch, and the hatched progeny range from severely deformed larvae that die soon after hatching (Figure 2-7 F) to morphologically normal larvae that develop into viable, fertile adults. In addition, among hermaphrodite-sired embryos, the proportion of embryos arresting at the two-fold

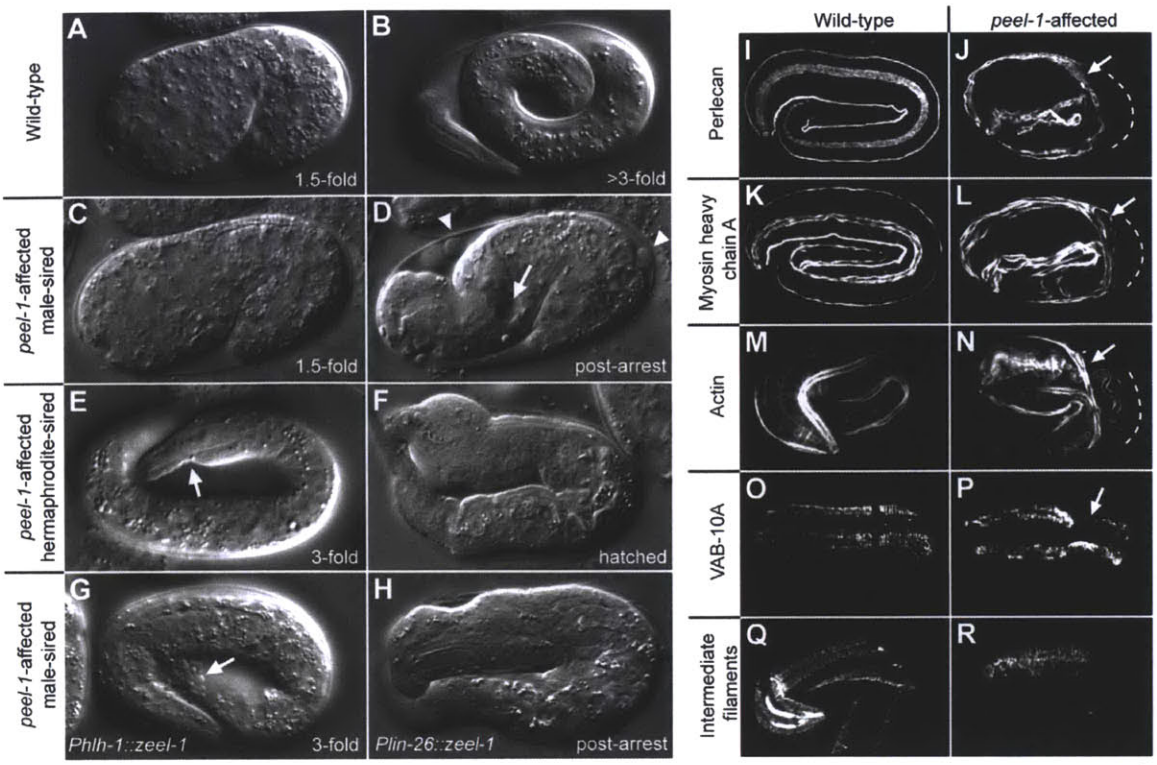

Figure 2-7: ***peel-1*-affected embryos exhibit late-occurring defects in muscle and epidermal tissue.** (A and B) Wild-type embryo at the 1.5-fold stage (A) and just before hatching (B). (C and D) *peel-1*-affected, male-sired embryo at the 1.5-fold stage (C) and approximately four hours after the two-fold arrest (D). Relative to its shape at the two-fold stage, the embryo in (D) has shortened longitudinally and thickened circumferentially. Thinning of the tail, distention of the excretory cell (arrow), and epidermal leakage (arrowheads) are visible. (E and F) *peel-1*-affected, hermaphrodite-sired embryos displaying less severe phenotypes than the embryo shown in (D). In (E), the embryo has elongated past the two-fold stage, but muscle detachment is visible (arrow). In (F), the embryo has hatched but is severely deformed. (G-H) *peel-1*-affected, male-sired embryos expressing *zeel-1* in only muscle (G) or only in epidermis (H). The embryo in (G) has elongated past the two-fold stage, but epidermal leakage is visible (arrow). The embryo in (H) has arrested paralyzed at the two-fold stage but has survived to hatching. (I-N) Perlecan, myosin heavy chain A, and F-actin were visualized in wild-type and *peel-1*-affected, male-sired embryos. In *peel-1*-affected embryos, muscle detachment is evident at the mid-embryo bend, where muscle fibers (arrows) are displaced inward relative to their proper locations (dashed lines). (O-R) VAB-10A and intermediate filaments were visualized in wild-type and *peel-1*-affected, male-sired embryos. In *peel-1*-affected embryos, VAB-10A and intermediate filaments are recruited properly to the four muscle quadrants, but they do not organize into evenly spaced, circumferentially oriented bands. In (P), VAB-10A staining is absent in one dorsal quadrant at the mid-embryo bend (arrow). Images in (O-P) are dorsal views.

stage and the proportion failing to hatch decreased dramatically with parental age (Figure 2-9 A-B, Figure 2-8). Among male-sired embryos, phenotypic severity was unaffected by parental age (Figure 2-9 C).

One explanation for the decreased phenotypic severity of hermaphrodite- versus male-sired embryos is PEEL-1 dosage. Male sperm are up to five-fold larger than hermaphrodite sperm [73], and as such, they may deliver more PEEL-1 protein to the embryo. In support of this hypothesis, we were able to alter the phenotype of *peel-1*-affected embryos, independent of sperm origin, by varying *peel-1* dosage. Among hermaphrodite-sired embryos, doubling *peel-1* copy number resulted in earlier onset of epidermal leakage (Figure 2-9 D). Among male-sired embryos, expression of *peel-1* exclusively from extra-chromosomal arrays, which are subject to germline silencing [66], had the opposite effect. For three of the *peel-1* arrays shown in Figure 1B, 3-10% of male-sired embryos elongated past the two-fold stage and hatched into deformed larvae ($n > 150$ embryos per array). When the same *peel-1* transgene was expressed from a single-copy genomic insertion, which is not silenced, no hatching was observed (Figure 1C).

Given the relationship between PEEL-1 dosage, sperm size, and phenotypic severity, we suspected that the age-related decrease in phenotypic severity among hermaphrodite-sired embryos might reflect underlying size differences and size-based competition among hermaphrodite sperm. Hermaphrodite sperm vary approximately two-fold in size [73] and are produced in a single bout of spermatogenesis at the onset of adulthood. Larger sperm in *C. elegans* experience a competitive advantage because they are able to crawl faster to reach the oocyte [73, 121]. One explanation for the age effect, therefore, is that larger-than-average sperm monopolize fertilization events early in life, leaving smaller, less toxic sperm to dominate fertilizations later on. In support of this hypothesis, we were able to reduce the age effect among hermaphrodite-sired embryos by delaying the hermaphrodites use of self-sperm via partial mating to a male (Figure 2-9 B). This result demonstrates that the age effect arises from a correlation between the competitive ability of each sperm and its toxicity to the embryo. Given the known biology of *C. elegans* sperm, the most parsimonious explanation for

this correlation is that larger hermaphrodite sperm both are more competitive and carry more PEEL-1 protein. This correlation might also arise from PEEL-1 having a direct effect on the competitive ability of each sperm, although we have no evidence for such an effect.

To our knowledge, the above results represent the first evidence of competition among hermaphrodite sperm in vivo, as well as the first evidence of naturally occurring differences in sperm size affecting embryonic development. Insofar as PEEL-1 levels scale with sperm size, the wide phenotypic variability among hermaphrodite-sired embryos implies that for low levels of PEEL-1, phenotypic severity is acutely sensitive to PEEL-1 dosage. By the same logic, however, the phenotypic homogeneity among male-sired embryos implies that above a certain threshold level of PEEL-1, phenotypic severity ceases to increase. In support of this threshold effect, doubling or tripling *peel-1* copy number among male-sired embryos did not produce a more severe phenotype, at least as measured by the onset of epidermal leakage (Figure 2-9 D).

zeel-1 is expressed transiently in the embryo, and tissue-specific expression of *zeel-1* produces tissue-specific rescue

Consistent with its function as an antidote to sperm-supplied PEEL-1, *zeel-1* is expressed in the embryo. Yet its expression is transient. By single-molecule FISH, *zeel-1* expression begins at the eight-cell stage, peaks at approximately the 150-cell stage, and then turns off (Figure 2-10 A). Transient expression was also observed for a GFP-tagged version of ZEEL-1, whose levels peaked during mid-embryogenesis (Figure 2-11), but whose expression was not observed in late-stage embryos, nor larvae or adults (data not shown).

Within embryos, ZEEL-1::GFP was expressed in all or almost all cell types (Figure 2-10 B-C, Figure 2-11). The protein localized most strongly to cell membranes (Figure 2-10 B-C), consistent with ZEEL-1 having an N-terminal transmembrane domain. In some tissues, such as the developing pharynx and intestine, ZEEL-1::GFP appeared more concentrated at the apical face (Figure 2-10 C).

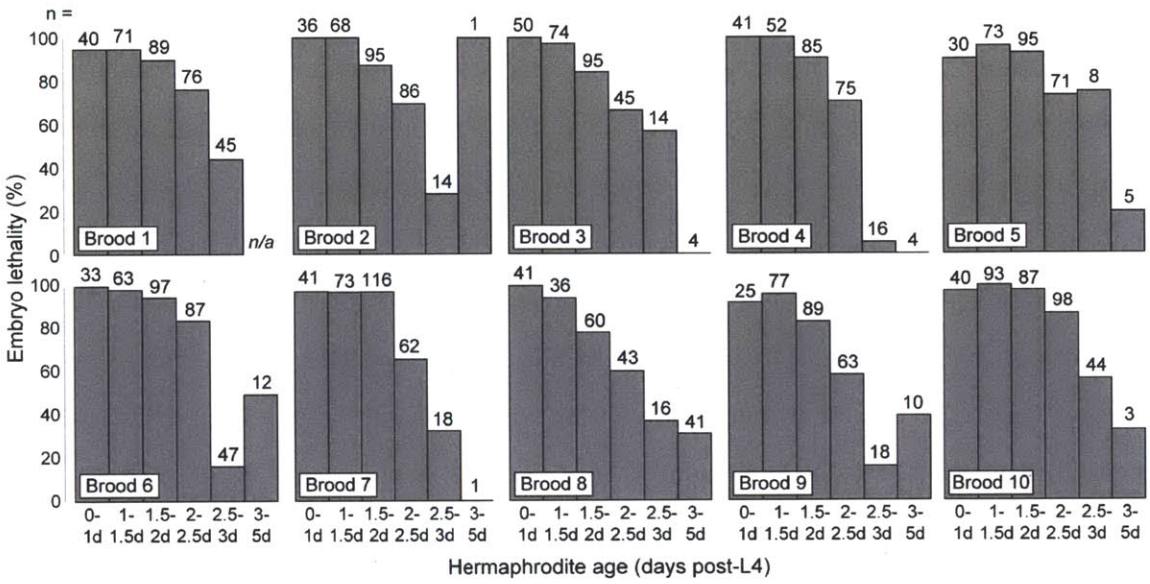

Figure 2-8: **Age-related decrease in the lethality of *peel-1*-affected, hermaphrodite-sired embryos in ten randomly selected broods.** The results for ten of the 91 broods used in the unmated experiment in Figure 2-9B are shown. Broods were selected using a random number generator. As described in Figure 2-9B, each hermaphrodite was followed from the onset of adulthood, and all embryos laid during the first five days of adulthood were collected. *n/a*, no embryos laid during this time period.

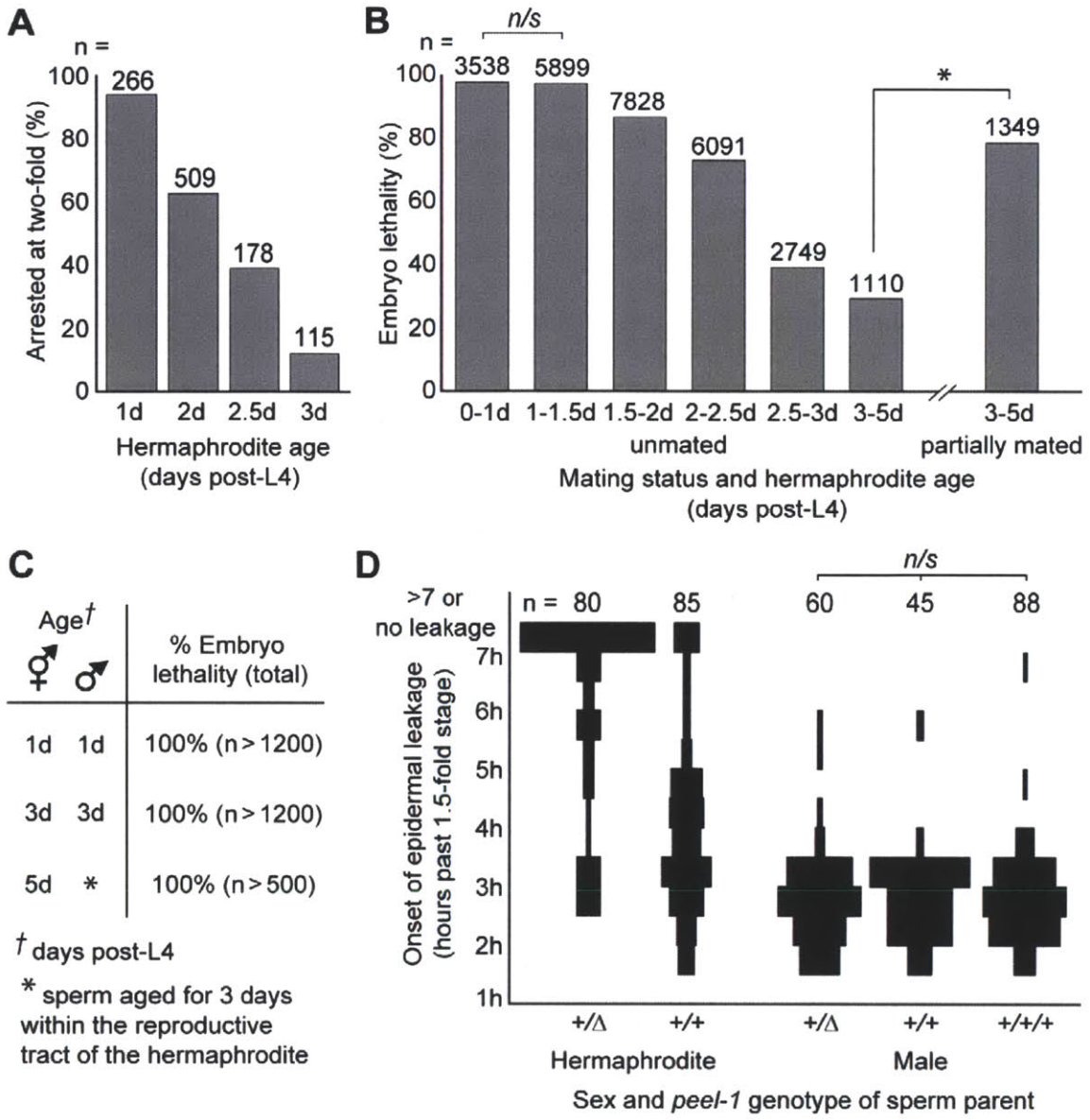

Figure 2-9: **The phenotypic effects of sperm-supplied PEEL-1 are dose-dependent.**

(A) The proportion of embryos arresting at the two-fold stage was calculated among *peel-1*-affected embryos sired by one- to three-day-old hermaphrodites. Within each age class, embryos derive from a total of approximately 50 to 150 hermaphrodites. All pair-wise combinations of age classes were compared using χ^2 tests. For all pairs, $p < 10^{-5}$.

(B) Embryo lethality was scored among *peel-1*-affected embryos sired by unmated, one- to five-day-old hermaphrodites and by partially mated, three- to five-day-old hermaphrodites. In the unmated experiment, 91 hermaphrodites were followed from the onset of adulthood, and all embryos laid during the first five days of adulthood were scored. The results for ten randomly selected broods are shown in Figure 2-8. To generate embryos sired by partially mated animals, 130 hermaphrodites were briefly

Figure 2-9:
mated to males following the L4 molt, and embryos were collected during days three to five from the 35 hermaphrodites that produced a mixture of self- and cross-progeny. Self- and cross-progeny were distinguished by the use of an integrated GFP marker carried by the male, and cross-progeny were excluded from analysis. χ^2 tests were used to compare the unmated and partially mated *3-5d* age classes, as well as all pair-wise combinations of age classes within the unmated experiment. *n/s*, $p > 0.05$. * and all unlabeled pairs within the unmated experiment, $p < 10^{-5}$.
(C) Embryo lethality was scored among *peel-1*-affected embryos derived from crosses between i) one-day-old males and hermaphrodites; ii) three-day-old males and hermaphrodites; and iii) five-day-old hermaphrodites that had been removed from males on day two in order to allow male sperm to age for three days within the reproductive tract of the hermaphrodite. In each cross, embryos derive from a total of 12 to 16 hermaphrodites.
(D) Spindle plots showing the onset of epidermal leakage in *peel-1*-affected embryos sired by hermaphrodites carrying one or two copies of *peel-1(+)*, or by males carrying one, two, or three copies of *peel-1(+)*. A third copy of *peel-1* was added using the single-copy insertion of the *peel-1* transgene marked in Figure 1B. The width of each bar reflects the proportion of embryos initiating leakage in each time interval. All pair-wise combinations of spindle plots were compared using Mann-Whitney U tests on the raw distributions of leakage times. *n/s*, $p > 0.05$. For all other pairs, $p < 10^{-5}$.

Ubiquitous *zeel-1* expression is consistent with *zeel-1*s ability to rescue the seemingly independent muscle and epidermal defects observed in peel-1-affected embryos. To test the tissue-autonomy of *zeel-1* rescue, we expressed *zeel-1* only in muscle and only in epidermis. We used the promoters of *hlh-1* and *lin-26*, respectively, [69, 74], which initiate expression at the 80- to 100-cell stage [72]. Consistent with sperm-supplied PEEL-1 affecting muscle and epidermis independently, tissue-specific expression of *zeel-1* produced tissue-specific rescue. In male-sired embryos, expression of *zeel-1* only in muscle rescued the muscle defect of paralysis and two-fold arrest, but it did not rescue epidermal leakage (n = 120 embryos; Figure 2-7G). (Muscle detachment and excretory cell distention could not be assayed because muscle movement, combined with epidermal leakage, ripped embryos apart entirely.) Conversely, expression of *zeel-1* only in the epidermis rescued the epidermal defects, but it did not rescue paralysis and two-fold arrest (n = 69 embryos; Figure 2-7H). In hermaphrodite-sired embryos, both constructs fully rescued a subset of embryos, and rescue activity increased with hermaphrodite age (Figure 2-12). This result is consistent with the

age effect among hermaphrodite-sired embryos and the fact that hermaphrodite-sired embryos do not always exhibit defects in both muscle and epidermal tissue.

The transmembrane domain of *zeel-1* is evolutionarily novel and partially sufficient for antidote activity

The structure of *zeel-1* — a *C*-terminal region (~700 amino acids) homologous to the highly conserved gene, *zyg-11*, and an N-terminus (~200 amino acids) predicted to form a six-pass transmembrane domain is highly unusual, and phylogenetic analysis indicates that this structure arose during a recent expansion of the *zyg-11* family. Most metazoan genomes contain one to two *zyg-11* orthologs, but in *C. elegans*, *C. briggsae* and *C. remanei*, the *zyg-11* family has expanded such that these species carry 19 to 37 *zyg-11*-like genes each (Figure 2-14). Most of these additional family members probably arose after the split with out-group *C. japonica*, because the genome of *C. japonica* contains only three *zyg-11*-like genes (including *Cja-zyg-11* itself).

Aside from *zeel-1*, only two other members of the *zyg-11* family paralogs *Y71A12B.17* and *Y55F3C.9* contain predicted transmembrane domains (Figure 2-13 A, 2-12). The transmembrane domains of these three genes are homologous to one another, but these domains show no detectable sequence similarity to any other gene in *C. elegans* or in the GenBank sequence database. This pattern, combined with the closest-paralog relationship between the soluble domains of *zeel-1*, *Y71A12B.17*, and *Y55F3C.9* (Figure 2-13 A, 2-12) implies that their shared transmembrane domain is evolutionarily novel and originated after the split between *C. elegans* and the *C. briggsae*/*C. remanei* lineage.

Analysis of gene order and sequence data suggests that *zeel-1* arose through duplication of the *Y71A12B.17* locus. *zeel-1* and *Y71A12B.17* are one anothers closest paralogs (Figure 2-13 A, 2-12), and the two genes are 55% identical at the amino acid level. *Y71A12B.17* is located 12 Mb from *zeel-1* in a tandem array of three additional *zyg-11* family members, none of which contain the N-terminal transmembrane domain. Assuming that these four genes originated in their current genomic location via repeated tandem duplication, then two scenarios for the origin of *zeel-1*

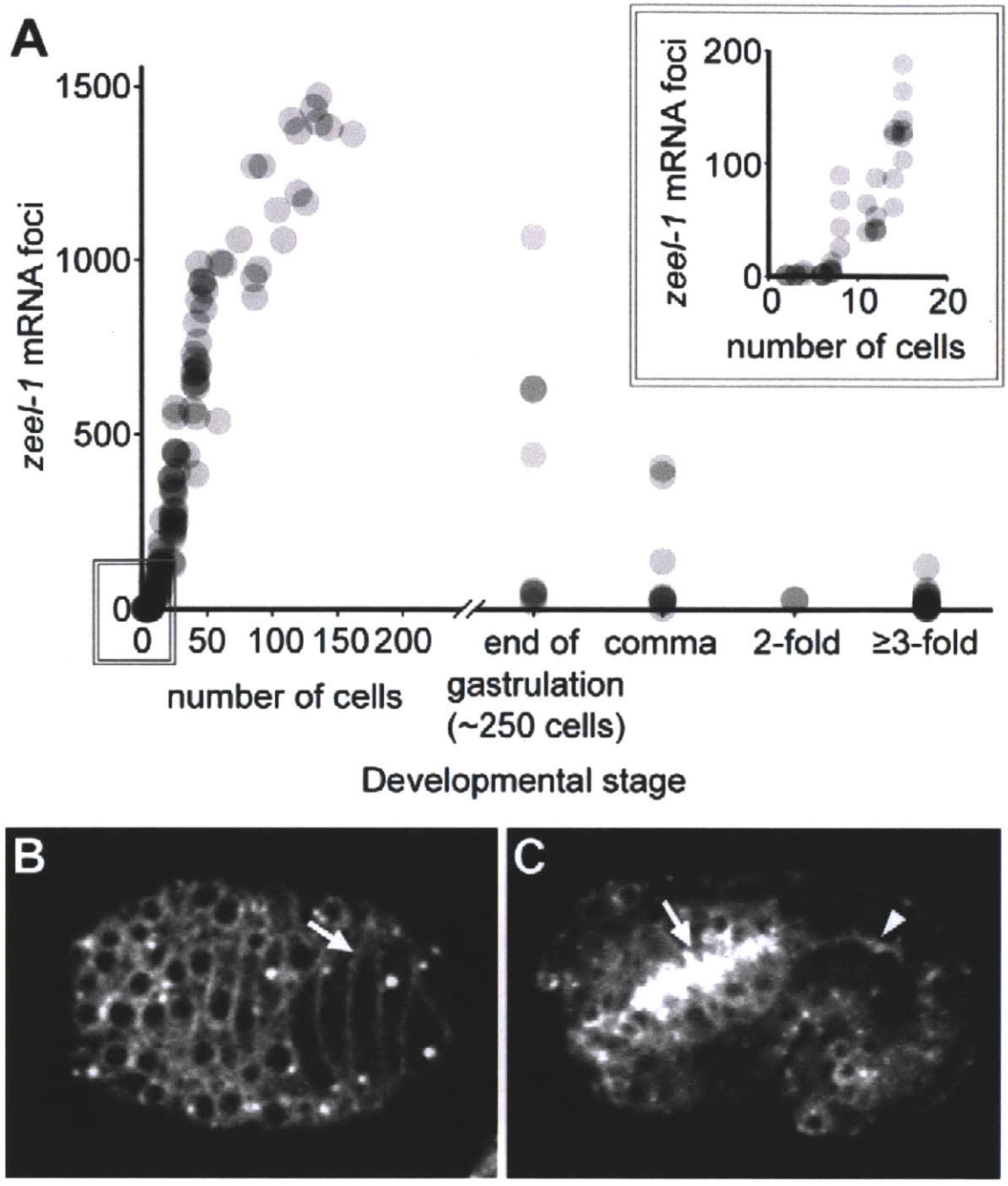

Figure 2-10: ***zeel-1* is transiently expressed during embryogenesis and localizes to cell membranes.** (A) *zeel-1* mRNAs were quantified in wild-type embryos via single-molecule fluorescence in situ hybridization [105]. Embryos were staged by counting nuclei manually (1- to 40-cell embryos); counting nuclei using image analysis software (41- to 200-cell embryos); or classifying embryos as end of gastrulation (~250-cells), comma, 2-fold, or $\geq$ 3-fold. Inset shows a magnification of the boxed area. Each circle represents an independent embryo. n = 130. (B-C) Embryos expressing *ZEEL-1::GFP*. Panel in (B) shows a dorsal view during intercalation of epidermal cells. Arrow indicates an epidermal cell membrane. Panel in (C) shows a lateral cross section of a 1.5-fold embryo. The apical face of the pharynx (arrow) and the intestine (arrowhead) are indicated.

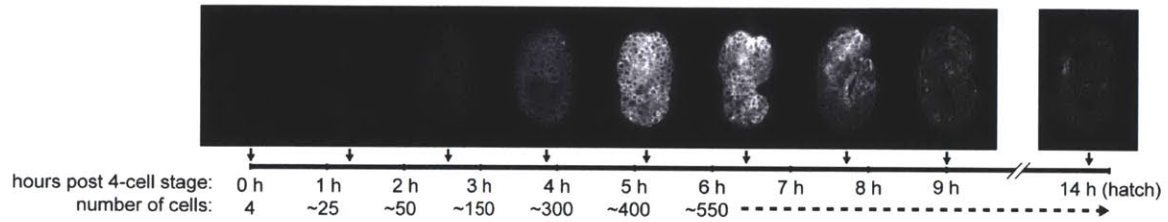

Figure 2-11: **ZEEL-1::GFP is expressed transiently during embryogenesis.** Time series images of a single embryo expressing ZEEL-1::GFP under the *zeel-1* promoter. Timeline indicates embryo age in hours post-4-cell stage.

and *Y71A12B.17* are possible. First, *Y71A12B.17* may have originated via duplication of another gene in the tandem array, gained its transmembrane domain during or after duplication, and later been duplicated again to produce *zeel-1*. Alternatively, the tandem array may have arisen through partial duplication *Y71A12B.17*. The second scenario is less parsimonious than the first, because it requires secondary loss of the transmembrane domain during creation of the tandem array. However, the second scenario still implies that the *Y71A12B.17* locus predates *zeel-1*, because if the opposite were true, then *zeel-1* would form an out-group to the tandem array, and it does not (Figure 2-13 A).

Given the chimeric structure of ZEEL-1, we tested whether either domain alone could rescue the lethality of *peel-1*-affected embryos. The soluble ZYG-11-like domain, $ZEEL{-}1_{SOL}$, provided no rescue (Figure 2-13B). The transmembrane domain, $ZEEL - 1_{TM}$, provided full rescue to hermaphrodite-sired embryos, but only partial rescue to male-sired embryos (Figure 2-13B-C). In contrast, the positive control transgene, full-length ZEEL-1 tagged with GFP, provided full rescue to both male- and hermaphrodite-sired embryos (Figure 2-13B-C). We conclude that the transmembrane domain of ZEEL-1 is required for antidote activity, and that this domain alone is able to neutralize the low doses of PEEL-1 delivered by hermaphrodite sperm but not the higher doses delivered by male sperm.

The partial rescue activity of $ZEEL - 1_{TM}$ demonstrates that $ZEEL - 1_{SOL}$ does contribute to the antidote activity of full-length ZEEL-1. To examine this contribution more carefully, we tested whether $ZEEL - 1_{SOL}$ could rescue the lethality

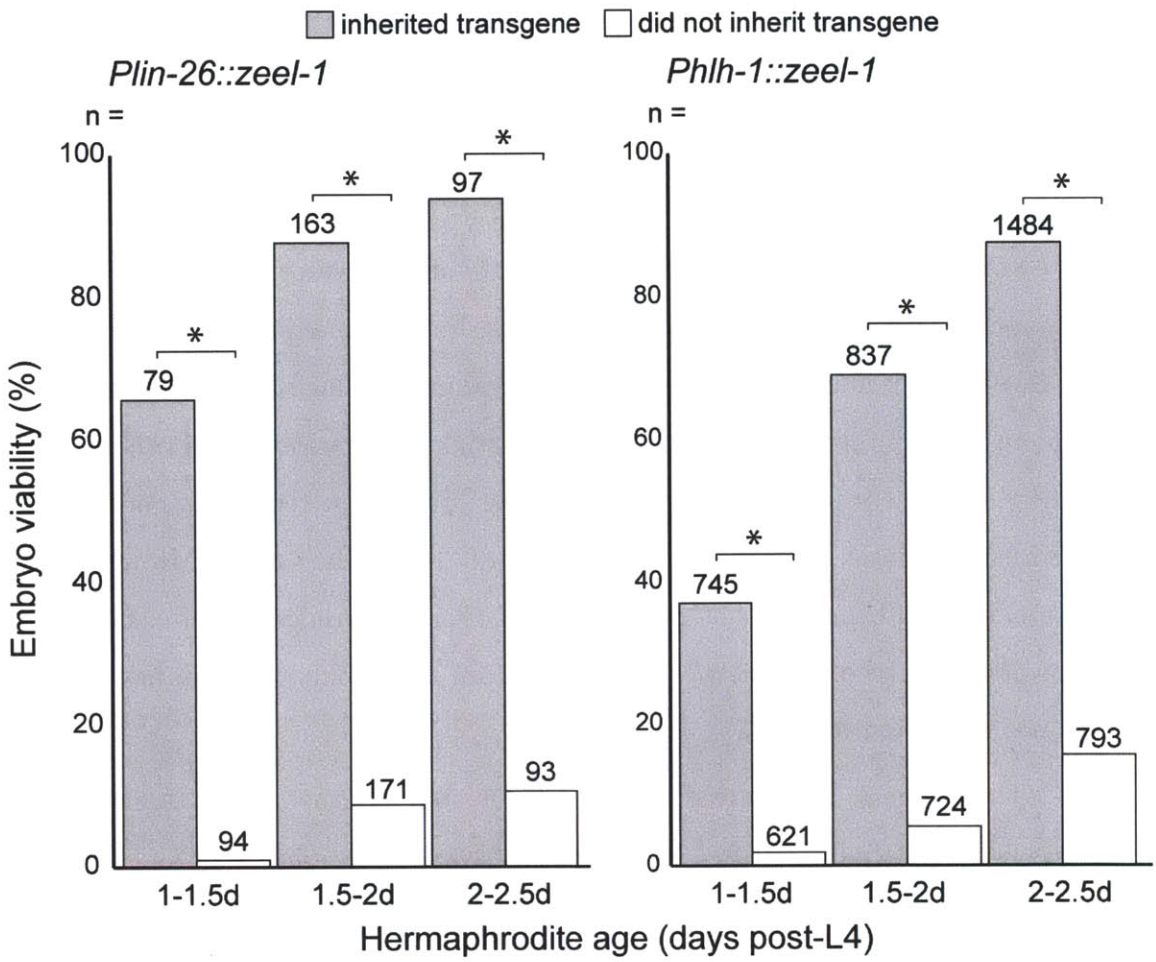

Figure 2-12: **Tissue-specific expression of *zeel-1* is partially sufficient for rescue of *peel-1*-affected, hermaphrodite-sired embryos.** Embryo viability was calculated among *peel-1*-affected, hermaphrodite-sired embryos inheriting either *Plin-26::zeel-1* or *Phlh-1::zeel-1*. Embryos are grouped according to the age of the parent hermaphrodite. White bars indicate sibling controls that did not inherit the transgene. *, $p < 10^{-5}$, χ^2 tests.

of *peel-1*-affected embryos when fused to the transmembrane domain of *zeel-1*s closest relative, *Y71A12B.17*. Like $ZEEL-1_{SOL}$, the chimeric transgene, *Y71A12B.17* TM::$ZEEL-1_{SOL}$, provided no rescue (Figure 2-13B). Assuming that this transgene was stably expressed, this result demonstrates that $ZEEL-1_{SOL}$ cannot confer antidote activity to a related transmembrane domain. Additionally, this result demonstrates that the transmembrane domains of *zeel-1* and *Y71A12B.17* have diverged functionally since their common ancestor. The molecular basis of this divergence remains unclear, however, because the transmembrane domains of *zeel-1* and *Y71A12B.17* are only 35% identical at the amino acid level, with substitutions distributed throughout their length (Figure 2-14).

Heat-shock expression of *peel-1* kills adult animals, and heat-shock expression of *zeel-1* rescues this lethality

To determine whether PEEL-1 can function as a toxin outside of embryos, we expressed *peel-1* ectopically in larvae and adults. *peel-1* was expressed using each of two heat-shock promoters, *Phsp-16.2* and *Phsp-16.41* [64]. For each promoter construct, we generated both single-copy genomic insertions and extra-chromosomal arrays, which typically contain tens to hundreds of copies of a transgene [85]. Both types of animals grew normally under standard laboratory conditions, but a one-hour heat shock at 34C was lethal to all: array-carrying adults died within two hours after the start of heat-shock, and insertion-carrying animals within 4.5 hours (Figure 2-15 A). Faster killing of array-carrying animals is consistent with their higher *peel-1* dosage, and similar results were observed for heat-shocked larvae (data not shown). In addition, aside from the gross phenotype of death, the heat-shocked animals showed defects in most, if not all, tissues. Beginning approximately 30 to 45 minutes before death, the body-wall and male-tail muscles hyper-contracted; vacuoles formed in many tissues (Figure 2-16 K); the lumen of the excretory cell distended (Figure 2-16 L); the gonad appeared to disintegrate (Figure 2-16 M); and in hermaphrodites, the gonad and intestine occasionally exploded through the vulva. We conclude that PEEL-1 is a nearly universal toxin, affecting many developmental stages and cell

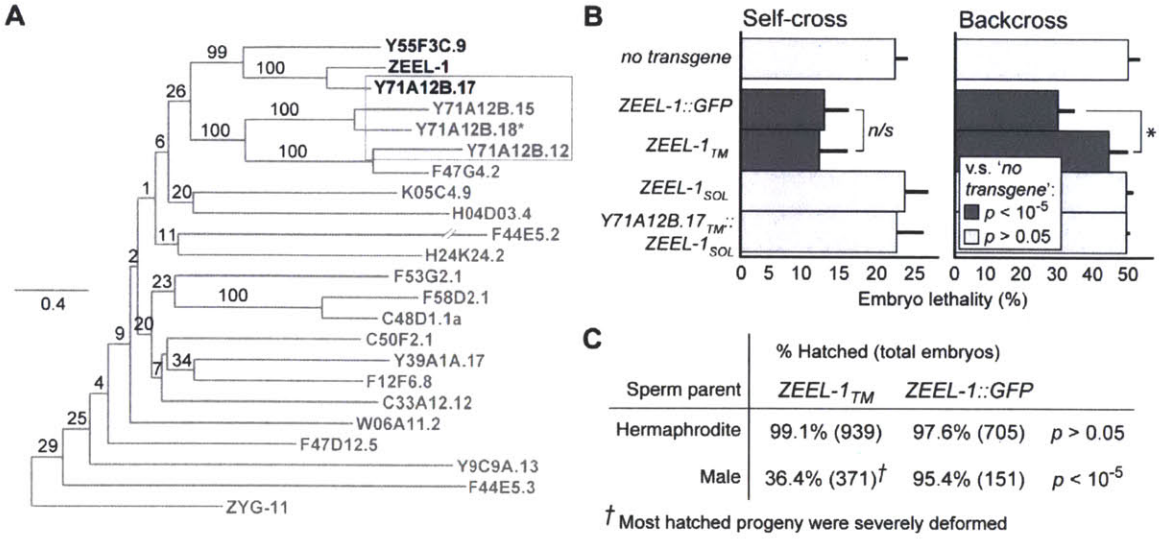

Figure 2-13: **The transmembrane domain of *zeel-1* is evolutionarily novel and partially sufficient for function.**
(A) Maximum likelihood phylogeny of the protein sequences of all *zyg-11* homologs in *C. elegans*. Genes containing predicted transmembrane domains are highlighted in black. The transmembrane domains of these genes were excluded prior to analysis. Genes located in the tandem array are highlighted by a shaded grey rectangle. Scale bar indicates amino acid substitutions per site. Values on branches indicate percent bootstrap support. The asterisk indicates that the reference sequence of *Y71A12B.18* contains a single frame-shift, corrected prior to analysis.
(B) Four *zeel-1*-derived transgenes were introduced into a strain carrying the *zeel-1* deficiency, *niDf9*, and tested for their ability to rescue *peel-1*-affected embryos. To test for rescue, transgenic animals were crossed to the Bristol strain, and lethality was scored among embryos derived from self-fertilizing F1 hermaphrodites (self-cross) and F1 males backcrossed to hermaphrodites of the original transgenic line (backcross). For each type of transgene, four to thirteen independent extra-chromosomal arrays were tested. For each array, 100 to 600 embryos were scored per self-cross or backcross. Ten control replicates were performed in parallel, each including 100 to 400 embryos (no transgene bars). Among arrays or control replicates, lethality scores were averaged to obtain global means and standard deviations. Each transgene was tested for a reduction in lethality compared to the control replicates (Students t-tests, p-values indicated by shading). Additionally, the two rescuing transgenes (*ZEEL-1*$_{TM}$ and *ZEEL-1::GFP*) were tested for significant differences relative to one another (Students t-tests; *, $p < 0.005$; *n/s*, $p > 0.05$). For the rescuing transgenes, lethality was not reduced to zero because extra-chromosomal arrays are not transmitted to all progeny.
(C) Hatch rates were compared between *peel-1*-affected embryos that we confirmed to have inherited either *ZEEL-1*$_{TM}$ or *ZEEL-1::GFP* (χ^2 tests, p-values shown). Separate comparisons were performed for male- and hermaphrodite-sired embryos. Unless otherwise specified, all hatched progeny appeared morphologically normal. Inheritance of the transgenes was determined by expression of the co-injection marker, *Pmyo-2::RFP*. Sibling embryos not inheriting the transgene were used as internal negative controls. The hatch rates of these controls were 2% (n = 601 - 653) among hermaphrodite-sired embryos and 0% (n = 341 - 933) among male-sired embryos.

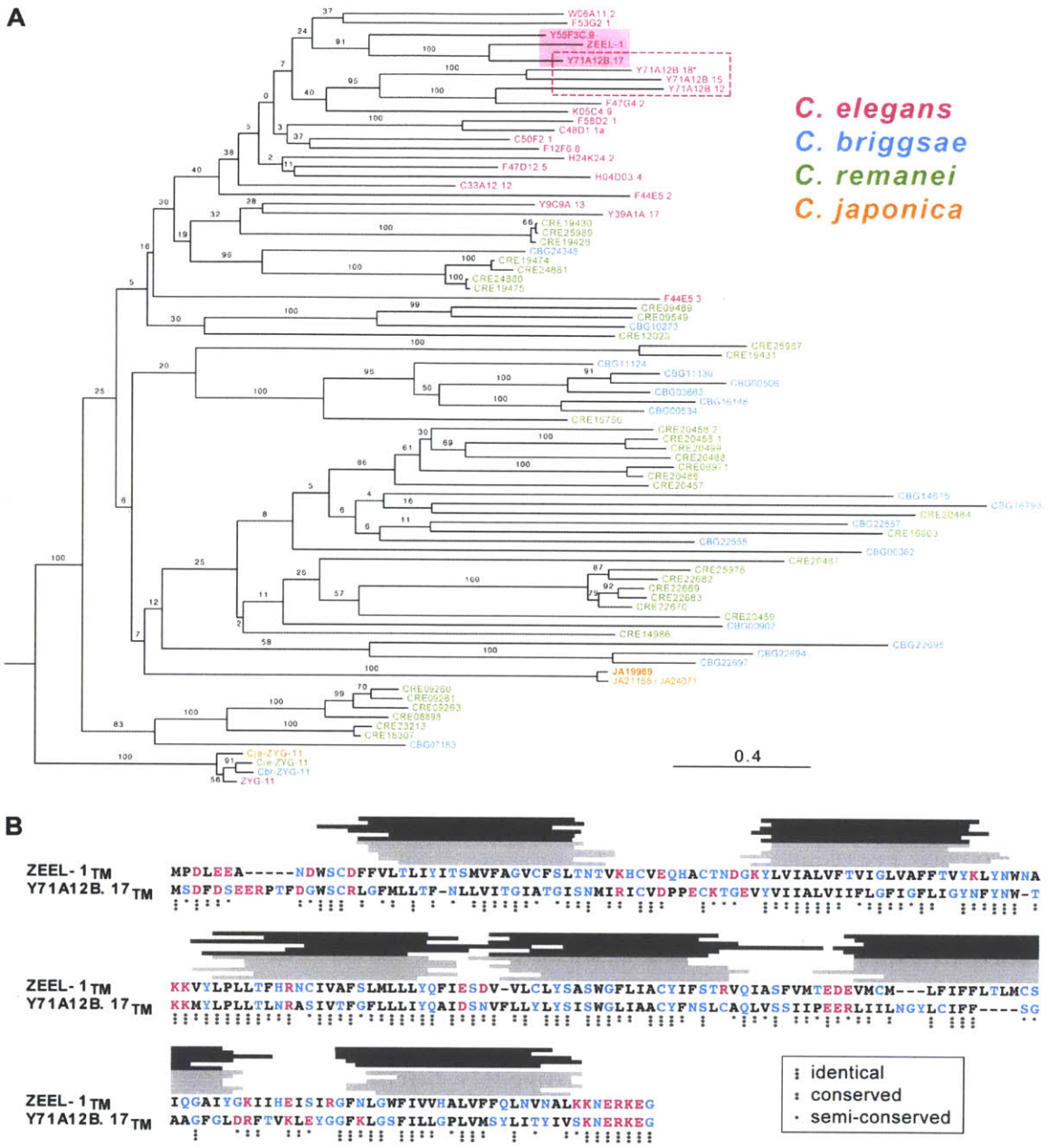

Figure 2-14: **The *zyg-11* family has expanded in *C. elegans*, *C. briggsae*, and *C. remanei*.**
(A) PhyML [49] was used to construct a maximum likelihood phylogeny of the protein sequences of all *zyg-11* homologs in *C. elegans*, *C. briggsae*, *C. remanei*, and *C. japonica*. As in Figure 2-13 A, full-length protein sequences of all genes were used, except for the three proteins containing predicted transmembrane domains, ZEEL-1, Y71A12B.17, and Y55F3C.9. For these three proteins, highlighted with a shaded pink rectangle, the predicted transmembrane domains were excluded. Y71A12B.17 and the other proteins encoded by genes located in the tandem array are outlined with a pink dashed box. The frameshift in *Y71A12B.18* was corrected prior to analysis. Scale bar indicates amino acid substitutions per site. This value is highly deflated from its true value because the sequence alignment was heavily trimmed prior to constructing the phylogeny. Values on branches indicate percent bootstrap support.

Figure 2-14: (B) Alignment of the amino acid sequences of the transmembrane domains of ZEEL-1 and Y71A12B.17. Sequences were aligned using MUSCLE [35], using default settings. Colors indicate amino acid classification: hydrophobic, including aromatic (black); acidic or basic (pink); and other (blue). Symbols below alignment indicate conservation. Above the alignment, horizontal bars indicate predicted transmembrane helices for ZEEL-1 (dark grey) and Y71A12B.17 (light grey). Predictions were generated using (from top to bottom): TopPred [54], Tmpred [123], TMHMM [53], SOSUI [112], PHDhtm [137], and HMMTOP [13].

types.

Next, we tested whether heat-shock expression of *zeel-1* could rescue the lethality caused by heat-shock expression of *peel-1*. We generated five extra-chromosomal arrays and one single-copy insertion of *Phsp-16.41*::*zeel-1*, and we tested these against one array and one insertion of *Phsp-16.41*::*peel-1*. Heat-shock expression of *zeel-1* was able to rescue the lethality caused by *Phsp-16.41*::*peel-1*, but only when *Phsp-16.41*::*peel-1* was expressed from insertions, not arrays (Figure 2-15 B). The ability of *Phsp-16.41*::*zeel-1* to rescue *Phsp-16.41*::*peel-1* even when both were expressed from single-copy insertions (Figure 2-15 B) indicates that insofar as these two transgenes produce equivalent levels of protein, *zeel-1*-mediated rescue does not require levels of ZEEL-1 to be higher than levels of PEEL-1.

Sperm-supplied PEEL-1 may act directly during the two-fold stage

The fact that *peel-1*-affected embryos do not exhibit defects until late in development at two-fold stage is surprising because sperm-supplied factors are thought to act only during egg-activation and first cleavage [77]. One explanation for this paradox is that the late-occurring defects might be a downstream manifestation of a cryptic defect earlier in development. Alternatively, sperm-supplied PEEL-1 might persist long after fertilization but only become toxic at the two-fold stage. While we have been unable to visualize PEEL-1 after fertilization, using either PEEL-1::GFP or the anti-PEEL-1 antibody (presumably because PEEL-1 becomes too diffuse), three observations are consistent with PEEL-1 acting directly during the two-fold stage.

First, pre-two-fold embryos were able to develop normally even when exposed

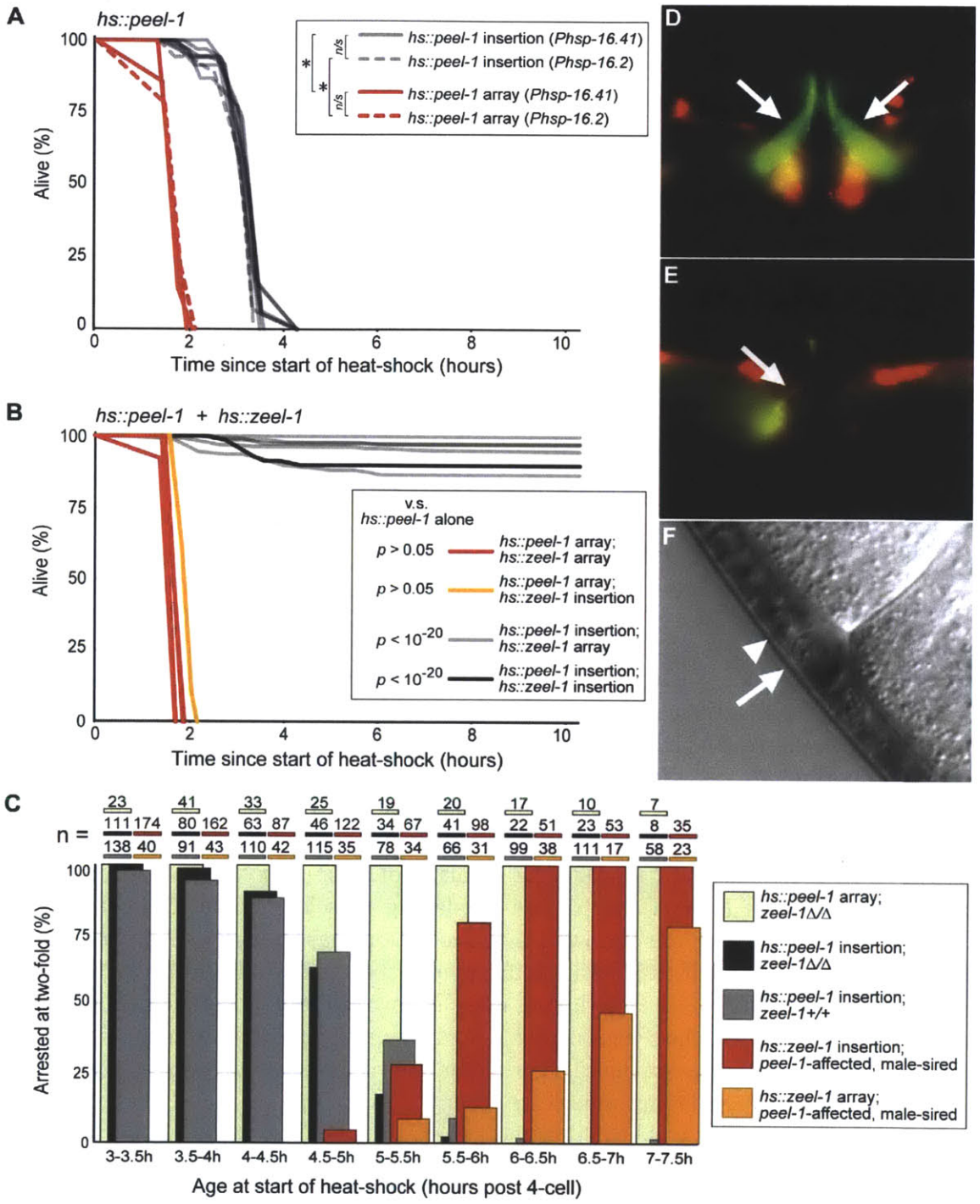

Figure 2-15: **Ectopic expression of *peel-1* and *zeel-1* replicates *peel-1*-mediated toxicity and *zeel-1*-mediated rescue.**
(A) Survival curves for heat-shocked adult animals carrying extra-chromosomal arrays or single-copy genomic insertions of *Phsp-16.2::peel-1* or *Phsp-16.41::peel-1*. Time zero indicates the start of a one-hour heat-shock at 34C. Curves represent one array and one insertion of *Phsp-16.2::peel-1* and two independent arrays and seven independent insertions of *Phsp-16.41::peel-1*. Log-rank tests were used to compare i) insertions *v.s.* arrays, and ii) *Phsp-16.2::peel-1 v.s. Phsp-16.41::peel-1*. Data for independent arrays or insertions of *Phsp-16.41::peel-1* were combined prior to analysis. *, $p < 10^{-16}$. *n/s*, $p > 0.05$. n = 40-70 animals per curve.

Figure 2-15:
(B) One array and one insertion of *Phsp-16.41::peel-1* were chosen from (A) to be tested against five independent arrays and one single-copy insertion of *Phsp-16.41::zeel-1.* Animals carrying both types of transgenes were heat-shocked as in (A). Assays were truncated at 10 hours post-heat-shock. Log-rank tests were used to compare each assay to the corresponding assay of *Phsp-16.41::peel-1* alone from (A) (p-values shown). n = 45-180 animals per curve.
(C) The following classes of embryos, aged three to 7.5 hours post-4-cell stage, were heat-shocked for 20 minutes at 34C: (i) *zeel-1(Δ)* embryos carrying a *Phsp-16.41::peel-1* array (pale green bars); (ii) *zeel-1(Δ)* and *zeel-1(+)* embryos carrying a *Phsp-16.41::peel-1* insertion (black and grey bars, respectively); and (iii) *peel-1*-affected, male-sired embryos carrying either an array or an insertion of *Phsp-16.41::zeel-1* (yellow and red bars, respectively). For each genotypic class, the proportion of embryos arresting at the two-fold stage relative to all embryos that elongated to the two-fold stage is plotted. Differences between the black and grey bars are not significant (p ¿ 0.05, χ^2 tests for each age class). See Figure 2-16 for the full dataset.
(D-E) Vulva regions of animals carrying an array of *Pexp-3::peel-1* and an integrated copy of *Pmyo-3::GFP*, a marker of the egg-laying muscles. Somatic inheritance of the *Pexp-3::peel-1* array was followed by co-injection markers, *Prab-3::mCherry* and *Pmyo-3::mCherry*, which express in neurons and the egg-laying and body-wall muscles, respectively. In (D), the egg-laying muscles (arrows) are morphologically normal and have not inherited the *Pexp-3::peel-1* array, as indicated by absence of *mCherry* expression. In (E), the left-hand egg-laying muscle is severely atrophied (arrow) and the right-hand egg-laying muscle is absent. The atrophied muscle cell expresses *mCherry*, indicating this cell has inherited the array of *Pexp-3::peel-1.* In both images, *mCherry* expression is also visible in body-wall muscles and neighboring neurons.
(F) Dead GABA neuron (arrow) in an animal carrying an array of *Punc-47::peel-1.* The surrounding tissue, including a neighboring, non-GABA neuron (arrowhead) is morphologically normal.

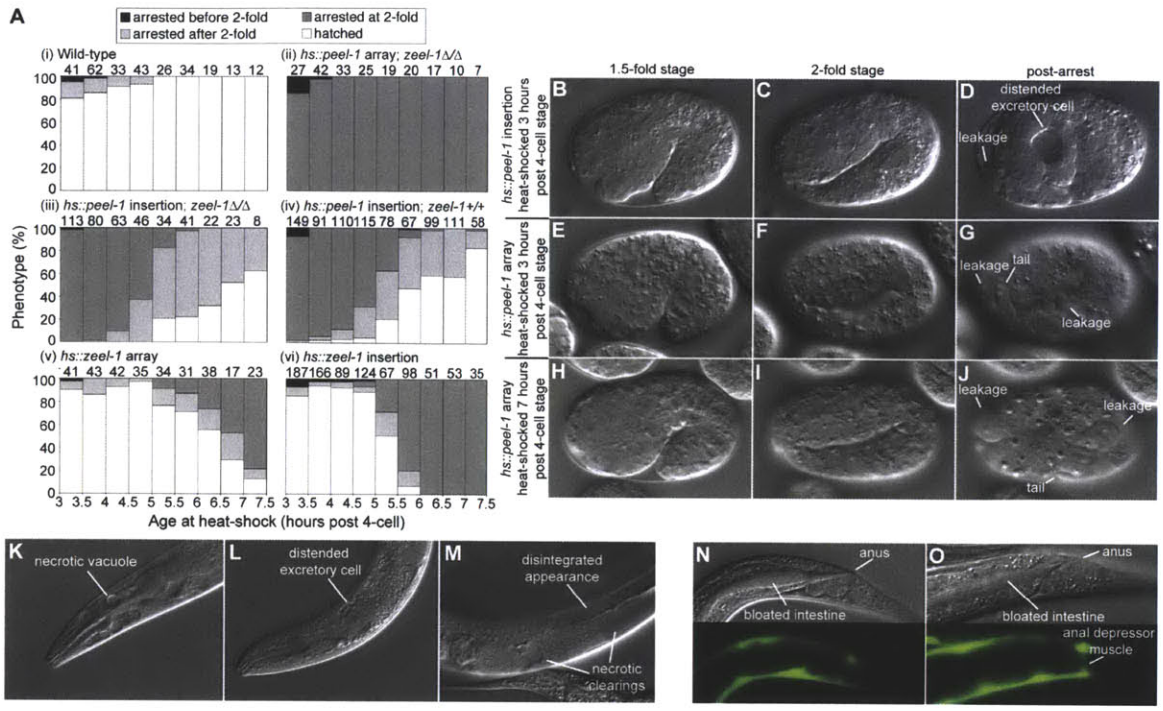

Figure 2-16: **Ectopic expression of *peel-1* and *zeel-1*.**
(A) The full dataset used to generate the plot in Figure 2-15 C is shown. As described in Figure 2-15 C, the following classes of embryos, aged three to 7.5 hours post-4-cell stage, were heat-shocked for 20 minutes at 34C: (i) wild-type (ii) *zeel-1(Δ)/zeel-1(Δ)* embryos carrying a *Phsp-16.41::peel-1* array (iii) *zeel-1(Δ)/zeel-1(Δ)* embryos carrying a *Phsp-16.41::peel-1* insertion (iv) *zeel-1(+)/zeel-1(+)* embryos carrying a *Phsp-16.41::peel-1* insertion (v) *peel-1*-affected, male-sired embryos carrying a *Phsp-16.41::zeel-1* array (vi) *peel-1*-affected, male-sired embryos carrying a *Phsp-16.41::zeel-1* insertion Each embryo was classified as hatching (white) or arresting before the two-fold stage (black), at the two-fold stage (dark grey), or after the two-fold stage (light grey). Numbers above bars indicate the total number of embryos in each age class.
(B-J) Time series images of heat-shocked, *zeel-1(Δ)/zeel-1(Δ)* embryos carrying either an insertion (B-D) or an array (E-J) of *Phsp-16.41::peel-1*. When visible, epidermal leakage and excretory cell distention are labeled. In (G, J), tails are indicated to help orient the viewer.
(K-M) Images of heat-shocked, adult hermaphrodites carrying an insertion of *Phsp-16.41::peel-1*. Animals were imaged shortly after paralysis had begun. Necrosis is visible in the head (K) and gonad (M), and the excretory cell is distended (L).
(N-O) Images of animals carrying an array of *Pexp-3::peel-1* and an integrated copy of *Pmyo-3::GFP*, which serves as a marker of the anal depressor muscle. Intestinal bloating is visible in both animals, but only in (N) is the anal depressor muscle absent.

to more PEEL-1 protein than is delivered by sperm. We heat-shocked pre-two-fold embryos, aged three to 7.5 hours after the 4-cell stage, carrying either an array or insertion of *Phsp-16.41*::*peel-1*. Embryos were heat-shocked for 20 minutes at 34C. Longer and earlier heat-shock were not possible because even in wild-type embryos, such conditions cause premature arrest (personal observations). Except for occasional subtle shape defects during early elongation, more than 97% of array- and insertion-carrying embryos developed normally to the two-fold stage ($n \geq 200$; Figure 2-16 A). This result is consistent with sperm-supplied PEEL-1 being able to persist until the two-fold stage without manifesting a visible phenotype earlier in development.

Second, heat-shock expression of *peel-1* as late as 30 minutes before the two-fold stage phenocopied the defects observed in *peel-1*-affected embryos. In the heat-shocked embryos described above, embryos carrying an array of *Phsp-16.41*::*peel-1* uniformly arrested at the two-fold stage and showed muscle detachment, epidermal leakage, and excretory cell distention (Figure 2-15 C, Figure 2-16 B-J). These defects were also observed among insertion-carrying embryos, although their occurrence required earlier induction of the transgene (Figure 2-15 C). In addition, consistent with heat-shock treatment exposing embryos to more PEEL-1 protein than is delivered by sperm, the defects induced by heat-shock were often more severe than those observed in *peel-1*-affected embryos, and even among insertion-carrying embryos, the defects could not be rescued by endogenous expression of *zeel-1* (Figure 2-15 C). These results demonstrate that as long as *peel-1* is expressed at or just before the two-fold stage, presence of PEEL-1 in the early embryo is dispensable for the two-fold arrest.

Finally, rescue of *peel-1*-affected embryos did not require early expression of *zeel-1*. We induced *zeel-1* expression in male-sired, *peel-1*-affected embryos by heat-shocking embryos carrying either an array or an insertion of *Phsp-16.41*::*zeel-1*. Heat-shock treatment rescued 53-100% of array-carrying embryos ($n = 17$-43), as long as heat-shock treatment occurred at least one hour before the two-fold stage (Figure 2-15 C). (Here rescue is defined as elongation past the two-fold stage. See Figure 2-16 A for the proportion of embryos that hatched.) Similar results were observed for insertion-carrying embryos, although rescue activity required earlier induction of the

transgene (Figure 2-15 C). These results imply that ZEEL-1 can neutralize sperm-supplied PEEL-1 at any time before the two-fold stage. This scenario is temporally discordant with PEEL-1 causing a cryptic defect early in development.

subsectionCell-specific expression of *peel-1* produces cell-specific ablation The test the cell-autonomy of *peel-1* killing, as well as the utility of *peel-1* as a tool for cell-specific ablation, we expressed *peel-1* under the control of each of two cell-specific promoters: *Punc-47*, which expresses in the GABA-ergic neurons [83]; and *Pexp-3*, which expresses in the egg-laying muscles and the anal depressor muscle (C. Frokjr-Jensen, personal communication). For each promoter construct, we examined the presence or absence of the corresponding cell types for four independent extra-chromosomal arrays.

In both muscle cells and neurons, cell-specific expression of *peel-1* produced cell-specific ablation, although the efficacy of ablation varied among arrays. Three of the *Punc-47*::*peel-1* arrays killed 94.2-99.8% (n = 241-453) of GABA-ergic neurons, although the fourth array killed only 28.6% (n = 350) of them. Each of the *Pexp-3*::*peel-1* arrays killed 6-27% (n = 83-90) of anal depressor muscles and 74-94% (n = 140-180) of egg-laying muscles. Of the egg-laying muscles that remained alive, all were severely atrophied (Figure 2-15 E). Lower toxicity to the anal depressor muscle may have been caused by selection bias among our arrays, because animals lacking the anal depressor muscle were very severely constipated and therefore more slow-growing than others. In addition, even among animals in which the anal depressor remained alive, constipation was prevalent (Figure 2-17), indicating that function of this muscle was impaired.

Aside from the defects caused by ablation of the corresponding cell types, animals carrying either type of construct were morphologically and behaviorally normal, consistent with PEEL-1 acting cell-autonomously. In addition, with one exception, no defects were observed outside the ablated cells types (Figure 2-15 F). The exception was that the three high kill *Punc-47*::*peel-1* arrays were lethal to the animal when inherited somatically along the lineage of the four RME neurons: for these three arrays, embryo and early larval lethality was very high (33.0-57.7%; n = 327-1095), and

the only animals surviving to adulthood were those that lost the arrays somatically in the four RME neurons. Given that the RME neurons are not required for survival [82], this lethality implies that either (i) expression of *peel-1* in the RME neurons kills a neighboring cell nonautonomously; or (ii) expression of *peel-1* is leaky and kills one or more essential cells along the RME lineage. While we did not distinguish between these possibilities, we note that the sister cell to one RME neuron is the excretory cell, which is essential for survival.

2.2.2 Materials and Methods

Strains

Strains were maintained at 19-23C on NGM plates spotted with *E. coli* strain OP50. In all age-effect experiments, strains were strictly maintained at 20C. For all transgenes described in this publication, only one array and/or one insertion is given in the strain list, although unless otherwise specified in the Results subsection, multiple independent arrays or insertions were examined.

CB4088 *him-5(e1490)* V.

CB4856 Hawaii natural isolate carrying *niDf9* I. *niDf9* designates the 19 kb deficiency spanning *peel-1* and *zeel-1*.

EG1285 *oxIs12[Punc-47::GFP; lin-15(+)] lin-15B(n765)* X.

EG4322 *ttTi5605 II; unc-119(ed3)* III.

EG4348 Utah natural isolate carrying *peel-1(qq99)* I. EG4348 was collected by M. Ailion from Salt Lake City, Utah (this publication). *qq99* designates the naturally-occurring nonsense mutation in *peel-1*.

EG5389 *qqIr7[peel-1(qq99)] I; oxIs494[Ppeel-1::GFP] II; unc-119(ed3)* III.

EG5655 *qqIr7[peel-1(qq99)] I; oxSi19[peel-1(+), Cbr-unc-119(+)] II; unc-119(ed3)* III.

EG5766 *qqIr7[peel-1(qq99)] I; oxSi77[Ppeel-1::peel-1::GFP] II; unc-119(ed3)* III.

EG5801 *oxSi87[Ppeel-1::peel-112a.a.::GFP] II; unc-119(ed3)* III.

EG5955 *qqIr7[peel-1(qq99)] I; ttTi5605 II; unc-119(ed3) III; oxEx1462[Phsp-16.41::peel-*

A Anal depressor muscle

Array	Dead/Absent	Alive: Inherited *Pexp-3::peel-1* array	Alive: Did **not** inherit *Pexp-3::peel-1* array	% Killing (total cells inheriting the array)	% Constipated (total animals)*
1	6	84	10	6.7% (90)	87% (90)
2	23	61	15	27.4% (84)	82% (84)
3	5	78	17	6.0% (83)	89% (83)
4	10	74	16	11.9% (84)	75% (84)

* Calculated among animals in which the array had been transmitted to the anal depressors muscle

B Egg-laying muscles

Array	Dead/Absent	Alive: Atrophied: Inherited *Pexp-3::peel-1* array	Alive: Atrophied: Did **not** inherit *Pexp-3::peel-1* array	Alive: Morphologically normal: Inherited *Pexp-3::peel-1* array	Alive: Morphologically normal: Did **not** inherit *Pexp-3::peel-1* array	% Killing (total cells inheriting the array)	% Egg-laying defective (total animals)**
1	169	11	0	0	20	93.4% (180)	100% (90)
2	160	10	0	0	30	94.1% (170)	100% (85)
3	104	36	0	0	60	74.3% (140)	100% (70)
4	135	19	0	0	46	87.7% (154)	100% (77)

** Calculated among animals in which the array had been transmitted to the egg-laying muscles

C GABA neurons

Array	Dead/Absent	Alive: Inherited *Punc-47::peel-1* array	Alive: Did **not** inherit *Punc-47::peel-1* array	% Killing (total cells inheriting the array)	% Embryo/larva arrest (total)	% Mosaics (total adults)
1	452	1	163	99.8% (453)	57.7% (1095)	100% (74)
2	232	8	210	96.7% (240)	42.4% (327)	100% (50)
3	227	14	273	94.2% (241)	33.0% (587)	100% (73)
4	100	250	0	28.6% (350)	2.4% (1059)	0% (50)

Figure 2-17: **Cell-specific killing via ectopic expression of *peel-1*.**
(A-B) The *Pexp-3::peel-1* arrays were crossed to a strain carrying an insertion of *Pmyo-3::GFP*, which serves as a marker of the egg-laying muscles and the anal depressor muscle. Live muscle cells were classified as inheriting the array if they expressed the co-injection marker, *Pmyo-3::mCherry*. One hundred animals were scored for each array, and two of the four egg-laying muscles were scored per animal.
(C) The *Punc-47::peel-1* arrays were crossed to a strain carrying an insertion of *Punc-47::GFP*, which serves as a marker for the GABA neurons. Live neurons were classified as inheriting the array if they expressed the co-injection marker, *Prab-3::mCherry*. For each array, 50-74 animals were scored, and six to ten neurons were scored per animal.

1, Cbr- unc-119(+), Pmyo-2::mCherry, Pmyo-3::mCherry, Prab-3::mCherry].

EG5958 *qqIr7[peel-1(qq99)] I; oxSi186[Phsp-16.41::peel-1, Cbr-unc-119(+)] II; unc-119(ed3)* III.

EG5960 *qqIr7[peel-1(qq99)] I; oxSi188[Phsp-16.2::peel-1, Cbr-unc-119(+)] II; unc-119(ed3)* III.

EG5961 *qqIr7[peel-1(qq99)] I; ttTi5605 II; unc-119(ed3) III; oxEx1464[Phsp-16.2::peel-1, Cbr- unc-119(+), Pmyo-2::mCherry, Pmyo-3::mCherry, Prab-3::mCherry].*

EG6297 *qqIr5[niDf9] I; oxSi298[Phsp-16.41::zeel-1::tagRFP, Cbr-unc-119(+)] II; unc-119(ed3)* III.

EG6298 *qqIr5[niDf9] I; ttTi5605 II; unc-119(ed3) III; oxEx1501[Phsp-16.41::zeel-1::tagRFP, Cbr- unc-119(+), Pmyo-2::GFP].*

EG6301 *qqIr5[niDf9] I; ttTi5605 II; unc-119(ed3) III; oxEx1504[Pexp-3::peel-1, Cbr-unc-119(+), Pmyo-2::mCherry, Pmyo-3::mCherry, Prab-3::mCherry].*

EG6306 *qqIr5[niDf9] I; ttTi5605 II; unc-119(ed3) III; oxEx1509[Punc-47::peel-1, Cbr-unc-119(+), Prab-3::mCherry].*

MT1344 *bli-3(e767) lin-17(n677)* I.

MT3301 *fem-1(hc17) IV; him-5(e1490)* V.

MY19 German natural isolate carrying *peel-1(qq98)* I. MY19 was collected from Roxel, Germany [51]. *qq98* designates the naturally-occurring nonsense mutation in *peel-1*.

N2 Laboratory reference strain, Bristol.

PD4790 *mIs12[myo-2::GFP, pes-10::GFP and gut::GFP].*

QX1015 *niDf9 I; qqIr8[N2 =¿ CB4856, unc-119(ed3)]* III.

QX1197 *qqIr5[CB4856 =¿N2, niDf9]* I. qqIr5 is an 140-370 kb introgression from CB4856 into N2. This strain was used in some experiments instead of CB4856, in order to reduce the genetic variation segregating in the background.

QX1257 *niDf9 I; qqIr8[unc-119(ed3)] III unc-119(ed3) III; qqIs2[zeel* $-1_{genomic}$*::GFP, unc-119(+)].*

QX1264 *niDf9 I; qqIr8[unc-119(ed3)] III unc-119(ed3) III; qqEx2[zeel* $-1_{genomic}$*::GFP, unc-119(+)].*

QX1319 *zeel-1(tm3419)/hT2[qIs48] I; +/hT2[qIs48]* III.

QX1320 *qqIr6[EG4348=¿N2, peel-1(qq99)] I; unc-119(ed3)* III.

QX1384 *niDf9 I; qqIr8[unc-119(ed3)] III unc-119(ed3) III; qqEx6[Pzeel-1:: zeel* -1_{SOL}*, unc-119(+)].*

QX1392 *qqIr6[peel-1(qq99)] I; unc-119(ed3) III; qqEx3[peel-1(+), unc-119(+)].*

QX1409 *qqIr7[EG4348=¿N2, peel-1(qq99)] I; ttTi5605 II; unc-119(ed3)* III.

QX1577 *qqIr5[niDf9] I; qqEx1[Pzeel-1::zeel* -1_{cDNA}*::GFP, Pmyo-2::RFP].*

QX1589 *qqIr5[niDf9] I; qqEx4[Pzeel-1::Y71A12B.17TM:: zeel* -1_{SOL}*, Pmyo-2::RFP].*

QX1605 *qqIr5[niDf9] I; ttTi5605 II; unc-119(ed3)* III.

QX1607 *qqIr5[niDf9] I; qqEx5[Pzeel-1:: zeel-1TM, Pmyo-2::RFP].*

QX1618 *qqIr5[niDf9] I; qqEx7[Plin-26::zeel-1, Pmyo-2::RFP].*

QX1619 *qqIr5[niDf9] I; qqEx8[Phlh-1::zeel-1, Pmyo-2::RFP].*

QX1624 *qqIr5[niDf9] I; oxSi186[Phsp-16.41::peel-1, Cbr-unc-119(+)] II; unc-119(ed3)* III.

QX1650 *oxSi19[peel-1(+), Cbr-unc-119(+)]* II.

QX1772 *qqIr5[niDf9] I; ttTi5605 II; unc-119(ed3) III; oxEx1462[Phsp-16.41::peel-1, Cbr-unc-119(+), Pmyo-2::mCherry, Pmyo-3::mCherry, Prab-3::mCherry].*

SJ4157 *zcIs21[Phsp-16::clpp-1(WT)::3xmyc-His tag + Pmyo-3::GFP]* V.

Scoring embryo lethality

In all experiments except the age-effect experiment, embryo lethality from self-fertilizing hermaphrodites was scored by isolating hermaphrodites at the L4 stage and singling them to fresh plates the following day. After laying eggs for 8-10 hours, the hermaphrodites were removed and embryos were counted. Unhatched embryos were counted ~24 hours later. To score embryo lethality from mated hermaphrodites, three or four L4 hermaphrodites were mated to six to ten L4 or young adult males for 24-36 hours. Hermaphrodites were then singled to fresh plates and embryo lethality was scored as above. Broods were examined for the presence of males 2-3 days later, and any broods lacking males were excluded. To allow male sperm to age within the reproductive tract of the hermaphrodite, mated hermaphrodites were removed from

males, and lethality was scored among embryos laid three days after removal.

In the age-effect experiment, 91 *zeel-1(tm3419)peel-1(+)/niDf9* hermaphrodites were singled at the L4 stage and transferred every 12 hours to fresh plates. Hermaphrodites were discarded after the first 12-hour period in which they failed to lay fertilized embryos. Total embryos were counted at the end of each laying period, and unhatched embryos were counted ~24 hours after each laying period had ended.

To score embryo lethality from partially mated hermaphrodites, 130 *zeel-1(tm3419)peel-1(+)/niDf9* hermaphrodites were mated at the L4 stage to an equal number of PD4790 males, which carry an insertion of the fluorescent marker, *Pmyo-2::GFP*. After 24 hours, hermaphrodites were singled and transferred every 12 hours to fresh plates until day five. Embryo lethality was scored as above, except that after unhatched embryos were counted, hatched and unhatched progeny were classified as self- or cross-progeny according to presence of pharyngeal GFP. Hermaphrodites laying 100% self-progeny or more than 95% cross-progeny were excluded. The remaining hermaphrodites, which we define as partially mated, laid ~10-50% self-progeny. In these broods, we calculated the portion of self-progeny, laid during days three to five, that failed to hatch.

Mapping *peel-1* mutations in MY19 and EG4348

Absence of the paternal-effect in EG4348 was mapped relative to *bli-3(e767)*, a visible marker located ~10 cM from the *peel-1* interval. Mapping was performed as described [115]. Briefly, EG4348 males were crossed to MT1344 hermaphrodites, and F1 hermaphrodites were mated to CB4856 males. The resulting hermaphrodite progeny were allowed to self-fertilize, and their broods were scored for embryo lethality (*i.e.* presence of *peel-1* activity) and presence of Bli animals. Directionality with respect to *bli-3* could be inferred because *bli-3* is located at the left-hand tip of chromosome I.

Preliminary sequence analysis of the *peel-1* interval in EG4348 was performed by genotyping EG4348 with a subset of the markers listed in Table S2 of [115]. These markers tile across the *peel-1* interval, and they distinguish all haplotypes carrying an

intact copy of the *peel-1/zeel-1* element from all haplotypes lacking it [115]. In other words, the Bristol-like alleles of these markers are in perfect linkage disequilibrium with presence of the *peel-1/zeel-1* element. At all markers we assayed, EG4348 carried the Bristol-like allele.

Fine-mapping in MY19 and EG4348 was performed by crossing each strain to MT1344 and collecting Lin Non-Bli and Bli Non-Lin recombinants in the F2 generation. Recombinant animals were genotyped (via a portion of their F3 broods) at each of two markers flanking the *peel-1* interval. The right-hand marker for the MY19 cross was a BstCI snip-SNP amplified with primers 5'-GTA TTC CGA CGA TTC GGA TG-3' and 5'-CAT TGA GAA CAC AAA AAC AAA CG-3'. The right-hand marker for EG4348 cross was an AfeI snip-SNP amplified with primers 5'- GAC ATA TTT CCC GCA ACC TG-3' and 5'- GTG ACG AGG CTT GAG GAT TC-3'. The left-hand marker for both crosses was a BanI snip-SNP amplified with primers 5'-CGC CAA ATA TGT TGT GCA GT-3' and 5'-CAC CAC GTG TCC TTT CTC ATT-3'.

Recombinants breaking within the *peel-1* interval were homozygosed for the recombinant chromosome, and the resulting homozygotes were phenotyped for *peel-1* activity. Phenotyping was performed by crossing each line to CB4856 and scoring embryo lethality from self-fertilizing, F1 hermaphrodites and from F1 males backcrossed to CB4856 hermaphrodites. Recombinants were classified as having *peel-1* activity if these crosses produced ~25% and ~50% embryo lethality, respectively. Next, the locations of recombination breakpoints were mapped more finely by sequencing six to ten sequence polymorphisms, located throughout the *peel-1* interval, that distinguish MY19 or EG4348 from Bristol. The MY19 polymorphisms were determined from the MY19 sequence described in [115], and the EG4348 polymorphisms were determined by amplifying and sequencing arbitrary fragments from this strain. Some polymorphisms are shared between MY19 and EG4348, and these were used in both crosses. For the most informative recombinants, we later sequenced across the entire breakpoint region in order to map these breakpoints to the level of adjacent polymorphisms. This approach mapped the *peel-1*-disrupting mutations to regions of 5 kb in

MY19 and 8 kb in EG4348. These intervals were then sequenced in the corresponding strains, and all sequence polymorphisms were identified. Finally, we genotyped these polymorphisms in a panel of 38 wild strains previously identified as having intact *peel-1* activity [115]. These strains, as well as the primers used for genotyping them, are given in Figure S2. The MY19 sequence was deposited in GenBank previously [115], and the EG4348 sequence was deposited under accession number HQ291558.

Identification of *peel-1* transcript

RNA was collected from mixed-staged Bristol animals by freeze-cracking and extracting in Trizol (Invitrogen) according to the manufacturers protocol. Reverse transcription-PCR (RT-PCR) was performed using pairs of primers flanking each candidate mutation in MY19 and EG4348. For each pair of primers, the forward and reverse primers were located ~100 bp apart, and two reactions were performed, one using each of the two primers as the RT primer. Product was observed for only one pair of primers, and for that pair, only in one direction. These primers were 5'-ACA TGT ATC TTG ATC TGC CTG A-3' (forward) and 5'-AAA AAT TAA CCA CAA TGA AGC AA-3' (reverse), and product was only observed using the reverse primer as the RT primer. To recover the remainder of this putative transcript, 3' and 5' RACE were performed using standard methods [55]. For 3' RACE, the RT reaction was performed using 5'-GTT TTC CCA GTC ACG ACT TTT TTT TTT TTT TTT TT-3', and PCR was performed using the gene-specific primer, 5'-ACA TGT ATC TTG ATC TGC CTG A-3' (forward) and the adaptor primer, 5'-GTT TTC CCA GTC ACG AC-3' (reverse). For 5' RACE, the RT reaction was performed using a gene-specific primer that spanned the putative stop codon, 5'-TCA ATT TCA TGG ATT TTC AAC A-3', and PCR was performed using 5'-GGC CAC GCG TCG ACT AGT ACG GGI IGG GII GGG IIG-3' (forward) and a nested, gene-specific primer, 5'-AAA AAT TAA CCA CAA TGA AGC AA-3' (reverse). Then, a second round of PCR was performed using the adaptor primer, 5'-GGC CAC GCG TCG ACT AGT AC-3' (forward) and another nested, gene-specific primer, 5'-AGA GCA ATA ACA TGC GCA AA-3' (reverse). SuperScript III (Invitrogen) was used in all RT

reactions, and PlatinumTaq (Invitrogen) was used for all PCR reactions. The *peel-1* transcript did not contain a splice leader sequence and was deposited in GenBank under accession number HQ291556. More recently, the *peel-1* transcript was identified independently by WormBase curators and assigned the identification number, *Y39G10AR.25*.

To search for transcripts carrying both *peel-1* and *zeel-1*, an RT reaction was performed using the *peel-1*-specific primer, 5'-AAA AAT TAA CCA CAA TGA AGC AA-3', and PCR was performed using a forward primer located in the 3' end of *zeel-1* (5'-CCA TCC GAG ATA ACC GAA AA-3') and a reverse primer located in the 5' end of *peel-1* (5'-AGA GCA ATA ACA TGC GCA AA-3'). No product was observed.

Quantitative RT-PCR

CB4088 and MT3301 animals were grow at 15C and synchronized at the L1 stage by bleaching and hatching overnight in M9. L1s were split into two populations, and one population was shifted to 25C. When animals had reached young adulthood, hermaphrodites and males were separated by hand, and RNA was collected as above. Real-time PCR of *peel-1*, *spe-9*, and *rpl-26* was performed in triplicate, for 40 cycles, on an ABI 7900HT using the QuantiTect SYBR Green Kit (Qiagen). Relative expression levels of *peel-1* and *spe-9* were calculated separately for males and hermaphrodites, using the $2^{\Delta\Delta Ct}$ method, with *rpl-26* as the endogenous control and the 15C MT3301 sample as the reference sample. Primers used to amplify *peel-1* were 5'-TAC ACC CGT CAC ACC AAC TG-3' and 5'-TCC GAC TAT GAT GTT CCA CAA-3'; primers for *spe-9* were 5'-CGG CTT GCA TAC ACA ATG AG-3' and 5'-ACG CCA TGA CTC TTG CTC TT-3'; and primers for *rpl-26* were 5'-TCC AAT CAG AAC CGA TGA TG-3' and 5'-GTG CAC AGT GGA TCC GTT AG-3'.

Among the hermaphrodite samples, relative expression levels of *peel-1* and *spe-9* were roughly equivalent, except for the 25C MT3301 sample, where expression of *peel-1* and *spe-9* was undetectable. That is, in this sample, signal for *peel-1* and *spe-9* failed to rise above the detection threshold, even after 40 cycles, despite *rpl-26* amplifying normally.

Single-molecule FISH

Single molecule FISH of was performed as in [105], with the embryos and hermaphrodites squashed down to ~9 μm thickness for imaging. Automated counting of nuclei in embryos was performed using software developed in [105, 104].

Rescue of *peel-1*

Transgenic animals carrying *peel-1(+)* were generated by two methods: bombardment [101] and Mos1-mediated, single-copy insertion [43]. For bombardment, a fragment containing the Bristol allele of *peel-1*, along with ~2.8 kb of upstream sequence and ~1 kb of downstream sequence, was excised from fosmid WRM0633bE09 (Bioscience LifeSciences, Nottingham, UK) using AhdI and NgoMIV. This fragment was cloned into the yeast shuttle vector, pRS246 (ATCC, Manassas, VA), via yeast-mediated ligation [106] of the fragments ends. The resulting plasmid, pHS11, was bombarded into QX1320, along with the *unc-119(+)* rescue vector, pDP#MM016B [81]. Bombardment was performed as in [88], although only extra-chromosomal arrays were recovered. Nine independent transgenic lines were tested for *peel-1* activity by crossing them to CB4856 and scoring embryo lethality from self-fertilizing, F1 hermaphrodites (self-cross) and F1 males backcrossed to CB4856 hermaphrodites (backcross).

For Mos1-mediated insertion, the *peel-1* fragment from pHS11 was amplified by PCR, using primers having NheI cut sites, and this amplicon was cut with NheI and ligated into pCFJ151 [43] linearized with AvrII. The resulting plasmid, pHS26, was injected into QX1409 along with the vectors needed to generate single-copy insertions [43]. Insertion-carrying animals were recovered by the direct insertion method [43], and five independent insertion-carrying lines were tested for *peel-1* activity as above. For one of the two insertions that did exhibit *peel-1* activity, the self-cross and backcross were repeated, and hatched progeny were collected and genotyped for a PCR-length polymorphism located less than 1 kb from *niDf9*. The primers used to amplify this polymorphism were 5'-TGG ATA CGA TTC GAG CTT CC-3' (forward) and 5'-CCC CCT AAT TTC CAA GTG GT-3' (reverse).

For three of the *peel-1* array lines, a small number of severely deformed L1s were observed in the backcross, similar to the escapers typically observed among *peel-1*-affected embryos sired by hermaphrodites. We suspected that these L1s had escaped the paternal-effect due to partial germline silencing of the *peel-1* arrays. Consistent with this hypothesis, we genotyped 13 of these animals, using the PCR-length polymorphism described above, and all were *zeel-1(niDf9)* homozygotes. We then calculated the frequency of these escapers relative to the total number of *peel-1*-affected progeny (*i.e.* relative to the total number of dead embryos and deformed L1s).

ZEEL-1::GFP fusion and domain swapping

ZEEL-1::GFP was generated by amplifying *GFP* from PD95.75 and inserting it into pHS4.1, a genomic subclone of *zeel-1(+)* described previously [115]. pHS4.1 was linearized with AhdI, and yeast-mediated ligation [106] was used to insert GFP just upstream of the *zeel-1* stop codon. Later, a second *ZEEL-1::GFP* construct was generated using the cDNA of *zeel-1*, instead of the genomic locus. This construct was generated by first cutting pHS4.1 with EcoNI and BglII, in order to remove the entire coding region of *zeel-1*, and then inserting a full cDNA of *zeel-1*, followed by *GFP*. The cDNA of *zeel-1* was cloned previously [115], and this replacement was performed using yeast-mediated ligation [106]. Both constructs showed full rescue of *peel-1*-affected embryos, and data from the two constructs were combined.

To generate $ZEEL-1_{SOL}$, pHS4.1 was cut with EcoNI and KpnI, and the fragment containing *zeel-1* codons 5 to 205 was removed. The remaining fragment was then re-circularized, using yeast-mediated ligation [106], to fuse codon 4 to codon 206. To generate $ZEEL-1_{TM}$, the entire coding region of *zeel-1* was excised from pHS4.1 using EcoNI and BglII, and this fragment was replaced with a partial cDNA of *zeel-1* encoding the first 205 amino acids of the protein. This replacement was performed using yeast-mediated ligation [106].

To generate $Y71A12B.17_{TM}::ZEEL-1_{SOL}$, the coding region of *zeel-1* was excised from pHS4.1, as above, and yeast mediated ligation [106] was used to replace this fragment with a partial cDNA of *Y71A12B.17*, followed by a partial cDNA of

zeel-1. The resulting construct contained the *N*-terminal 207 codons of *Y71A12B.17* fused to the *C*-terminal 712 codons of *zeel-1*. The junction of this fusion was chosen to overlap a string of seven amino acids (KNERKEG) that are perfectly conserved between the two proteins. The *Y71A12B.17* cDNA was cloned by reverse transcribing RNA from the Bristol strain using primer 5'-TTG AAC AAA AAC AAT GGA TAT GTA A-3', and then performing PCR using primers 5'-GGG GAC AAG TTT GTA CAA AAA AGC AGG CTT CAT GTC GGA TTT CGA CTC AGA-3' (forward) and 5'-GGG GAC CAC TTT GTA CAA GAA AGC TGG GTC ATT TAT TAA CTC CAA CAA TGA TTC G-3' (reverse). This PCR product was then cloned into the vector, pDONR221 (Invitrogen), using the Gateway cloning kit (Invitrogen). The *Y71A12B.17* cDNA differs slightly from the WormBase gene prediction and was deposited in GenBank under accession number HQ291557.

All constructs were bombarded [88] into QX1015 along with the *unc-119(+)* rescue vector, pDP#MM016B [81], or they were injected [39] into QX1197 at ~80ng/μl, along with the fluorescent marker, *Pmyo-2::RFP* at 3 ng/μl. To test each transgene for its ability to rescue *peel-1*-affected embryos, transgenic animals were crossed to the Bristol strain, and lethality was scored among embryos derived from two crosses: self-fertilizing F1 hermaphrodites (self-cross); and F1 males backcrossed to hermaphrodites of the original transgenic line. To calculate hatch rates among *peel-1*-affected embryos inheriting *ZEEL-1::GFP* and $ZEEL-1_{TM}$, transgenic animals were crossed to QX1319, and embryos were collected from: (i) transgenic, self-fertilizing, F1, *zeel-1(tm3419)peel-1(+)/niDf9* hermaphrodites; and (ii) transgenic, F1, *zeel-1(tm3419)peel-1(+)/niDf9* males backcrossed to non-transgenic, *niDf9/niDf9* hermaphrodites. Inheritance of *ZEEL-1::GFP* and $ZEEL-1_{TM}$ was inferred by expression of the co-injection marker, *Pmyo-2::RFP*, which can be scored even in arrested embryos.

Other transgenes

All other transgenes were generated using the three-site Gateway system from Invitrogen. This method allows three separate DNA fragments to be joined together and inserted into pCFJ150, which contains *Cbr-unc-119(+)* and the sequences needed for

Mos1-mediated insertion at the *ttTi5605* Mos site on chromosome II [43]. In most cases, this method was used to join together a promoter of interest, a coding sequence, and a 3' UTR.

Ppeel-1::GFP, *Ppeel-1::PEEL-1*$_{12a.a.}$*::GFP*, and the *PEEL-1::GFP* fusion

For *Ppeel-1::GFP*, we joined together the *peel-1* promoter, *GFP*, and the *peel-1* 3'UTR. For the *peel-1* promoter, we used all intergenic sequence between the *peel-1* start codon and last coding segment of *zeel-1* (*i.e.* 2473 bp of sequence). The *peel-1* 3' UTR was determined empirically and extended 86 bp downstream of the *peel-1* stop codon. For *GFP*, we used a variant containing S65C and three internal introns (identical to the variant in pPD95.75).

For *Ppeel-1::PEEL* $-$ $1_{12a.a.}$*::GFP*, the PEEL-1 leader peptide was added by extending the promoter fragment to include the first 12 amino acids of PEEL-1. This signal peptide was discovered while we were investigating a possible regulatory role of the first intron of *peel-1*. We had generated a GFP reporter driven by the *peel-1* promoter and the first intron of *peel-1*, and this construct also happened to carry the first 12 amino acids of PEEL-1. GFP driven by this construct was packaged into sperm (data not shown), and in order to confirm that sperm packaging was caused by the leader peptide, rather than the intron, we generated *Ppeel-1::PEEL* $-$ $1_{12a.a.}$*::GFP* (which excludes the first intron). Conversely, we also generated a reporter carrying the first intron and a randomized leader peptide, and for this construct, no sperm packaging was observed (data not shown).

To tag PEEL-1 with GFP, the promoter fragment was extended even further to include the entire *peel-1* gene, up to (but excluding) the stop codon.

All three constructs were injected into EG4322 or QX1409, and single-copy insertions were obtained using the direct insertion MosSCI method [43]. Three to six independent insertions were analyzed for each construct, and no differences were observed among insertions of the same construct. We note that although PEEL-1::GFP appears to localize normally, it failed to exhibit *peel-1* activity (data not shown), presumably because the GFP tag inhibited function.

Plin-26::zeel-1 and *Phlh-1::zeel-1*

For *Plin-26::zeel-1* and *Phlh-1::zeel-1*, the promoters of *lin-26* or *hlh-1* were joined to the cDNA of *zeel-1* and the 3' UTR of *let-858*. For the promoters of lin-26 and hlh-1, 7122 bp of sequence and 3037 bp of sequence upstream of the respective start codons were used. For the *let-858* 3' UTR, 434 bp of sequence downstream of the stop codon was used. Transgenic animals were generated by injecting *Plin-26::zeel-1* and *Phlh-1::zeel-1* into QX1197 at ~80 ng/μl, along with the fluorescent marker, *Pmyo-2::RFP* at 3 ng/μl.

To evaluate rescue among male-sired embryos, transgenic animals were crossed to QX1319, and transgenic, F1, *zeel-1*(tm3419)*peel-1*(+)/*niDf9* males were backcrossed to non-transgenic, *niDf9*/*niDf9* hermaphrodites. Embryos were dissected from these hermaphrodites and imaged every 10-20 minutes, starting before the two-fold stage and ending at least six hours after the two-fold stage. To evaluate rescue among hermaphrodite-sired embryos, transgenic lines were crossed to QX1319, and embryo viability was scored among embryos collected from transgenic, self-fertilizing, F1, *zeel-1*(tm3419)*peel-1*(+)/*niDf9* hermaphrodites. Among both male- and hermaphrodite-sired embryos, inheritance of the transgene was inferred by expression of *Pmyo-2::RFP*.

Heat-shock constructs and constructs for cell-specific expression of *peel-1*

Phsp-16.41::*peel-1*, *Phsp-16.2*::*peel-1*, *Pexp-3*::*peel-1*, and *Punc-47*::*peel-1* were generated by joining the *peel-1* cDNA downstream of the appropriate promoter and upstream of the *tbb-2* 3' UTR. We describe the promoter and 3'UTR fragments in terms of length of sequence upstream or downstream of the appropriate start or stop codons: *Phsp-16.41* (501 bp), *Phsp-16.2* (493 bp), *Pexp-3* (2877 bp), and *Punc-47* (1251 bp), and *tbb-2* 3' UTR (331 bp). *Phsp-16.41*::*peel-1* and *Phsp-16.2*::*peel-1* were injected into QX1409 at 25 ng/μl, and arrays and MosSCI insertions were recovered as in [43]. The arrays carry co-injection markers *Pmyo-2*::*mCherry*, *Pmyo-3*::*mCherry*, and *Prab-3*::*mCherry*. *Pexp-3*::*peel-1* and *Punc-47*::*peel-1* were

injected into QX1605 at 25 and 10 ng/μl respectively, along with co-injection markers *Prab-3*::*mCherry*, *Pmyo-2*::*mCherry*, and *Pmyo-3*::*mCherry* (for *Pexp-3*::*peel-1*) and marker *Prab-3*::*mCherry* (for *Punc-47*::*peel-1*). In all cases, *Pmyo-3*::*mCherry* and *Prab-3*::*mCherry* were injected at 10 ng/μl, and *Pmyo-2*::*mCherry* was injected at 5 ng/μl.

Phsp-16.41::*zeel-1* was generated using the *hsp-16.41* promoter described above, the *zeel-1* cDNA, and the *let-858* 3'UTR fused downstream of *tagRFP*. *tagRFP* was added to confirm expression of *zeel-1* after heat-shock. *Phsp-16.41*::*zeel-1* was injected at 10 ng/μl into QX1605 and the arrays and the MosSCI insertion were recovered as in [43], except that a GFP-based co-injection marker (*Pmyo-2*::GFP injected at 2.5 ng/μl) was used in order to distinguish these arrays from the *Phsp-16.41*::*peel-1* arrays.

Microscopy and analysis of live embryos

Imaging of fixed embryos and live imaging of *ZEEL-1*::*GFP* embryos was performed on a PerkinElmer RS3 spinning disk confocal. All other imaging was performed on a Nikon 90i equipped with a CoolSNAP HQ2 camera and a X-Cite 120 Series fluorescent light source. Images were acquired and background subtracted with either Volocity (PerkinElmer) or NIS Elements (Nikon), and (in some cases) multiple channels were overlaid in Adobe Photoshop. To image dissected gonads, spermatocytes, and sperm, adult males or mated hermaphrodites were dissected into sperm media containing dextrose (50 mM Hepes, 1 mM $MgSO_4$, 25 mM KCl, 45 mM NaCl, 5 mM $CaCl_2$, 10 mM dextrose).

To measure the onset of epidermal leakage in *peel-1*-affected embryos, pre-arrest embryos were dissected from the following crosses. Hermaphrodite-sired embryos were dissected from (i) self-fertilizing, *zeel-1*(tm3419)*peel-1*(+)/*niDf9* hermaphrodites; and (ii) self-fertilizing, *zeel-1(tm3419)peel-1(+)/zeel-1(tm3419)peel-1(+)* hermaphrodites. Male-sired embryos were dissected from *niDf9/niDf9* hermaphrodites mated to three types of males: (i) *zeel-1(tm3419)peel-1(+)/niDf9*; (ii) *zeel-1(tm3419)peel-1(+)/zeel-1(+)peel-1(+)*; and (iii) *zeel-1(tm3419)peel-1(+)/zeel-1(+)peel-1(+)*; *oxSi19[peel-1(+)]/+*.

The self-fertilizing hermaphrodites were aged 24 hours post-L4 at the time of dissubsection, and mated hermaphrodites were aged 24-48 hours at the time of dissubsection. After dissubsection, embryos were imaged every 10 minutes, starting before the 1.5-fold stage and ending seven or more hours after the 1.5-fold stage. The onset of epidermal leakage was calculated as the time between the 1.5-fold stage and the first frame in which leakage was observed. Calculations were truncated at seven hours past the 1.5-fold stage because this represents one hour after the average hatching time of wild-type embryos. Finally, embryos were binned into 30-minute intervals in order to generate the inverted histograms shown in Figure 4A.

To calculate the percentage of *peel-1*-affected embryos elongating past two-fold, *zeel-1(tm3419)peel-1(+)/niDf9* hermaphrodites were isolated at the L4 stage and allowed to age for 24, 48, 60, and 72 hours. Embryos were then dissected and imaged every 20 or 30 minutes for at least 10 hours.

Fixation of sperm and embryos

Anti-PEEL-1 is a rabbit polyclonal generated against the *C*-terminal 15 amino acids of PEEL-1. This antibody was generated and purified by GenScript, Piscataway, NJ. 1CB4 is a mouse monoclonal used to stain FB-MOs [96]. 1CB4 was a gift from Steven L'Hernault. To stain sperm, adult males were dissected into sperm media on charged slides, freeze-cracked in liquid nitrogen, and fixed overnight in -20C methanol. Slides were washed with PBST (PBS + 0.1% Triton-X 100), blocked for 30 minutes with PBST + 0.5% BSA, and incubated for four hours with anti-PEEL-1 (1/100) and 1CB4 (1/2000), diluted in PBST + 0.5% BSA. Slides were then washed three times in PBST and incubated for two hours with Alexa568-labeled anti-mouse (1/500) and Alexa488-labeled anti-rabbit (1/500) (Invitrogen), diluted in PBST + 0.5% BSA. Slides were washed again three times in PBST and mounted in Vectashield mounting media with DAPI.

To visualize actin filaments in *peel-1*-affected embryos, embryos were stained with Alexa568-labeled Phalloidin (Invitrogen) according to Protocol 7 in [120]. To visualize all the other proteins, embryos were stained with monoclonal antibodies MH2

(perlecan), DM5.6 (myosin heavy chain A), MH5 (VAB-10A), and MH4 (intermediate filaments). All monoclonals were obtained from The Developmental Studies Hybridoma Bank, Iowa City, Iowa. For these experiments, embryos were fixed for 10 minutes in 3% paraformaldehdye, freeze cracked in liquid nitrogen, and incubated for 5-10 minutes in -20C methanol. Embryos were then washed three times in PBST and incubated overnight with the primary antibody diluted in PBST + 1% BSA. MH2, MH4, and MH5 were diluted 1/150, and DM5.6 was diluted 1/1000. Embryos were washed three times in PBST and incubated overnight with Alexa488-labeled anti-mouse (1/500) (Invitrogen), diluted in PBST + 1% BSA. Embryos were washed again three times in PBST and mounted in Vectashield mounting media with DAPI.

Phylogenetic analysis of *zeel-1*

Separate phyolgenetic trees were built for: (i) *zyg-11* and all *zyg-11* homologs in *C. elegans*; and (ii) *zyg-11* and all *zyg-11* homologs in *C. elegans*, *C. briggsae*, *C. remanei*, and *C. japonica*. *zyg-11* homologs were defined as all genes carrying the *zyg-11*-like leucine-rich repeat region. After removing the predicted transmembrane domains of ZEEL-1, Y71A12B.17, and Y55F3C.9, all protein sequences were aligned using MUSCLE [35]. The alignments were performed using the BLOSUM30 substitution matrix, a gap open penalty of -10, and a gap extend penalty of -1. The *C. elegans*-only alignment was trimmed to exclude residues having gaps in more than 90% of sequences, and the multi-species alignment was trimmed using the heuristic method, *automated1*, from TrimAL [24], which is optimized for maximum likelihood tree construction. Finally, phylogenetic trees were constructed using PhyML [49], using the LG substitution model [75], zero invariant sites, and four substitution rate categories. Branch support was determined using bootstrap sampling with 100 replicates.

Divergence between *zeel-1* and *Y71A12B.17* was determined by aligning the two proteins with MUSCLE [35], trimming the alignment of gaps, and using PAML [46] to calculating synonymous site divergence on the corresponding nucleotide sequences. (The total length of gaps was less than 0.1% of the length of the total alignment.)

The summary statistics are as follows: number of synonymous sites = 715.5; number of non-synonymous sites = 2002.5; synonymous substitutions per site (d_S) = 1.0709; non-synonymous substitutions per site (d_N) = 0.3267.

Heat-shock

Adults and larvae were heat-shocked by submerging sealed, agar plates in a 34C water bath for one hour. Embryos were heat-shocked by mounting embryos on an agar pad, incubating the slide at 19-20C for the prescribed number of hours before placing the slide on the floor of a sealed, 1 cm x 8 cm x 8 cm plastic box, and submerging the box in a 34C water bath for 20 minutes. After heat-shock, embryos were imaged every 20 minutes for at least 10 hours. Initially, embryos were staged directly by collecting and mounting 4-cell embryos. Later, when it became clear that the vast majority of heat-shocked embryos developed to the two-fold stage without defects or delay, throughput was increased by collecting mixed stage embryos and mounting, incubating, and heat-shocking as above. These embryos were staged relative to the time at which they initiated elongation and by comparing their morphology before heat-shock to images of embryos that had been staged using the direct method.

Cell-specific killing

To quantify *peel-1*-mediated killing of the egg-laying muscles and the anal depressor muscle, the *Pexp-3::peel-1* arrays were crossed to SJ4157, which carries an integrated array of the muscle marker, *Pmyo-3::GFP*. In day-one, F1 hermaphrodites, two of the four egg-laying muscles and the single anal depressor muscle were observed and classified as live or dead based on expression of *GFP*. Live egg-laying muscles were classified as morphologically normal or atrophied, and both live egg-laying muscles and live anal depressor muscles were then classified as $mCherry^+$ or $mCherry^-$, indicating that they had or had not inherited the *Pexp-3::peel-1* array. For each cell type, the percent of cells killed by the arrays was calculated assuming that all dead cells had inherited the array. In addition, each F1 animal was classified as constipated if it contained bacteria in the posterior intestine and as egg-laying defective if it

contained three-fold embryos in the uterus.

To quantify *peel-1*-mediated killing of GABA neurons, the *Punc-47::peel-1* arrays were crossed to EG1285, which carries an integrated array of the GABA-neuron marker, *Punc-47::GFP*. GABA-neurons were observed in F1 hermaphrodites, and *peel-1*-mediated killing was quantified as above. Typically, the DVB neuron and five to nine ventral cord neurons were scored per hermaphrodite. In addition, each animal was classified as mosaic or non-mosaic based on expression of the co-injection marker, *Prab-3::mCherry*.

2.3 Discussion

We have shown that the *peel-1/zeel-1* element in *C. elegans* is composed of two, tightly linked genes: a sperm-delivered toxin, *peel-1*, and an embryo-expressed antidote, *zeel-1*. *peel-1* and *zeel-1* are located adjacent to one another in the genome, and both genes encode transmembrane proteins. *peel-1* is expressed in the male germline, and its product is delivered to the embryo via fibrous body-membranous organelles. In the absence of *zeel-1*, sperm-supplied PEEL-1 causes dose-dependent, late-occurring defects in muscle and epidermal tissue. *zeel-1* is expressed transiently in the embryo, and tissue-specific expression of *zeel-1* produces tissue-specific rescue. The transmembrane domain of *zeel-1* is required and partially sufficient for function, and like *peel-1*, this domain is evolutionarily novel and does not occur outside *C. elegans*. Finally, although PEEL-1 and ZEEL-1 normally function in embryos, *peel-1* is lethal when expressed ectopically in adults, and this lethality is rescued by ectopic expression of *zeel-1*.

2.3.1 Sperm and early embryos may be protected from PEEL-1

Given the evidence that sperm-supplied PEEL-1 may persist throughout embryogenesis and act directly during the two-fold stage, PEEL-1 must be a remarkably potent toxin. Sperm are tiny in size compared to the oocyte, roughly 1% as large by volume [21], so PEEL-1 concentrations in the embryo are necessarily low. Moreover, assum-

ing that PEEL-1 localizes to plasma membranes in the embryo, as might be expected for a FB-MO protein, then with each cell division, PEEL-1 will become more and more dilute relative to the total membrane component of the embryo.

Equivalently, the two-fold stage of development must be remarkably sensitive to the toxic effects of PEEL-1. While the cause of this hypersensitivity remains unclear, we emphasize that the morphogenetic processes occurring at the two-fold stage involve changes in cell shape and cell adhesion that are vastly more dramatic than those in earlier development. In addition, the two tissues most affected by PEEL-1 muscle and epidermis are also the two tissues in which these morphogenetic changes are most pronounced.

The high potency of PEEL-1, combined with its widespread toxicity to a variety of cell types, highlights an unusual aspect of sperm cell biology: sperm are able to function normally, despite high concentrations of PEEL-1. While the mechanism of sperm protection remains unclear, we note that sperm differ from other cell types in three ways. First, sperm contain only a nucleus, some mitochondria, and FB-MOs; all other organelles and all ribosomes, are excluded [146, 140]. Second, sperm lack an actin-based cytoskeleton [93], and instead crawl using polymers of the Major Sperm Protein [62]. Third, sperm sequester PEEL-1 in FB-MOs. Such sequestration is not possible in other cell types because FB-MOs are sperm-specific. In addition, although FB-MOs fuse with the plasma membrane upon sperm activation, they persist as permanent fusion pores [141]. This morphology prevents at least some FB-MO proteins from diffusing into the plasma membrane [142], and it may prevent diffusion of PEEL-1 as well.

The fact that pre-two-fold embryos are able to develop normally even when *peel-1* is induced by heat-shock indicates that pre-two-fold development is less sensitive than the two-fold stage to the toxic effects of PEEL-1. However, given the hypersensitivity of the two-fold stage, it remains unclear whether pre-two-fold embryos are fully resistant to PEEL-1 (like sperm), or whether PEEL-1 levels in the heat-shocked, pre-two-fold embryos were too low to produce general cytotoxic effects. While we cannot discount the possibility of full resistance, we note that in the heat-shocked embryos,

the time interval between heat-shock and the two-fold stage was five hours, at most. Five hours was sufficient for necrosis to develop in heat-shocked adults, but the two heat-shock experiments are not directly comparable because the heat-shock response in adults and embryos may not be equivalent, and the duration of heat-shock was shorter in embryos than in adults.

2.3.2 Possible mechanisms of PEEL-1 toxicity and ZEEL-1-mediated rescue

Because PEEL-1 has no sequence similarity to any other protein, the PEEL-1 sequence cannot be used to infer the mechanism of its toxicity. The fact that PEEL-1 is toxic even in extremely tiny amounts suggests that PEEL-1 might act catalytically for example, by nucleating aggregation events or by acting as a transmembrane protease. The muscle hyper-contraction observed in heat-shocked adults, as well as the paralysis and two-fold arrest observed in *peel-1*-affected embryos (which may in theory result from too much muscle contraction rather than too little), suggests that PEEL-1 might act by releasing intracellular calcium, perhaps by generating a membrane pore. It remains unclear, however, how calcium release alone can account for the epidermal defects observed in *peel-1*-affected embryos, because increased calcium signaling alone does not cause embryonic arrest [22] and is even known to suppress certain defects in epidermal morphogenesis [100]. In addition, it remains unclear how sperm might be protected from increased calcium, given the role of calcium in sperm activation [142].

Given the uncertain mechanism of PEEL-1 toxicity, there are also many possible mechanisms of ZEEL-1-mediated rescue. ZEEL-1 might promote degradation of PEEL-1, or it might prevent PEEL-1 from binding to its target, either by acting as a competitive inhibitor or by neutralizing PEEL-1 through direct interaction. While we have been unable to demonstrate a direct physical interaction between PEEL-1 and ZEEL-1, several observations are consistent with it. First, both PEEL-1 and ZEEL-1 are transmembrane proteins. ZEEL-1 localizes to cell membranes, and

PEEL-1 localizes to FB-MOs. Assuming that FB-MOs do not endocytose during fertilization, localization to these organelles should deliver PEEL-1 to the plasma membrane of the zygote, where it should have the opportunity to encounter ZEEL-1 later in development. Second, the transmembrane domain of ZEEL-1 is required and partially sufficient for function, consistent with this domain binding directly to PEEL-1. Third, tissue-specific expression of *zeel-1* produces tissue-specific rescue, consistent with ZEEL-1 being able to neutralize PEEL-1 only when both proteins are present within the same cell. Fourth, ZEEL-1 can neutralize PEEL-1 toxicity even in adults, demonstrating that the genetic interaction between *peel-1* and *zeel-1* does not require any intermediaries specific to embryogenesis. Fifth, in both embryos and adults, ZEEL-1 is able to neutralize small but not large doses of PEEL-1. This dose-dependence implies that the genetic interaction between *peel-1* and *zeel-1* requires a minimum ratio of ZEEL-1 to PEEL-1.

2.3.3 Comparison with other genetic elements causing transmission ratio distortion

Like nearly all other selfish genetic elements whose genetic basis is known [30, 79, 80], the *peel-1/zeel-1* element experiences a suppression of recombination between component parts: the insertion/deletion of *peel-1* and *zeel-1* removes both genes at once, so the two genes cannot be separated by homologous recombination. This genomic organization has undoubtedly allowed *peel-1* to persist in spite of its toxic effects, because recombination breaking apart *peel-1* and *zeel-1* would have generated haplotypes carrying *peel-1* alone, and such haplotypes are effectively suicidal.

The *peel-1/zeel-1* elements mode of action is similar to that of *Wolbachia*, in that both types of elements act through paternal-effect killing [117, 144]. *Wolbachia*s molecular mechanism is very different, however, because *Wolbachia* does not load sperm with an extra-nuclear toxin, but instead modifies the sperm pronucleus to undergo a chromatin condensation defect during the first mitotic division [18, 102]. In addition, *Wolbachia* is an intracellular bacterium, not a nuclear-encoded locus, and

rescue of *Wolbachia*-mediated killing depends upon the contents of maternal ooplasm, not zygotic transcription of a nuclear-encoded gene. The *peel-1/zeel-1* elements mode of action is also similar to the maternal-effect killing and zygotic self-rescue of Medea-factors [11], although the extent of this similarity at the molecular level is unclear because the mechanism of Medea-factor killing is unknown [79].

2.3.4 Sheltering of the *peel-1/zeel-1* element by near perpetual homozygosity

Previously, we demonstrated that haplotypes carrying the *peel-1/zeel-1* element and haplotypes lacking it are maintained by balancing selection [115]. We hypothesized that the target of selection may be a linked polymorphism, rather than the *peel-1/zeel-1* element itself [115]. Under this scenario, *peel-1* may represent an unprecedented case of inverted sheltered load. Sheltered load refers to the incidental maintenance of deleterious alleles tightly linked to sites under balancing selection [138]. Ordinarily, sheltered load occurs when deleterious recessives arise on haplotypes maintained in persistent heterozygosity, such as those of major histocompatibility complex loci in vertebrates [55] or self-incompatibility loci in plants [125]. *peel-1* is like these deleterious recessives in that although it has the potential to impose substantial genetic load on the species, its effects are rarely visible to natural selection. In the case of *peel-1*, however, sheltering is inverted because *peel-1* is only visible when heterozygous, and in *C. elegans*, heterozygosity is the exception rather than the norm.

Like any locus promoting its own transmission to the detriment of the rest of the genome, the *peel-1/zeel-1* element creates a selective environment favoring its own suppression. From a genic perspective, loci unlinked to the *peel-1/zeel-1* element suffer a fitness cost every time they are transmitted to a *peel-1*-affected embryo. As a consequence, mutations unlinked to *peel-1* and *zeel-1* that either suppress the activity of *peel-1* or mimic the activity of *zeel-1* will be favored by natural selection. Insofar as such alleles are accessible in mutational space, their absence further attests to the sheltering of the *peel-1/zeel-1* element by near perpetual homozygosity. (The *peel-1*

mutations in strains MY19 and EG4348 do not represent favored alleles because they do not arise on haplotypes suffering a fitness cost.)

2.3.5 Evolutionary origins of the *peel-1/zeel-1* element

The insertion/deletion polymorphism of *peel-1* and *zeel-1* raises the following question: Did this indel polymorphism arise by an insertion event or by deletion of pre-existing sequence? With respect to *zeel-1*, this polymorphism probably arose by a deletion event, because the divergence between *zeel-1* and its presumed ancestor, *Y71A12B.17*, predates allelic divergence at the *peel-1/zeel-1* locus. *zeel-1* and *Y71A12B.17* are 45% diverged at the amino acid level, and divergence at synonymous sites is saturated (see Materials and Methods). In comparison, the Bristol and Hawaii alleles of genes surrounding the indel polymorphism of *peel-1* and *zeel-1* are roughly 2% diverged at the amino acid level and 10-16% diverged at synonymous sites [115], this level of divergence is representative of the divergence between all haplotypes carrying the *peel-1/zeel-1* element and all haplotypes lacking it [115].

It is reasonable to suppose that the *peel-1/zeel-1* element originated as a weak toxin-antidote pair and then co-evolved into its current form. Yet given the low selective pressure for transmission ratio distortion in a self-fertilizing species, it is unlikely that *peel-1* and *zeel-1* co-evolved within *C. elegans* as result of this type of selective pressure alone. One possible solution to this paradox is that *peel-1* and *zeel-1* co-evolved in the out-crossing ancestor of *C. elegans*, where the selective pressure for transmission ratio distortion would have been much stronger. Another, non-mutually exclusive hypothesis is that *peel-1* was originally favored because it aided in another cellular process, such as sperm competition, and its toxicity to the embryo was initially mild and incidental. Under this scenario, *zeel-1* would have arisen to counteract the toxicity of *peel-1*, and once *zeel-1* became established, the presence of *zeel-1* would have allowed for stronger toxicity on the part of *peel-1* and, eventually, lethality in *zeel-1*s absence. Regardless of the initial selective pressures favoring *peel-1* and *zeel-1*, however, the fact that both *peel-1* and the transmembrane domain of *zeel-1* are evolutionarily novel indicates that the self-promoting activity of the *peel-1/zeel-1*

element arose fundamentally from the co-evolution of two novel proteins.

2.4 Acknowledgements

Foremost, we are very grateful to Michel Labouesse for his generous advice regarding the analysis of peel-1-affected embryos. We also thank Michael Brauchle for help with microscopy; Arjun Raj for providing the nuclei counting code; Joshua Bloom for help with phylogenetic analysis; Andy Singson, Steve LHernault, Christian Frokjr-Jensen, and Indrani Chatterjee for reagents and protocols; three anonymous reviewers for comments on the manuscript; and Marie-Anne Flix, Antoine Barrire, Elie Dolgin, Erik Andersen, the National Bioresource Project of Japan, and the *Caenorhabditis* Genetics Center, funded by the NIH National Center for Research Resources, for strains. MA thanks Erik Jorgensen for allowing him to work on this project in his laboratory.

Chapter 3

E- and N-cadherin in the developing mouse limb

3.1 Introduction

The vertebrate limb is a good model for studying pattern formation and morphogenesis (for review see [150]). The growth of a limb starts with the appearance of a small protrusion called the limb bud at specific locations of the developing embryo. The limb bud consists of undifferentiated mesenchymal cells covered by ectoderm. The epithelial-mesenchymal interactions between the two layers are important for induction, outgrowth, and patterning of the limb. Several specialized regions called organizing centers form to coordinate these processes. Among them, the Apical Ectodermal Ridge (AER) is particularly important for the limb outgrowth.

The AER is a thickened layer of ectodermal cells at the tip of a growing limb bud. The AER is found to be important for limb outgrowth, in that surgical removal of the AER caused truncation of the limb. Removal of the AER at progressively later stages results in progressively more distal truncation [95]. The Apical Ectodermal Cap (AEC), the equivalent structure of AER in amphibians, is the key for triggering limb regenerative response [113]. The AER is thought to be induced and maintained by the surrounding ectodermal and underlying mesenchymal cells through Wnt and FGF signaling, though the specifics are not well-understood [23]. The AER lies at

the boundary between dorsal and ventral sides of the limb, and this positioning is controlled by *Wnt7a* and *En1* in mouse [67].

3.1.1 Cadherin switch and Epithelial-mesenchymal transition (EMT) in development

All cells in our body come from one single cell. One strategy to enhance cellular diversity, as an alternative to the differentiation of stem cells, is for differentiated cells to retain plasticity and to be able to transition back and forth between different cell types. During development (and adulthood), certain cells in the epithelia have the ability to convert between epithelial and mesenchymal states via EMT and MET (Mesenchymal-epithelial transition) [65]. In particular, the transition from epithelial to mesenchymal state allows increased cell motility and invasiveness.

E-cadherin and N-cadherin are biomarkers of epithelial and mesenchymal cells, respectively. Therefore, the cadherin switch from E-cadherin to N-cadherin has been used to monitor the progress of EMT [149]. At the molecular level, EMT transcriptional reprogramming can be activated through common transcription factors such as Snail, Slug, Twist, ZEB1/2, FOXC [133], which can also be used as markers of EMT [149].

3.2 Preliminary Results

In this preliminary study, we examined the expression of E-cadherin and N-cadherin in the forelimb of E9.5 mouse embryos. We have observed E-cadherin to be expressed exclusively in the limb ectoderm including the AER (Figure 3-1 A). N-cadherin is expressed in both the underlying limb mesenchyme and the AER but not in the surrounding ectoderm (Figure 3-1 B). To our surprise, the cadherin expressions in the AER resemble neither those of epithelial cells undergoing EMT nor those of normal non-transitioning epithelial cells. In other words, the expression patterns of E- and N-cadherin are mutually exclusive, except for in the AER, where substantial levels

of both cadherins are observed. Further cell dissociation and sorting experiments using combined expression levels of E- and N-cadherin as biomarkers can isolate cells within the AER from those within the ectoderm and mesenchyme layers, and help further elucidate the molecular mechanisms behind the induction and maintenance of the AER as well as the epithelial-mesenchymal interactions driving the induction, outgrowth, and patterning of the limb.

3.2.1 Image stitching method

One big technical difficulty in imaging large mammalian tissue section was customizing automated image stitching software. Commercial and open source packages work to various degrees. We have adapted a method based on correlation [107] and used pre-recorded microscope positions for efficient and accurate image registration. The normalized 2-dimensional(2-D) correlation function measures the similarity between two input images. The translational offset between two partially overlapping images can be retrieved by maximizing the 2-D correlation function for each translation. One efficient way to calculate the normalized 2-D correlation function, using the correlation theorem, is to use fast Fourier transform to calculate the cross-power spectrum first. The cross-power spectrum, namely, the Fourier transform of the normalized 2-D correlation function of two input images, is equal to the product of the Fourier transform of one image and the complex conjugate of the Fourier transform of the other. By applying the inverse Fourier transform on the cross-power spectrum, one obtains the normalized 2-D correlation function. To speed up image processing time, we pre-crop the 1024-pixel-by-1024-pixel images down to a size of 50-pixel-by-50-pixel based on pre-recorded microscope positions. In theory, the 2-D correlation function has a single peak, indicating the translational offset between the two input image patches. But in reality, multiple peaks can result from bright auto-fluorescent spots in the background and thus become a source of registration error. Pre-cropping reduces the number of bright auto-fluorescent spots down to essentially zero in the to-be-matched image patches, and therefore drastically improves the accuracy of image stitching. Eighteen 1024-pixel-by-1024-pixel images were stitched together and

shown in (Figure 3-1 A).

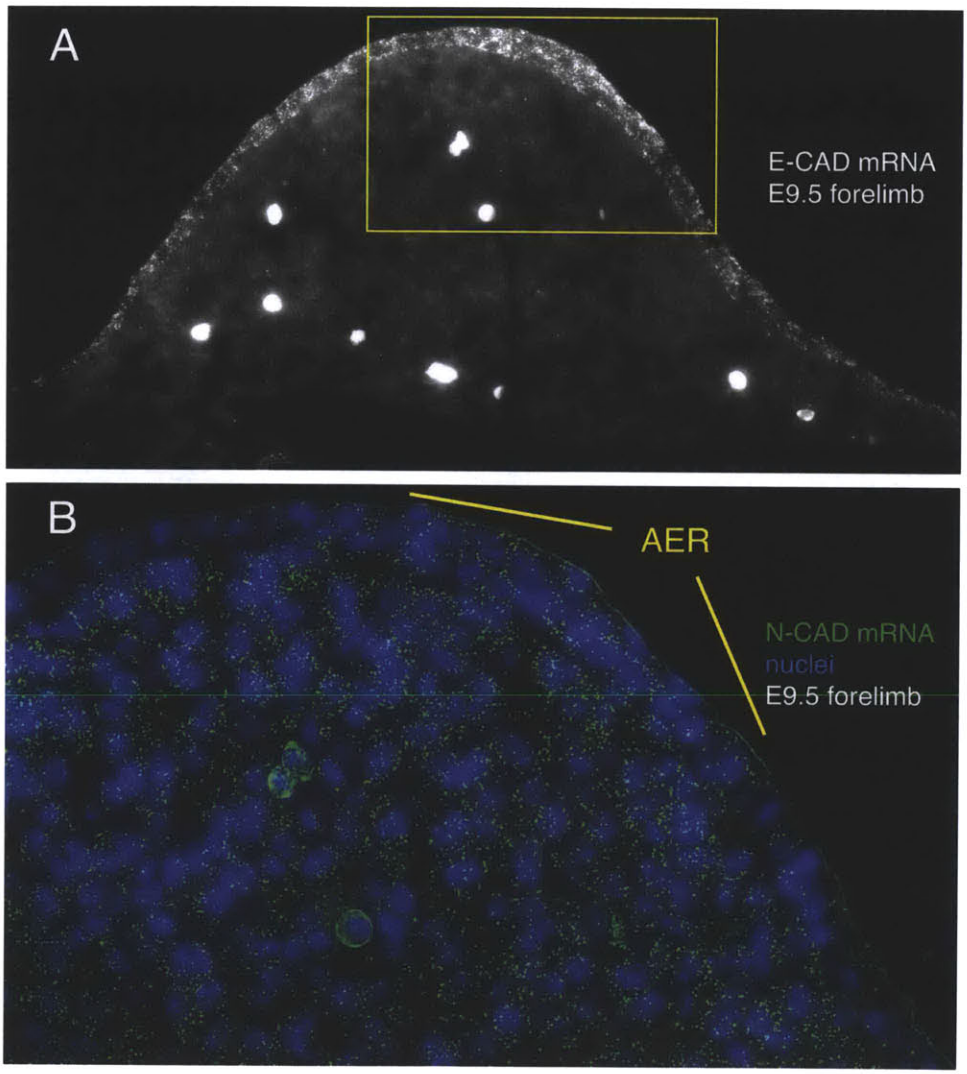

Figure 3-1: **E- and N-cadherin in forelimb of mouse E9.5 embryo.** E- and N-cadherin mRNAs were visualized in the forelimb of a wild-type, E9.5 mouse embryo using single-molecule fluorescence *in situ* hybridization. (A) E-cadherin mRNAs are shown in white. (B) shows a magnification of the boxed area in (A), with N-cadherin mRNAs shown in green, and nuclei are stained with DAPI (blue).

Appendix A

Supplementary Information

The oligonucleotide sequences of all the probes generated in this study are included below:

pie-1

atcggctttgtttgagccat, gagtgcagccatttgctcgg, acgacgtgtcatctgagttg, ctgttcgatcgatcggcagc, cgggcacgtcgcattcagaa, ctactgaattttgaattctc, gatcgattgattttccgttg, ggacgacagcgaatcattga, cgaagccattttccactata, tcttgagcgcttcacgcttt, tcaatctgagccaatggagt, tcttttagttgccggcgcct, gcttatccttcgccgagcta, agtcgcgttttgtattctgt, ttcacggcggaacgcatcac, tgtcgttgtacgggcagtat, tgtccgtgagcatatgtgca, tctcggaactctcagctcat, gggaataatactcttggcgg, acggcgctcacgtggtg-gat, cgtctcgtctagaacgagaa, cgattgattgttgtatccac, cttcgatgctgaagaactcg, gtctccgattct-catcatga, ttcgagcttccgtggttgtt, attgtgacaaatctgacgac, tatctgcagtttcctctctc, aatgaagcg-gcatcttggac, aatgttgcatttgttcgacg, taaaccgtcgcattcgcatt, acaatcggaagaaggtggcg, tg-gtagtaggcaatcggcgg, ttgctgatgttgtggatgat, gcattggaaatggcaggaat, ggcggtggagccaagaaata, aggagctccttgttgagctt, gtggaatatattgcactgga, ggctattcatcaaatcatgt, gccattggtgcatacattgg, tggttgatagtagtatgtcg, tgggcatgccattcgaatta, cggatcaatagtcacatcca, acttcaaacgcaccgc-ccgt, agagaagaatccatcgggga, aaataatagttggtggtggc

nos-2

cttggagtacccagagacat, ttcgagagtcgaagtcggtt, aaagatcgtcaaaaatgtct, acatcctctagataat-acaa, cggcgttgtggcggaaagga, cactcaaatcaaatgttggc, gaaagtgatggatccgatgg, ccattcact-

gtcaaacgaat, ttgagcatggagtcattggt, gttgaggtctccggtctttc, ttcaaacgagaagattgatg, gcggcgttttgatgggtcta, agtcgaagatattcggcagg, attcgttgacaggaatgtcg, ctgaatcgaaaaatccggaa, aaattgaaatccgaagcgac, ccaatcattgaacttcccgt, tgcgaggcttgctgtcattc, gattcaatcgcaaacgatcc, attcctcgcgagctcttcag, gctcggagcgagtttctctt, ttgaacaatgatggcacttc, atccacatccatattcacgc, catatatccaacggaacgac, tacgtgtatgcgtttcccat, gagctgagcttgtcgcattt, cacaaattttacatggagcc, tgtgattcatttcaccgcga, ttcattgggcagtacgtctc, ttgaagaacaactggctcga, gaagtctcggctgaaatcct, tgcgctggaatcgtcggttt, tgcttgtaaaattgataacg, gatcttctgaattaatgagg, aagaatcttcggatgatgcg

gfp:h2b

agttcttctcctttactcat, aattgggacaactccagtga, catcaccatctaattcaaca, gacagaaaatttgtgcccat, catcaccttcaccctctcca, agggtaagttttccgtatgt, tccagtagtgcaaataaatt, ttggccatggaacaggtagt, taacagaaagtagtgacaag, tctcgagaagcattgaacac, tgccgtttcatatgatctgg, gcatggcactcttgaaaaag, ctttcctgtacataaccttc, gtcatctttgaaaaatatag, cagcacgtgtcttgtagttc, gtatcaccttcaaacttgac, taactcgattctattaacaa, cttctttaaaatcaatacct, ttgtgtccaagaatgtttcc, tgagttatagttgtattcca, ctgccatgatgtatacattg, ttgattccattcttttgttt, gtgtctaattttgaagttaa, gaacgcttccatcttcaatg, tgttgataatggtctgctag, gccatcgccaattggagtat, ggttgtctggtaaaaggaca, gcagattgtgtggacaggta, ttcgttgggatctttcgaaa, gaaggaccatgtggtctctc, ccagcagctgttacaaactc, ttcatccatgccatgtgtaa

peel-1

aaaaccacagttggtgtgac, ggaaatcaaagcgcatcctt, ccgactatgatgttccacaa, caggcagatcaagatacatg, gcaaaccgatttacccatac, gacgagacagaaaatcttcc, gcaaacaagaagcaggatag, ggcgaaaatctgtgcaagaa, catgggtcaatgtaaaggac, gaacagtgcagagttcaatg, gcaccacgagactcataata, ctaattccatcaacggatgg, ttaaatcgtacagcagcgca, atgagcagttgagttgagac, gccttctacacatcgatcaa

zeel-1

acaactccagtcatttgcct, cagcaaaaaccattgaggtg, cacgcaatgtttcaccgtat, cgttggtacaagcatgttgt, cgagcgctataacaagatac, caactagaccaatgaccgta, ggagatacacttttttcgcg, tttcggt-

gaaacgtcagaag, gaactggtacagaagcaaca, aaaggaccacatcagactca, ttaaaaaaccccagctggct, gcaatctgaacacgagtaga, ctcgtcctcagtcataacaa, gagcacatcaaggtgagaaa, ccaacccaaattgaaacctc, ccagtgcatgaaccacaata, gctcattctttttgagtgcg, gctgtgttgcaatggttcaa, tgtcattttgtgaggaaggc, cagtgatgtttgccagagaa, catcgttgatatgccttgca, gggtcgtctttgctataaac, ccaattgacagcgacttttc, ctcgcactctctaatgtcta, aacccatcctggagtcaatt, gggaagagagcataatacca, cgcagagttctgagaaatct, cggtgtcgcttatatccaat, ccagcatatcagaggaacat, cagttaggcctgttagtttg, cgcattccacaaattgcatg, ggaagcatctagaaacgtca, ggatgagatgctaaggagtt, gtctgtagattaccgaagct, ctggtggctacagatctttt, gcttctatcgcatgccttaa, ctgctcattgggtctaaaag, gcggatggaatatatgggat, cgttcggaggcaataagtaa, tgatgatgtaaggggagaa, tactgcttgacaaggatgct, gccagtcaaactcttgatca, cactggtgccaatttgatca, atagacttccagcgcaaaac, tcaagaaacgatcgggtctt, tctcgtacaggtttccacaa, tccactgaaatcctgacttg, cgctcttactgcataatgtc

Bibliography

[1] Z. Alizadeh, S. Kageyama, and F. Aoki. Degradation of maternal mRNA in mouse embryos: selective degradation of specific mRNAs after fertilization. *Mol. Reprod. Dev.*, 72(3):281–290, Nov 2005.

[2] E. Alvarez-Saavedra and H. R. Horvitz. Many families of C. elegans microRNAs are not essential for development or viability. *Curr. Biol.*, 20(4):367–373, Feb 2010.

[3] A. Audhya, F. Hyndman, I. X. McLeod, A. S. Maddox, J. R. Yates, A. Desai, and K. Oegema. A complex containing the Sm protein CAR-1 and the RNA helicase CGH-1 is required for embryonic cytokinesis in *Caenorhabditis elegans*. *J. Cell Biol.*, 171(2):267–279, Oct 2005.

[4] A. F. Baas, L. Smit, and H. Clevers. LKB1 tumor suppressor protein: PARtaker in cell polarity. *Trends Cell Biol.*, 14(6):312–319, Jun 2004.

[5] Z. Bao, J. I. Murray, T. Boyle, S. L. Ooi, M. J. Sandel, and R. H. Waterston. Automated cell lineage tracing in *Caenorhabditis elegans*. *Proc. Natl. Acad. Sci. U.S.A.*, 103(8):2707–2712, Feb 2006.

[6] A. Barriere and M. A. Felix. High local genetic diversity and low outcrossing rate in *Caenorhabditis elegans* natural populations. *Curr. Biol.*, 15(13):1176–1184, Jul 2005.

[7] A. Bashirullah, R. L. Cooperstock, and H. D. Lipshitz. Spatial and temporal control of RNA stability. *Proc. Natl. Acad. Sci. U.S.A.*, 98(13):7025–7028, Jun 2001.

[8] A. Bashirullah, S. R. Halsell, R. L. Cooperstock, M. Kloc, A. Karaiskakis, W. W. Fisher, W. Fu, J. K. Hamilton, L. D. Etkin, and H. D. Lipshitz. Joint action of two RNA degradation pathways controls the timing of maternal transcript elimination at the midblastula transition in *Drosophila melanogaster*. *EMBO J.*, 18(9):2610–2620, May 1999.

[9] H. Bauer, N. Veron, J. Willert, and B. G. Herrmann. The t-complex-encoded guanine nucleotide exchange factor Fgd2 reveals that two opposing signaling pathways promote transmission ratio distortion in the mouse. *Genes Dev.*, 21(2):143–147, Jan 2007.

[10] L. R. Baugh, A. A. Hill, D. K. Slonim, E. L. Brown, and C. P. Hunter. Composition and dynamics of the *Caenorhabditis elegans* early embryonic transcriptome. *Development*, 130(5):889–900, Mar 2003.

[11] R. W. Beeman, K. S. Friesen, and R. E. Denell. Maternal-effect selfish genes in flour beetles. *Science*, 256(5053):89–92, Apr 1992.

[12] P. R. Boag, A. Atalay, S. Robida, V. Reinke, and T. K. Blackwell. Protection of specific maternal messenger RNAs by the P body protein CGH-1 (Dhh1/RCK) during *Caenorhabditis elegans* oogenesis. *J. Cell Biol.*, 182(3):543–557, Aug 2008.

[13] D. G. Bonett and R. M. Price. Confidence intervals for a ratio of binomial proportions based on paired data. *Stat Med*, 25(17):3039–3047, Sep 2006.

[14] J. M. Bosher, B. S. Hahn, R. Legouis, S. Sookhareea, R. M. Weimer, A. Gansmuller, A. D. Chisholm, A. M. Rose, J. L. Bessereau, and M. Labouesse. The *Caenorhabditis elegans vab-10* spectraplakin isoforms protect the epidermis against internal and external forces. *J. Cell Biol.*, 161(4):757–768, May 2003.

[15] B. Bowerman, B. A. Eaton, and J. R. Priess. *skn-1*, a maternally expressed gene required to specify the fate of ventral blastomeres in the early *C. elegans* embryo. *Cell*, 68(6):1061–1075, Mar 1992.

[16] B. Bowerman, M. K. Ingram, and C. P. Hunter. The maternal *par* genes and the segregation of cell fate specification activities in early *Caenorhabditis elegans* embryos. *Development*, 124(19):3815–3826, Oct 1997.

[17] L. Boyd, S. Guo, D. Levitan, D. T. Stinchcomb, and K. J. Kemphues. PAR-2 is asymmetrically distributed and promotes association of P granules and PAR-1 with the cortex in *C. elegans* embryos. *Development*, 122(10):3075–3084, Oct 1996.

[18] J. A. Breeuwer and J. H. Werren. Microorganisms associated with chromosome destruction and reproductive isolation between two insect species. *Nature*, 346(6284):558–560, Aug 1990.

[19] S. Brenner. The genetics of behaviour. *Br. Med. Bull.*, 29(3):269–271, Sep 1973.

[20] S. Brenner. The genetics of *Caenorhabditis elegans*. *Genetics*, 77(1):71–94, May 1974.

[21] H Browning and S Strome. A sperm-supplied factor required for embryogenesis in *C. elegans*. *Development Cambridge England*, 122(1):391–404, 1996.

[22] Y. K. Bui and P. W. Sternberg. *Caenorhabditis elegans* inositol 5-phosphatase homolog negatively regulates inositol 1,4,5-triphosphate signaling in ovulation. *Mol. Biol. Cell*, 13(5):1641–1651, May 2002.

[23] J. Capdevila and J. C. Izpisua Belmonte. Patterning mechanisms controlling vertebrate limb development. *Annual Review of Cell and Developmental Biology*, 17(1):87–132, 2001.

[24] S. Capella-Gutierrez, J. M. Silla-Martinez, and T. Gabaldon. trimAl: a tool for automated alignment trimming in large-scale phylogenetic analyses. *Bioinformatics*, 25(15):1972–1973, Aug 2009.

[25] B. J. Cha, B. S. Koppetsch, and W. E. Theurkauf. In vivo analysis of *Drosophila bicoid* mRNA localization reveals a novel microtubule-dependent axis specification pathway. *Cell*, 106(1):35–46, Jul 2001.

[26] A. D. Chisholm and J. Hardin. Epidermal morphogenesis. *WormBook*, pages 1–22, 2005.

[27] D. Cohen, P. J. Brennwald, E. Rodriguez-Boulan, and A. Musch. Mammalian PAR-1 determines epithelial lumen polarity by organizing the microtubule cytoskeleton. *J. Cell Biol.*, 164(5):717–727, Mar 2004.

[28] A. D. Cutter, A. Dey, and R. L. Murray. Evolution of the *Caenorhabditis elegans* genome. *Mol. Biol. Evol.*, 26(6):1199–1234, Jun 2009.

[29] I. D'Agostino, C. Merritt, P. L. Chen, G. Seydoux, and K. Subramaniam. Translational repression restricts expression of the *C. elegans* Nanos homolog NOS-2 to the embryonic germline. *Dev. Biol.*, 292(1):244–252, Apr 2006.

[30] R. K. Dawe and E. N. Hiatt. Plant neocentromeres: fast, focused, and driven. *Chromosome Res.*, 12(6):655–669, 2004.

[31] S. De Renzis, O. Elemento, S. Tavazoie, and E. F. Wieschaus. Unmasking activation of the zygotic genome using chromosomal deletions in the *Drosophila* embryo. *PLoS Biol.*, 5(5):e117, May 2007.

[32] D. Ding, S. M. Parkhurst, S. R. Halsell, and H. D. Lipshitz. Dynamic Hsp83 RNA localization during *Drosophila* oogenesis and embryogenesis. *Mol. Cell. Biol.*, 13(6):3773–3781, Jun 1993.

[33] C. Duval, P. Bouvet, F. Omilli, C. Roghi, C. Dorel, R. LeGuellec, J. Paris, and H. B. Osborne. Stability of maternal mRNA in Xenopus embryos: role of transcription and translation. *Mol. Cell. Biol.*, 10(8):4123–4129, Aug 1990.

[34] L. G. Edgar, N. Wolf, and W. B. Wood. Early transcription in *Caenorhabditis elegans* embryos. *Development*, 120(2):443–451, Feb 1994.

[35] R. C. Edgar. MUSCLE: multiple sequence alignment with high accuracy and high throughput. *Nucleic Acids Res.*, 32(5):1792–1797, 2004.

[36] B. Etemad-Moghadam, S. Guo, and K. J. Kemphues. Asymmetrically distributed PAR-3 protein contributes to cell polarity and spindle alignment in early *C. elegans* embryos. *Cell*, 83(5):743–752, Dec 1995.

[37] T. C. Evans, S. L. Crittenden, V. Kodoyianni, and J. Kimble. Translational control of maternal *glp-1* mRNA establishes an asymmetry in the *C. elegans* embryo. *Cell*, 77(2):183–194, Apr 1994.

[38] T. C. Evans and C. P. Hunter. Translational control of maternal RNAs. *WormBook*, pages 1–11, 2005.

[39] Thomas C. Evans. *Transformation and microinjection.* 2006.

[40] B. M. Farley and S. P. Ryder. Regulation of maternal mRNAs in early development. *Crit. Rev. Biochem. Mol. Biol.*, 43(2):135–162, 2008.

[41] L. Fishman and J. H. Willis. A novel meiotic drive locus almost completely distorts segregation in *mimulus* (monkeyflower) hybrids. *Genetics*, 169(1):347–353, Jan 2005.

[42] K. R. Fitch, G. K. Yasuda, K. N. Owens, and B. T. Wakimoto. Paternal effects in *Drosophila*: implications for mechanisms of early development. *Curr. Top. Dev. Biol.*, 38:1–34, 1998.

[43] C. Frokjaer-Jensen, M. W. Davis, C. E. Hopkins, B. J. Newman, J. M. Thummel, S. P. Olesen, M. Grunnet, and E. M. Jorgensen. Single-copy insertion of transgenes in *Caenorhabditis elegans*. *Nat. Genet.*, 40(11):1375–1383, Nov 2008.

[44] C. M. Gallo, E. Munro, D. Rasoloson, C. Merritt, and G. Seydoux. Processing bodies and germ granules are distinct RNA granules that interact in *C. elegans* embryos. *Dev. Biol.*, 323(1):76–87, Nov 2008.

[45] A. J. Giraldez, Y. Mishima, J. Rihel, R. J. Grocock, S. Van Dongen, K. Inoue, A. J. Enright, and A. F. Schier. Zebrafish MiR-430 promotes deadenylation and clearance of maternal mRNAs. *Science*, 312(5770):75–79, Apr 2006.

[46] N. Goldman and Z. Yang. A codon-based model of nucleotide substitution for protein-coding DNA sequences. *Mol. Biol. Evol.*, 11(5):725–736, Sep 1994.

[47] B. Goldstein. Induction of gut in *Caenorhabditis elegans* embryos. *Nature*, 357(6375):255–257, May 1992.

[48] K. S. Guimaraes, A. Panchenko, and T. M. Editors Przytycka, editors. *Advances in Bioinformatics and Computational Biology*, volume 5676. Springer, Berlin, Heidelberg, 2009.

[49] S. Guindon and O. Gascuel. A simple, fast, and accurate algorithm to estimate large phylogenies by maximum likelihood. *Syst. Biol.*, 52(5):696–704, Oct 2003.

[50] S. Guo and K. J. Kemphues. *par-1*, a gene required for establishing polarity in *C. elegans* embryos, encodes a putative Ser/Thr kinase that is asymmetrically distributed. *Cell*, 81(4):611–620, May 1995.

[51] M. Haber, M. Schungel, A. Putz, S. Muller, B. Hasert, and H. Schulenburg. Evolutionary history of *Caenorhabditis elegans* inferred from microsatellites: evidence for spatial and temporal genetic differentiation and the occurrence of outbreeding. *Mol. Biol. Evol.*, 22(1):160–173, Jan 2005.

[52] O. Hachet and A. Ephrussi. *Drosophila* Y14 shuttles to the posterior of the oocyte and is required for *oskar* mRNA transport. *Curr. Biol.*, 11(21):1666–1674, Oct 2001.

[53] T. Hirokawa, S. Boon-Chieng, and S. Mitaku. SOSUI: classification and secondary structure prediction system for membrane proteins. *Bioinformatics*, 14(4):378–379, 1998.

[54] K Hofmann and W Stoffel. Tmbase - a database of membrane spanning protein segments. *Biol Chem HoppeSeyler*, 374(374):166, 1993.

[55] A. L. Hughes and M. Nei. Pattern of nucleotide substitution at major histocompatibility complex class I loci reveals overdominant selection. *Nature*, 335(6186):167–170, Sep 1988.

[56] T. J. Hung and K. J. Kemphues. PAR-6 is a conserved PDZ domain-containing protein that colocalizes with PAR-3 in *Caenorhabditis elegans* embryos. *Development*, 126(1):127–135, Jan 1999.

[57] C. P. Hunter and C. Kenyon. Spatial and temporal controls target *pal-1* blastomere-specification activity to a single blastomere lineage in *C. elegans* embryos. *Cell*, 87(2):217–226, Oct 1996.

[58] M. S. Hunter, S. J. Perlman, and S. E. Kelly. A bacterial symbiont in the Bacteroidetes induces cytoplasmic incompatibility in the parasitoid wasp Encarsia pergandiella. *Proc. Biol. Sci.*, 270(1529):2185–2190, Oct 2003.

[59] G. D. Hurst and J. H. Werren. The role of selfish genetic elements in eukaryotic evolution. *Nat. Rev. Genet.*, 2(8):597–606, Aug 2001.

[60] H. Hutter and R. Schnabel. *glp-1* and inductions establishing embryonic axes in *C. elegans*. *Development*, 120(7):2051–2064, Jul 1994.

[61] V. Irish, R. Lehmann, and M. Akam. The *Drosophila* posterior-group gene *nanos* functions by repressing *hunchback* activity. *Nature*, 338(6217):646–648, Apr 1989.

[62] J. E. Italiano, T. M. Roberts, M. Stewart, and C. A. Fontana. Reconstitution in vitro of the motile apparatus from the amoeboid sperm of *Ascaris* shows that filament assembly and bundling move membranes. *Cell*, 84(1):105–114, Jan 1996.

[63] J. Jaenike. Sex chromosome meiotic drive. *Annual Review of Ecology and Systematics*, 32(2001):25–49, 2001.

[64] D. Jones, R. H. Russnak, R. J. Kay, and E. P. Candido. Structure, expression, and evolution of a heat shock gene locus in *Caenorhabditis elegans* that is flanked by repetitive elements. *J. Biol. Chem.*, 261(26):12006–12015, Sep 1986.

[65] R. Kalluri and R. A. Weinberg. The basics of epithelial-mesenchymal transition. *J. Clin. Invest.*, 119(6):1420–1428, Jun 2009.

[66] W. G. Kelly, S. Xu, M. K. Montgomery, and A. Fire. Distinct requirements for somatic and germline expression of a generally expressed Caernorhabditis elegans gene. *Genetics*, 146(1):227–238, May 1997.

[67] R. A. Kimmel, D. H. Turnbull, V. Blanquet, W. Wurst, C. A. Loomis, and A. L. Joyner. Two lineage boundaries coordinate vertebrate apical ectodermal ridge formation. *Genes Dev.*, 14(11):1377–1389, Jun 2000.

[68] S. Kondo and T. Miura. Reaction-diffusion model as a framework for understanding biological pattern formation. *Science*, 329(5999):1616–1620, Sep 2010.

[69] M. Krause, S. W. Harrison, S. Q. Xu, L. Chen, and A. Fire. Elements regulating cell- and stage-specific expression of the *C. elegans* MyoD family homolog *hlh-1*. *Dev. Biol.*, 166(1):133–148, Nov 1994.

[70] A. Kusano, C. Staber, H. Y. Chan, and B. Ganetzky. Closing the (Ran)GAP on segregation distortion in *Drosophila*. *Bioessays*, 25(2):108–115, Feb 2003.

[71] M. Labouesse. Epithelial junctions and attachments. *WormBook*, pages 1–21, 2006.

[72] M. Labouesse and S. E. Mango. Patterning the *C. elegans* embryo: moving beyond the cell lineage. *Trends Genet.*, 15(8):307–313, Aug 1999.

[73] C. W. LaMunyon and S. Ward. Larger sperm outcompete smaller sperm in the nematode *Caenorhabditis elegans*. *Proc. Biol. Sci.*, 265(1409):1997–2002, Oct 1998.

[74] F. Landmann, S. Quintin, and M. Labouesse. Multiple regulatory elements with spatially and temporally distinct activities control the expression of the epithelial differentiation gene *lin-26* in *C. elegans*. *Dev. Biol.*, 265(2):478–490, Jan 2004.

[75] S. Q. Le and O. Gascuel. An improved general amino acid replacement matrix. *Mol. Biol. Evol.*, 25(7):1307–1320, Jul 2008.

[76] D. J. Levitan, L. Boyd, C. C. Mello, K. J. Kemphues, and D. T. Stinchcomb. *par-2*, a gene required for blastomere asymmetry in *Caenorhabditis elegans*, encodes zinc-finger and ATP-binding motifs. *Proc. Natl. Acad. Sci. U.S.A.*, 91(13):6108–6112, Jun 1994.

[77] S. W. L'Hernault. Spermatogenesis. *WormBook*, pages 1–14, 2006.

[78] D. Lin, A. S. Edwards, J. P. Fawcett, G. Mbamalu, J. D. Scott, and T. Pawson. A mammalian PAR-3-PAR-6 complex implicated in Cdc42/Rac1 and aPKC signalling and cell polarity. *Nat. Cell Biol.*, 2(8):540–547, Aug 2000.

[79] M. D. Lorenzen, A. Gnirke, J. Margolis, J. Garnes, M. Campbell, J. J. Stuart, R. Aggarwal, S. Richards, Y. Park, and R. W. Beeman. The maternal-effect, selfish genetic element Medea is associated with a composite Tc1 transposon. *Proc. Natl. Acad. Sci. U.S.A.*, 105(29):10085–10089, Jul 2008.

[80] T. W. Lyttle. Segregation distorters. *Annu. Rev. Genet.*, 25:511–557, 1991.

[81] M. Maduro and D. Pilgrim. Identification and cloning of *unc-119*, a gene expressed in the *Caenorhabditis elegans* nervous system. *Genetics*, 141(3):977–988, Nov 1995.

[82] S. L. McIntire, E. Jorgensen, J. Kaplan, and H. R. Horvitz. The GABAergic nervous system of *Caenorhabditis elegans*. *Nature*, 364(6435):337–341, Jul 1993.

[83] S. L. McIntire, R. J. Reimer, K. Schuske, R. H. Edwards, and E. M. Jorgensen. Identification and characterization of the vesicular GABA transporter. *Nature*, 389(6653):870–876, Oct 1997.

[84] C. C. Mello, B. W. Draper, M. Krause, H. Weintraub, and J. R. Priess. The *pie-1* and *mex-1* genes and maternal control of blastomere identity in early *C. elegans* embryos. *Cell*, 70(1):163–176, Jul 1992.

[85] C. C. Mello, J. M. Kramer, D. Stinchcomb, and V. Ambros. Efficient gene transfer in C.elegans: extrachromosomal maintenance and integration of transforming sequences. *EMBO J.*, 10(12):3959–3970, Dec 1991.

[86] C. C. Mello, C. Schubert, B. Draper, W. Zhang, R. Lobel, and J. R. Priess. The PIE-1 protein and germline specification in *C. elegans* embryos. *Nature*, 382(6593):710–712, Aug 1996.

[87] C. Merritt, D. Rasoloson, D. Ko, and G. Seydoux. 3' UTRs are the primary regulators of gene expression in the *C. elegans* germline. *Curr. Biol.*, 18(19):1476–1482, Oct 2008.

[88] C. Merritt and G. Seydoux. Transgenic solutions for the germline. *WormBook*, pages 1–21, 2010.

[89] T. Miura, K. Shiota, G. Morriss-Kay, and P. K. Maini. Mixed-mode pattern in *Doublefoot* mutant mouse limb–Turing reaction-diffusion model on a growing domain during limb development. *J. Theor. Biol.*, 240(4):562–573, Jun 2006.

[90] D. G. Moerman and B. D. Williams. Sarcomere assembly in *C. elegans* muscle. *WormBook*, pages 1–16, 2006.

[91] D. G. Morton, D. C. Shakes, S. Nugent, D. Dichoso, W. Wang, A. Golden, and K. J. Kemphues. The *Caenorhabditis elegans par-5* gene encodes a 14-3-3 protein required for cellular asymmetry in the early embryo. *Dev. Biol.*, 241(1):47–58, Jan 2002.

[92] J. Nagler, A. Levina, and M. Timme. Impact of single links in competitive percolation – how complex networks grow under competition. *Nature Physics*, 7(3):265–270, 2011.

[93] G. A. Nelson, T. M. Roberts, and S. Ward. *Caenorhabditis elegans* spermatozoan locomotion: amoeboid movement with almost no actin. *J. Cell Biol.*, 92(1):121–131, Jan 1982.

[94] S. A. Newman and H. L. Frisch. Dynamics of skeletal pattern formation in developing chick limb. *Science*, 205(4407):662–668, Aug 1979.

[95] L. Niswander. Pattern formation: old models out on a limb. *Nat. Rev. Genet.*, 4(2):133–143, Feb 2003.

[96] H. Okamoto and J. N. Thomson. Monoclonal antibodies which distinguish certain classes of neuronal and supporting cells in the nervous tissue of the nematode *Caenorhabditis elegans*. *J. Neurosci.*, 5(3):643–653, Mar 1985.

[97] O. J. O'Loan and M. R. Evans. Alternating steady state in one-dimensional flocking. *Journal of Physics A: Mathematical and General*, 32(8):L99, 1999.

[98] I. M. Palacios and D. St Johnston. Getting the message across: the intracellular localization of mRNAs in higher eukaryotes. *Annu. Rev. Cell Dev. Biol.*, 17:569–614, 2001.

[99] F. Pardo-Manuel de Villena and C. Sapienza. Nonrandom segregation during meiosis: the unfairness of females. *Mamm. Genome*, 12(5):331–339, May 2001.

[100] J. Pilipiuk, C. Lefebvre, T. Wiesenfahrt, R. Legouis, and O. Bossinger. Increased IP3/Ca2+ signaling compensates depletion of LET-413/DLG-1 in *C. elegans* epithelial junction assembly. *Dev. Biol.*, 327(1):34–47, Mar 2009.

[101] V. Praitis, E. Casey, D. Collar, and J. Austin. Creation of low-copy integrated transgenic lines in *Caenorhabditis elegans*. *Genetics*, 157(3):1217–1226, Mar 2001.

[102] D. C. Presgraves. A genetic test of the mechanism of Wolbachia-induced cytoplasmic incompatibility in Drosophila. *Genetics*, 154(2):771–776, Feb 2000.

[103] J. R. Priess and J. N. Thomson. Cellular interactions in early *C. elegans* embryos. *Cell*, 48(2):241–250, Jan 1987.

[104] A. Raj, S. A. Rifkin, E. Andersen, and A. van Oudenaarden. Variability in gene expression underlies incomplete penetrance. *Nature*, 463(7283):913–918, Feb 2010.

[105] A. Raj, P. van den Bogaard, S. A. Rifkin, A. van Oudenaarden, and S. Tyagi. Imaging individual mRNA molecules using multiple singly labeled probes. *Nat. Methods*, 5(10):877–879, Oct 2008.

[106] C. K. Raymond, T. A. Pownder, and S. L. Sexson. General method for plasmid construction using homologous recombination. *BioTechniques*, 26(1):134–138, Jan 1999.

[107] B S Reddy and B N Chatterji. An fft-based technique for translation, rotation, and scale-invariant image registration. *Image Processing IEEE Transactions on*, 5(8):1266–1271, 1996.

[108] C. E. Rocheleau, W. D. Downs, R. Lin, C. Wittmann, Y. Bei, Y. H. Cha, M. Ali, J. R. Priess, and C. C. Mello. Wnt signaling and an APC-related gene specify endoderm in early *C. elegans* embryos. *Cell*, 90(4):707–716, Aug 1997.

[109] M. V. Rockman and L. Kruglyak. Recombinational landscape and population genomics of *Caenorhabditis elegans*. *PLoS Genet.*, 5(3):e1000419, Mar 2009.

[110] T. M. Rogalski and D. L. Riddle. A *Caenorhabditis elegans* RNA polymerase II gene, *ama-1* IV, and nearby essential genes. *Genetics*, 118(1):61–74, Jan 1988.

[111] L. S. Rose and K. J. Kemphues. Early patterning of the *C. elegans* embryo. *Annu. Rev. Genet.*, 32:521–545, 1998.

[112] B. Rost, R. Casadio, and P. Fariselli. Refining neural network predictions for helical transmembrane proteins by dynamic programming. *Proc Int Conf Intell Syst Mol Biol*, 4:192–200, 1996.

[113] A. Satoh, G. M. Graham, S. V. Bryant, and D. M. Gardiner. Neurotrophic regulation of epidermal dedifferentiation during wound healing and limb regeneration in the axolotl (Ambystoma mexicanum). *Dev. Biol.*, 319(2):321–335, Jul 2008.

[114] A. F. Schier. The maternal-zygotic transition: death and birth of RNAs. *Science*, 316(5823):406–407, Apr 2007.

[115] H. S. Seidel, M. V. Rockman, and L. Kruglyak. Widespread genetic incompatibility in *C. elegans* maintained by balancing selection. *Science*, 319(5863):589–594, 2008.

[116] J. L. Semotok, R. L. Cooperstock, B. D. Pinder, H. K. Vari, H. D. Lipshitz, and C. A. Smibert. Smaug recruits the CCR4/POP2/NOT deadenylase complex to trigger maternal transcript localization in the early *Drosophila* embryo. *Curr. Biol.*, 15(4):284–294, Feb 2005.

[117] L. R. Serbus, C. Casper-Lindley, F. Landmann, and W. Sullivan. The genetics and cell biology of *Wolbachia*-host interactions. *Annu. Rev. Genet.*, 42:683–707, 2008.

[118] G. Seydoux and A. Fire. Soma-germline asymmetry in the distributions of embryonic RNAs in *Caenorhabditis elegans*. *Development*, 120(10):2823–2834, Oct 1994.

[119] G. Seydoux, C. C. Mello, J. Pettitt, W. B. Wood, J. R. Priess, and A. Fire. Repression of gene expression in the embryonic germ lineage of *C. elegans*. *Nature*, 382(6593):713–716, Aug 1996.

[120] Shai Shaham. Methods in cell biology. *WormBook*, 107(3):1–75, 2006.

[121] A. Singson, K. L. Hill, and S. W. L'Hernault. Sperm competition in the absence of fertilization in *Caenorhabditis elegans*. *Genetics*, 152(1):201–208, May 1999.

[122] A. Singson, K. B. Mercer, and S. W. L'Hernault. The *C. elegans spe-9* gene encodes a sperm transmembrane protein that contains EGF-like repeats and is required for fertilization. *Cell*, 93(1):71–79, Apr 1998.

[123] E. L. Sonnhammer, G. von Heijne, and A. Krogh. A hidden Markov model for predicting transmembrane helices in protein sequences. *Proc Int Conf Intell Syst Mol Biol*, 6:175–182, 1998.

[124] A. Spirov, K. Fahmy, M. Schneider, E. Frei, M. Noll, and S. Baumgartner. Formation of the *bicoid* morphogen gradient: an mRNA gradient dictates the protein gradient. *Development*, 136(4):605–614, Feb 2009.

[125] J. L. Stone. Sheltered load associated with S-alleles in *Solanum carolinense*. *Heredity (Edinb)*, 92(4):335–342, Apr 2004.

[126] J. E. Sulston. Neuronal cell lineages in the nematode *Caenorhabditis elegans*. *Cold Spring Harb. Symp. Quant. Biol.*, 48 Pt 2:443–452, 1983.

[127] J. E. Sulston and H. R. Horvitz. Post-embryonic cell lineages of the nematode, *Caenorhabditis elegans*. *Dev. Biol.*, 56(1):110–156, Mar 1977.

[128] J. E. Sulston, E. Schierenberg, J. G. White, and J. N. Thomson. The embryonic cell lineage of the nematode *Caenorhabditis elegans*. *Dev. Biol.*, 100(1):64–119, Nov 1983.

[129] H. Tabara, R. J. Hill, C. C. Mello, J. R. Priess, and Y. Kohara. *pos-1* encodes a cytoplasmic zinc-finger protein essential for germline specification in *C. elegans*. *Development*, 126(1):1–11, Jan 1999.

[130] W. Tadros and H. D. Lipshitz. The maternal-to-zygotic transition: a play in two acts. *Development*, 136(18):3033–3042, Sep 2009.

[131] C. Tenenhaus, C. Schubert, and G. Seydoux. Genetic requirements for PIE-1 localization and inhibition of gene expression in the embryonic germ lineage of *Caenorhabditis elegans*. *Dev. Biol.*, 200(2):212–224, Aug 1998.

[132] C. Tenenhaus, K. Subramaniam, M. A. Dunn, and G. Seydoux. PIE-1 is a bifunctional protein that regulates maternal and zygotic gene expression in the embryonic germ line of *Caenorhabditis elegans*. *Genes Dev.*, 15(8):1031–1040, Apr 2001.

[133] J. P. Thiery and J. P. Sleeman. Complex networks orchestrate epithelial-mesenchymal transitions. *Nat. Rev. Mol. Cell Biol.*, 7(2):131–142, Feb 2006.

[134] C. J. Thorpe, A. Schlesinger, J. C. Carter, and B. Bowerman. Wnt signaling polarizes an early *C. elegans* blastomere to distinguish endoderm from mesoderm. *Cell*, 90(4):695–705, Aug 1997.

[135] A. M. Turing. The chemical basis for morphogenesis. *Philosophical transactions of the royal society of london Series B Biological sciences*, 237:37–72, 1952.

[136] B. C. Turner and D. D. Perkins. Spore killer, a chromosomal factor in neurospora that kills meiotic products not containing it. *Genetics*, 93(3):587–606, 1979.

[137] G. E. Tusnady and I. Simon. The HMMTOP transmembrane topology prediction server. *Bioinformatics*, 17(9):849–850, Sep 2001.

[138] M. K. Uyenoyama. Genealogical structure among alleles regulating self-incompatibility in natural populations of flowering plants. *Genetics*, 147(3):1389–1400, Nov 1997.

[139] G. von Heijne. Membrane protein structure prediction. Hydrophobicity analysis and the positive-inside rule. *J. Mol. Biol.*, 225(2):487–494, May 1992.

[140] S. Ward. *Asymmetric localization of gene products during the development of* C. elegans *spermatozoa.*, pages 55–75. Alan R. Liss, NY, 1986.

[141] S. Ward, Y. Argon, and G. A. Nelson. Sperm morphogenesis in wild-type and fertilization-defective mutants of *Caenorhabditis elegans*. *J. Cell Biol.*, 91(1):26–44, Oct 1981.

[142] N. L. Washington and S. Ward. FER-1 regulates Ca2+ -mediated membrane fusion during *C. elegans* spermatogenesis. *J. Cell. Sci.*, 119(Pt 12):2552–2562, Jun 2006.

[143] J. L. Watts, D. G. Morton, J. Bestman, and K. J. Kemphues. The *C. elegans par-4* gene encodes a putative serine-threonine kinase required for establishing embryonic asymmetry. *Development*, 127(7):1467–1475, Apr 2000.

[144] J. H. Werren, L. Baldo, and M. E. Clark. *Wolbachia*: master manipulators of invertebrate biology. *Nat. Rev. Microbiol.*, 6(10):741–751, Oct 2008.

[145] B. D. Williams and R. H. Waterston. Genes critical for muscle development and function in *Caenorhabditis elegans* identified through lethal mutations. *J. Cell Biol.*, 124(4):475–490, Feb 1994.

[146] N. Wolf, D. Hirsh, and J. R. McIntosh. Spermatogenesis in males of the free-living nematode, *Caenorhabditis elegans*. *J. Ultrastruct. Res.*, 63(2):155–169, May 1978.

[147] U. Wolke, G. Weidinger, M. Koprunner, and E. Raz. Multiple levels of posttranscriptional control lead to germ line-specific gene expression in the zebrafish. *Curr. Biol.*, 12(4):289–294, Feb 2002.

[148] W. B. Wood, editor. *The Nematode Caenorhabditis elegans*. Cold Spring Harbor Laboratory Press, Cold Spring Harbor, New York, 1988.

[149] M. Zeisberg and E. G. Neilson. Biomarkers for epithelial-mesenchymal transitions. *J. Clin. Invest.*, 119(6):1429–1437, Jun 2009.

[150] R. Zeller, J. Lopez-Rios, and A. Zuniga. Vertebrate limb bud development: moving towards integrative analysis of organogenesis. *Nat. Rev. Genet.*, 10(12):845–858, Dec 2009.